Special Issue

VYTÁPĚNÍ VĚTRÁNÍ INSTALACE

6 2017
VOL. 26

Journal of Heating, Ventilation and Sanitary Installation

ISSN 1210-1389 / MK ČR E 6050

Special Issue of Journal of Heating, Ventilation and Sanitary Installation

VVI Journal brings information:

- about the latest trends in heating, ventilation, air conditioning, cooling, humidification, dehumidification, hygiene, sanitation installation, measurement and control, lighting, noise, air quality, energy conservation, traditional and alternative energy sources at home and abroad;
- about new products, techniques and domestic or foreign technology for accurate and efficient operation of buildings with examples of practical use;
- about testing and measures improving quality of domestic production and enhancing sales of domestic products at foreign markets;
- about theoretical works dealing with new knowledge characteristics of new products, new computational methods and application of computer technology in the field of environmental engineering;

More information: www.stpcr.cz/en

Since 2014 the VVI journal is included into the SCOPUS database

Scopus

Journal of Heating, Ventilation and Sanitary Installation Vol. 26 Issue 6
VYTÁPĚNÍ, VĚTRÁNÍ, INSTALACE 26. ročník Číslo 6

60. ročník Zdravotní technika a vzduchotechnika (323. číslo) Prosinec 2017 / December 2017

Vydává: Společnost pro techniku prostředí / Publisher: Society of Environmental Engineering
Novotného lávka 5, 116 68 Praha 1, tel./fax: 221 082 201, stp@stpcr.cz, www.stpcr.cz

Vedoucí redaktor / Editor in chief: doc. Ing. Vladimír Zmrhal, Ph.D.
Výkonná redaktorka / Text editor: Ing. Štěpánka Homolová

VYTÁPĚNÍ VĚTRÁNÍ INSTALACE

Editorial

Vážení čtenáři,

nebývá zvykem zabírat místo v našem technickém časopisu podobnou rubrikou, nicméně dovolte mi několik úvodních slov. Právě si prohlížíte zvláštní vydání časopisu Vytápění, větrání, instalace 6/2017, což je v historii časopisu s 60letou tradicí ojedinělý počin, který jistě stojí za zmínku. Toto zvláštní číslo obsahuje články psané v anglickém jazyce, vychází pouze elektronicky a je dostupné on-line všem zájemcům. Obecným cílem našeho časopisu je přinášet kvalitní informace z oborů techniky prostředí a k tomu jsou zapotřebí i kvalitní autoři, ochotní podělit se s námi o nové poznatky v oboru. Abychom podpořili autory v prezentaci výsledků jejich práce i v zahraničí, rozhodli jsme se vydat jedno číslo časopisu „navíc" v angličtině. Již v minulosti byl časopis zařazen do prestižní mezinárodní databáze SCOPUS a věříme, že předkládané číslo v anglickém jazyce přispěje ke zvýšení prestiže časopisu v zahraničí. Zejména pro mladé autory z akademické sféry může mít tento počin do budoucna motivační účinek.

Vážení čtenáři, přeji Vám příjemné „anglické" čtení

Vladimír Zmrhal
vedoucí redaktor

Pokyny pro autory naleznete na www.stpcr.cz/vvi

Odborný recenzovaný časopis Společnosti pro techniku prostředí

Člen Českého svazu VTS, člen REHVA, asociovaný člen ASHRAE

REDAKCE
Vladimir.Zmrhal@fs.cvut.cz, tel.: 224 352 433, homolova.vvi@gmail.com, tel.: 778 444 677.

PŘEDPLATNÉ
Česká republika: **SEND Předplatné**, s. r. o., Ve Žlíbku 77/1800, hala 3, 193 00 Praha 9, tel.: 225 985 225, fax: 225 341 425, send@send.cz, www.send.cz. Administrace: Marek Rybenský, marek@send.cz.

Roční předplatné **250 Kč**, studenti **125 Kč** včetně poštovného.

Slovenská republika: **MAGNET PRESS, SLOVAKIA s. r. o.**, P. O. Box 169, 830 00 Bratislava. Předplatné: predplatne@press.sk, tel./fax: +421 267 201 930-1. Sídlo firmy Šustekova 8, 851 04 Bratislava. Roční předplatné **10,80 €**.

Volný prodej a zasílání na dobírku: Univerzitní knihkupectví ČVUT, budova NTK, Technická 6, 160 80 Praha 6, vera.mikulkova@ctn.cvut.cz, tel.: 224 355 003 nebo osobně v redakci.

Inzeráty přijímá a informace o podmínkách inzerce podává Věra Jírová, tel.: 241 401 229, 603 180 596, vera.jirova.vvi@gmail.com nebo Vladimír Zmrhal, vladimir.zmrhal@fs.cvut.cz, tel.: 224 352 433.

Za obsah inzerce ručí objednatel.

Podávání novinových zásilek v ČR povoleno Ředitelstvím pošt, Praha čj. NP 1727/1993 ze dne 23. 3. 1993.

Jazyková korektura: Harvey Cook

STP je plátcem DPH. Expedice online.
ISSN 1210-1389. Registrace MK ČR E 6050.

Časopis je zařazen do mezinárodní databáze SCOPUS.

Scopus

Ing. Jan KRÁLÍČEK [1),2)]
Ing. Miroslav KUČERA, Ph.D. [2),3)]

[1)] AKUSTPROJEKT s.r.o.
[2)] CTU in Prague, Faculty of Mechanical Engineering, Department of Environmental Engineering
[3)] University Centre for Energy Efficient Buildings

Acoustic Assessment and Design of Acoustic Protection for Heat Pumps

Akustické posouzení a návrh protihlukových opatření u tepelných čerpadel

The paper deals with the acoustic assessment and design of acoustic protection for an actual heat pump system for a residential building with a shop installed in the courtyard of an older residential building. The heat pump system is used for the cooling and heating of the residential and non-residential premises, hence the night operation of the heat pumps, which is subject to stricter hygiene limits on noise. The installation of the units and the construction were already under implementation, therefore, there was little room for acoustic design adjustments.

Keywords: *heat pumps, noise, residential courtyard, design of acoustic protection*

Článek se věnuje akustickému posouzení a návrhu akustických opatření u reálné soustavy tepelných čerpadel pro bytový dům s prodejnou instalované ve vnitrobloku starší bytové zástavby. Soustava tepelných čerpadel slouží pro chlazení a vytápění bytových a nebytových prostor, tudíž byl vyžadován i noční provoz tepelných čerpadel, na který se vztahují přísnější hygienické limity hluku. Instalace jednotek a stavba byly již v realizaci, tudíž nezbývalo příliš možností pro návrhy akustických úprav.

Klíčová slova: *tepelná čerpadla, hluk, obytný vnitroblok, návrh protihlukových opatření*

INTRODUCTION

Nowadays, heat pumps (HP) are used as a part of air conditioning and heating systems, not only for the commercial sphere, but also in the communal sphere for family and residential buildings. Noise from heat pumps is assessed by hygienic noise limits, e.g., in the protected outdoor area of buildings (up to 2 m from the windows of protected rooms), in this case, especially residential buildings. The hygienic noise limits for these sources according to [4] are the level $L_{Aeq,8h}$ = 50dB for 8 consecutive noisy and consecutive hours of the day and $L_{Aeq,1h}$ = 40 dB for one of the loudest hours of the night. In addition, if a noise component is present, 5 dB is subtracted, thus $L_{Aeq,8h}$ = 45 dB for the day and $L_{Aeq,1h}$ = 35 dB for the night.

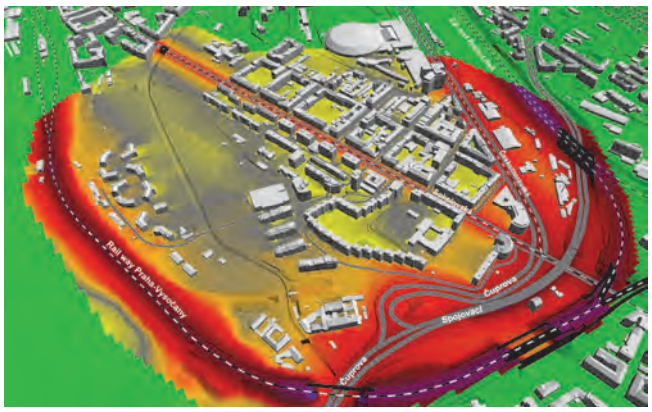

Figure 1 An example of a 3D view of the real computational situation of traffic noise sources with the display of noise bands, see [3].

The cooling or heating designer solves the design of the heat pumps in terms of thermal requirements, but often neglects the acoustic assessment. There are cases when an acoustics issue comes up only after the installation of the heat pumps and once the noise is noticed on site. In such cases, however, there are no longer many possibilities to reduce the noise. The danger of installing heat pumps in terms of acoustics occurs especially when it is not possible to install the equipment outside a protected area e.g., on the roof, but it is necessary to install the equipment, for example, in the interior of a residential building. There is very low background noise in the inner courtyard, and an inadequate noise source can be easily demonstrated by on-site measurements.

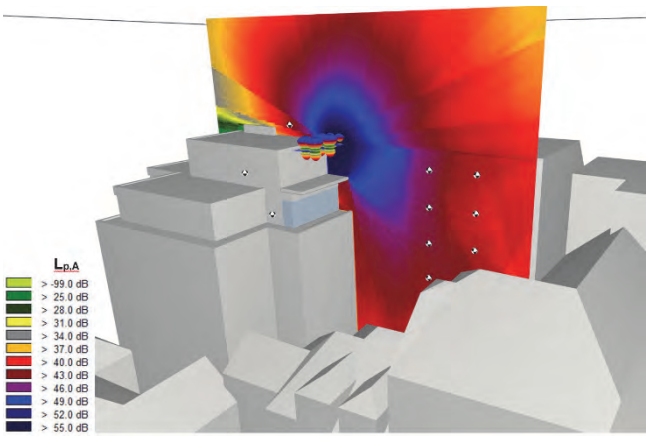

Figure 2 A 3D view of a computational model showing the distribution of the noise field around the cooling unit installed on the roof near the protected area, see [3].

For acoustic assessment, a number of computational software products exist today, whose differences mainly lay in the possibilities of entering more complicated geometric situations, the possibility of entering parameters for sound characteristics of the materials, the directionality of the sources, and in the computational methodology also. The more sophisticated the software is, of course, the more expensive it is, so it is always necessary to assess each situation and make decisions as to how large the monitored area will be and what details are decisive for assessing the noise. These may include reflections from the facade, the frequency composition of the sound, the proximity of the point to the source and the size of the sound source, its directivity, and the number of resources to be considered in the model. It is not possible to use the same approach for the acoustic assessment of, e.g., traffic noise in the city, see Fig. 1, or to provide a detailed explanation of the noise propagation from the cooling unit to

the protected area near the installation, see Fig. 2. Also, a completely different approach is required for a noise source model, such as aerodynamic noise. Physical principals must be simulated there. The model simulates noise generation by solving fluid mechanics equations, which describe fluctuations of air mass, and subsequently describe sound propagation by wave equations, see [5] and [8]. This detailed access, when the sound propagation is described by wave and fluid mechanics equations or detailed measurement around the source [6] and [7], is not convenient for practical application due to the huge demands on the solution time.

A HEAT PUMP AIR/WATER PROBLEM FROM A NOISE POINT OF VIEW

The main source of air/water heat pump noise is the axial fan at the condenser section and the compressors, which are mostly installed in one compact outdoor unit. The noise generated by the unit is composed of medium and higher frequencies generated by the axial fan, which can be effectively dampened by absorption, and lower frequencies occurring at the compressor section, which are difficult to dampen. It is not necessary to invest in a less noisy unit because the fans are designed for certain conditions in terms of air flow and transport pressure only. If the load is in the form of a cover or noise suppression device, the unit can no longer overcome the pressure loss and loses functionality. It may be more advantageous to install a more powerful and noisy unit, which can withstand the intake and displacement of the additional pressure loss, to dampen the sound with absorption dampers, which are acoustically, significantly more efficient than the silent unit. The manufacturer usually reports noise from the unit without load. If the pressure drop, in the form of silencers, is added to the heat pump intake and discharge, the whole noise generation system will be re-tuned. In general, the noise generated by the unit will increase but noise components in the noise spectrum may be generated also. This means that the resulting noise must be considered with the noise component at the reference point, i.e., by 5 dB more stringent than the normal hygienic noise limits in the protected outdoor area of buildings, i.e., $L_{Aeq,8h}$ = 45 dB per day and $L_{Aeq,1h}$ = 35 dB per night, see [4]. Another difficulty in selecting a unit is often that the reported noise at a certain distance from the unit in the manufacturer's catalogue applies to the free acoustic field. However, if the unit is inserted into a wall, a corner or even a canopy, the noise may increase by 8 dB. In addition to the sound pressure level at a certain distance from the unit, it is also necessary to check the sound power level, which actually testifies to the device parameters and reliably defines its noise level. Another difference between the catalogue and real acoustic emissions of the HP could be that producers present data of the HP for nominal conditions, according to the European norms [1] and [2], which is not with the HP at full power.

DESCRIPTION OF THE SOLVED SITUATION

The solved heat pump installation is located in the interior of a residential building of a listed building in the city centre, similarly as was solved in [9]. The original design for effective acoustic modifications was an air/water heat pump installed in an inner courtyard only, in the canopy with one free side for air exchange, see Fig. 3. The heat pumps provide air conditioning for the interior of the flats, heating and air conditioning to the shop and cooling the server technology in the adjacent building. The total installed cooling power, resp. heating, is about 190 kW. There are 6 heat pump units in total. The internal space of the canopy, including the walls and the roof, is covered with mineral insulation thickness of. 60 mm + a non-woven fabric on the surface. The inside height of the canopy is approximately 3.6 m, above the upper planar unit is the height of 1.2 m of free space.

At maximum operation of all refrigeration units (6 pieces), the air flow through the fans is 60,000 m³/hour. The closest window of the living room from the free opening of the canopy is 6 m away. The noise of the cooling units, see Fig. 3, is L_{WA} = 64 dB, L_{WA} = 72 dB and L_{WA} = 79 dB for 1 unit, 1 unit and 4 units, respectively. The smallest heat pump on the left in Fig. 3 has a fan wheel vertical to the ground (a classic split unit with the exhaust on the sides). Other larger heat pumps have an axial fan wheel in the horizontal plane at the top (the exhaust at the top), the compressor is at the bottom, similar to Fig. 4. The heat pumps are installed outside the residential building, so the propagation of vibration (structural noise) from the heat pumps to the inside of the residential building was not solved. The pipeline network dilatation from the construction of the building can also be a difficult problem as well [10].

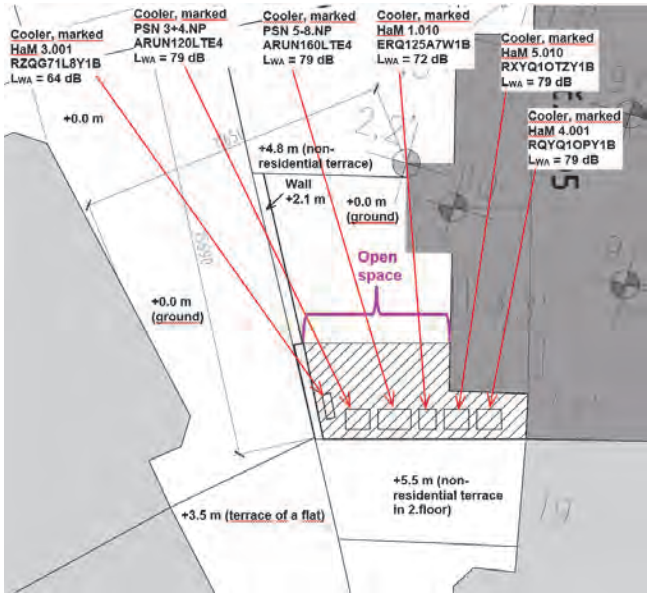

Figure 3 Situation of the heat pump installation in the assessed courtyard.

DESCRIPTION OF THE CALCULATION MODEL

The noise calculation was taken using the CADNA R software (Datakustik GmbH). It is a planar model of calculation with the base plane at the surface level of the courtyard. The area of the model was limited to the interior of the project only - the closest protected area of the building to the noise sources - the cooling unit in the courtyard shed. The computational model includes the entire courtyard and parts of the adjacent buildings, an area of 36 x 60 x 40 m (width x length x height - court-ceiling of the computing area). The boundary areas of the computational area are considered without reflection and perfectly absorbed - the space behind the boundary surfaces continues. The surface of the individual buildings - facades of the buildings, the surface of the courtyard is considered reflective – they are mainly concrete, brick and glass surfaces. The solved installation of the heat pumps is located in the courtyard of the residential building. The calculation is performed in the frequency range of 31.5 to 8000 Hz. The uncertainty of the calculation is 2 dB.

In the computational model, it is always necessary to consider how real sources of noise will be entered. If the calculation is to investigate short distances from the source, i.e., the case solved, the real noise source needs to be described in detail by alternative theoretical sources (point, area, volume), with due consideration being given to the directionality

of the noise sources. It is always necessary to check that the logarithmic sum of the sound power levels of all the theoretical noise sources is at the level of the real noise source. When simulating the sound pressure levels at a certain distance (at the calculation point) and the overall sound power level (sum of the replacement sources of noise) in the octave frequency spectrum must be checked, and not only to control the total values of the theoretical noise only. In the calculation, it can easily occur that the replacement of real sources with theoretical and tuning calculations will lead to another definition of the noise spectrum of the theoretical source, although the overall sound power level or power level in the model with the measured data from the manufacturer will be the same level.

If larger distances are resolved, real sources can be replaced by a less accurate description, i.e., only point sources that are the easiest to calculate. The more theoretical the model will try to describe the real source of noise, the more complex and the longer it will take. In assessing the noise of the above-mentioned situation in the courtyard, it was necessary to replace the real sources of noise with real sources as much as possible, see Fig 4.

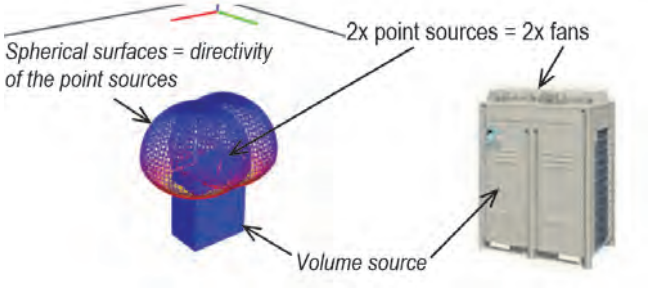

Figure 4 Comparison of the actual noise source – the actual heat pump on the right with the theoretical one on the left, used in the calculation model of the heat pump installation in the courtyard

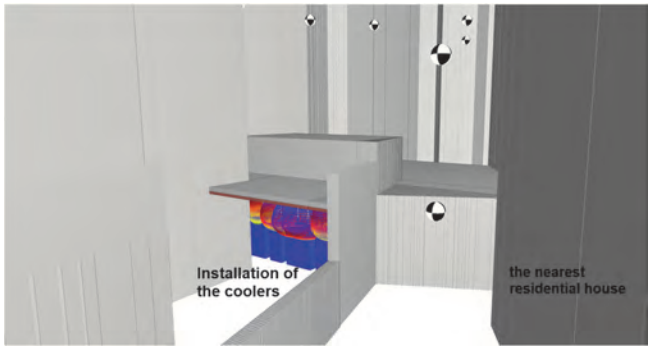

Figure 5 The 3D view of the calculation model with the installation of the HP in the canopy before the modifications

The description of the heat pump noise sources can be made as follows: The theoretical volume source replaces the basic dimensions of the HP unit, the body of the unit in which the compressor part of the cooling/heating cycle is located (the dominant area of noise emission is at low frequencies and the directionality is evenly distributed throughout). The point sources of noise replace the axial fan in the upper plane of the unit, the dominant area of radiation is in the region of the middle frequencies and it is the directional source of the noise dominant in the direction of flow, in the hemisphere direction from the upper plane of the unit. The smaller cooling/heating unit of a split-type HP with a vertical fan can only be replaced by a vertical surface source and there is no need to define the directivity also, since this unit is significantly quieter than the other heat pumps, and will not have a significant effect. Fig. 5 shows a 3D view of a computational model showing the theoretical sources of noise replacing the real heat pumps.

VALIDATION OF THE CALCULATION MODEL

Since the installation of some of the heat pumps had already been completed, it was possible to verify the correctness of the calculation model. During the noise measurement, the heat pumps of Figure 6 were in operation, the units were running at full power. Other units were out of order (they were disconnected or switched off, but were present at the installation site). The control points, i.e., MP no. 1 to 3, were selected around the installation site and adjacent objects. Table 1 shows the measured and calculated values of the A-weighted equivalent sound pressure level from the operation of the selected heat pumps.

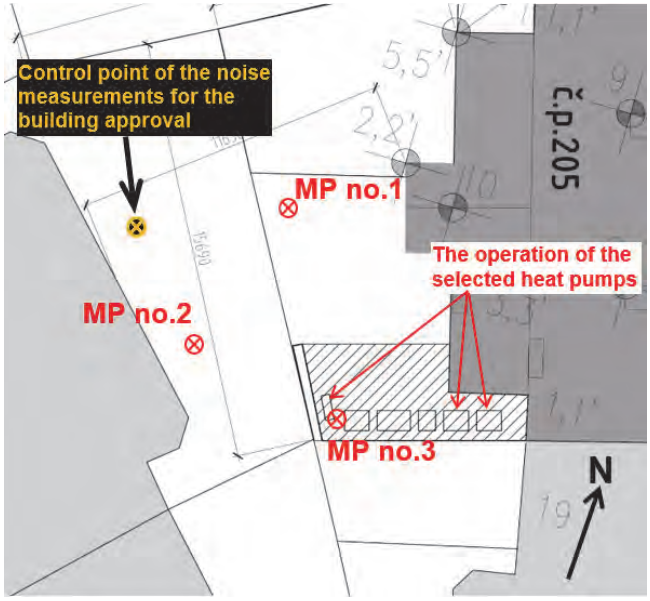

Figure 6 The noise measurement situation for verifying the computational model and control point of the noise measurements for the building approval, see the article's conclusion

Table 1 Verification of the calculation model - full power of the cooling units shown in Figure 6

Measurement point (MP)/ calculation point (CP)	Measured $L_{Aeq,T}$ (dB)	Calculated $L_{Aeq,T}$ (dB)
MP no.1 – before the installation of the heat pumps	58.6 ± 2 dB	58.8 ± 2 dB
MP no.2 – 1 m in front of the nearest residential building facade, window level 1st floor	51.0 ± 2 dB	51.9 ± 2 dB
MP no.3 – above the roof canopy of the coolers installation	51.3 ± 2 dB	50.5 ± 2 dB

The differences between the measured and calculated A-weighted equivalent sound pressure level in Table 1 are up to 0.9 dB. The justification may be that the model considers the pure courtyard space, that is, only the building construction of the facades of the buildings and any walls. The model does not take the presence of building material or scaffolding into account that was present on site during the control measurement of the noise.

RESULTS OF THE CALCULATION BEFORE ACOUSTIC ADJUSTMENTS

The sum of all the heat pumps at full power, i.e., approx. 190 kW, representing the highest daily operation of the heat pumps, generates noise at the nearest residential building (about 6 m beside the canopy, further north of MP no.2) at the level $L_{Aeq,8h}$ = 56 dB, see the noise field in Fig. 7 and 8. For the night reduced regime of the HP (operation of parts of the limited power units only, a total of about 50 kW), the noise level $L_{Aeq,1h}$ = 51 dB was calculated for the neighbouring residential object, see the noise field in Fig. 9 and 10. The hygienic noise limits of $L_{Aeq,8h}$ = 50 dB per day and $L_{Aeq,1h}$ = 40 dB for night are significantly exceeded, not to mention the possibility of the presence of a noise component in the noise spectrum.

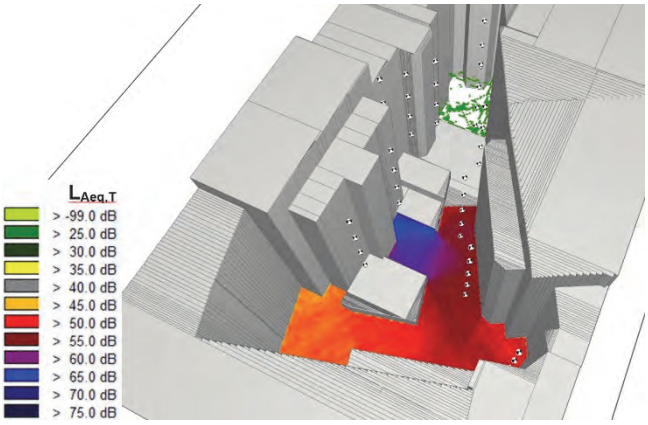

Figure 7 Noise field at 3 m above the ground before adjustments for maximum HP operation (in the daytime)

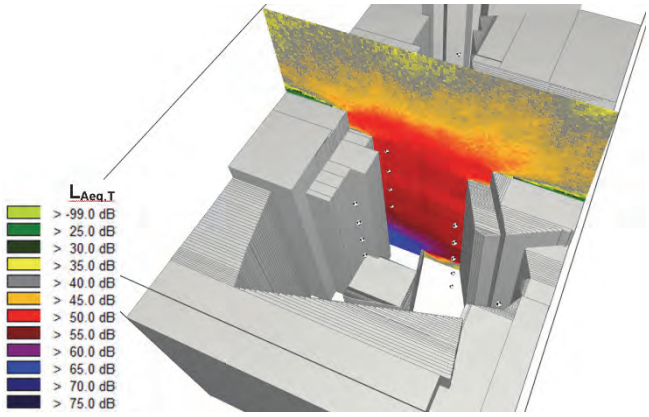

Figure 8 Noise field in the vertical plane before adjustments for maximum HP operation (in the daytime)

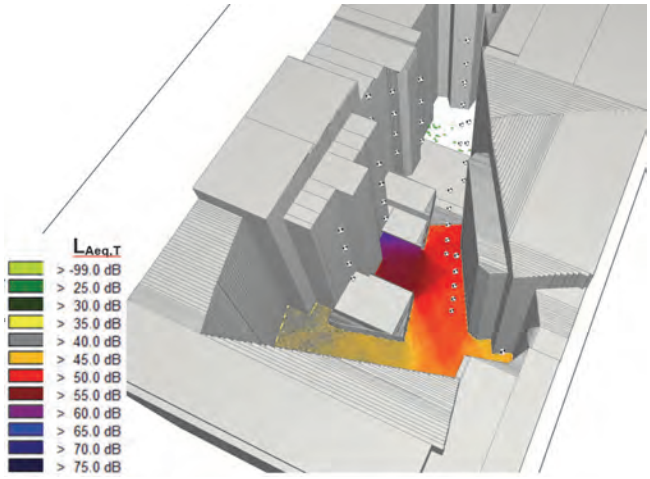

Figure 9 Noise field at 3 m above the ground before adjustments for reduced HP operation (at night)

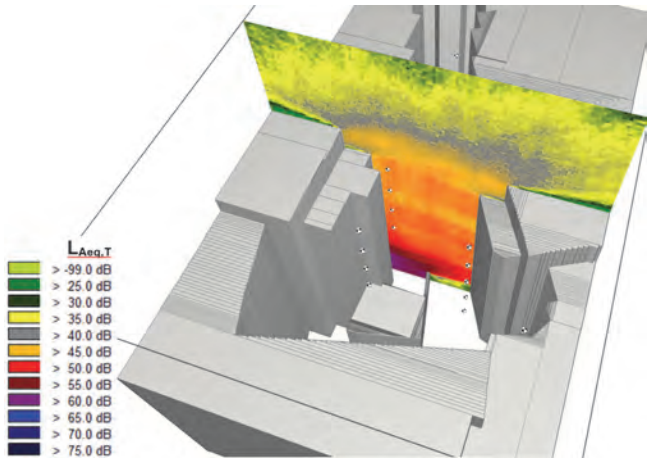

Figure 10 Noise field in the vertical plane before adjustments for reduced HP operation (at night)

PROPOSAL FOR ACOUSTIC ADJUSTMENTS AND NOISE EVALUATION

Due to the already finished work of the canopy and the location of the HP in its position, it was no longer possible to carry out larger structural modifications. The limitation was also due to the fact that the planned HP installation was a long-discussed solution with conservationists. So, the only solution was to use the free space between the heat pumps and the end of the canopy. The solution, see Fig. 11, was the horizontal distribution of the open canopy's opening to the bottom of the intake's opening and the expansive upper opening. The intake has a dimension of 4x2 m (width x height), a top exhaust port of 5x1.5 m. The holes were completely cross-sectioned with cell silencers measuring 250x500x1500 mm with a leading edge on each side, see the section in Fig. 11. The induced pressure loss at a full flow rate of 60,000 m³/h is 18 Pa and 21 Pa at the intake. An arch was created above the HP fans for a better exhalation.

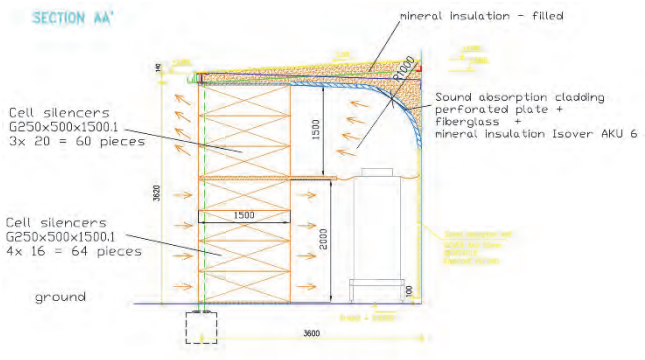

Figure 11 Section of the canopy with acoustic modifications in the form of cellular silencers.

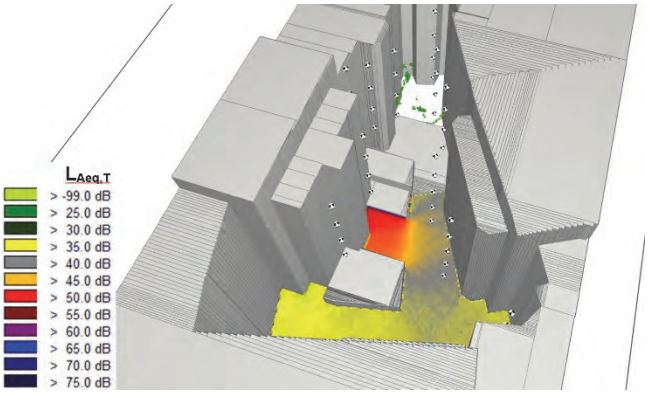

Figure 12 Noise field at 3 m above the ground after acoustic modifications, maximum HP operation (at night)

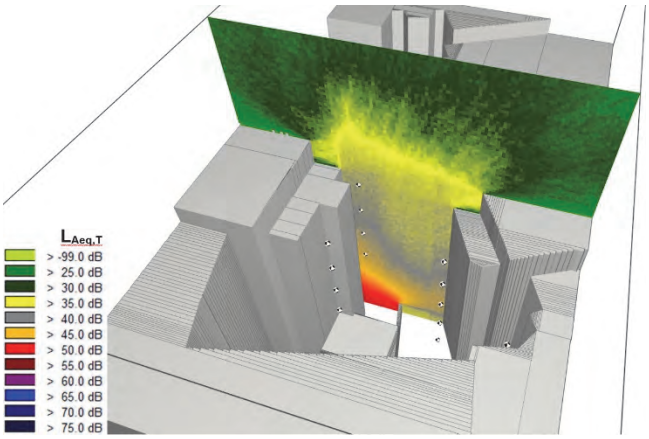

Figure 13 Noise field in the vertical plane after acoustic modifications, maximum HP operation (in the daytime)

Problems of the HP installation could arise during heating, because the freezing air generated by the fans can cool down the courtyard. But the basic solution with a canopy only (without buffers) was chosen by the builder in the early phase of the project and were discussed with heating and cooling professionals.

The calculation results for the sum of all the heat pumps at full power, i.e., approx. 190 kW, are at the level $L_{Aeq,8h}$ = 42 dB at the nearest residential building (approx. 6 m beside the canopy, further north of MP no.2), see the noise field in Fig. 12 and 13. For the night reduced mode, the noise level was calculated at $L_{Aeq,1h}$ = 33 dB in the next residential object, see noise field in Fig. 14 and 15. The hygienic noise limits of $L_{Aeq,8h}$ = 50 dB per day and $L_{Aeq,1h}$ = 40 dB for night operation are also met as well as with the assumption that the noise component of the spectrum is present.

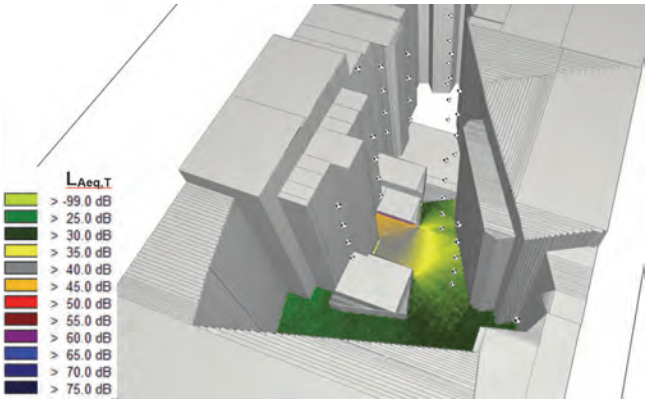

Figure 14 Noise field at 3 m above the ground after acoustic modifications, reduced HP operation (at night)

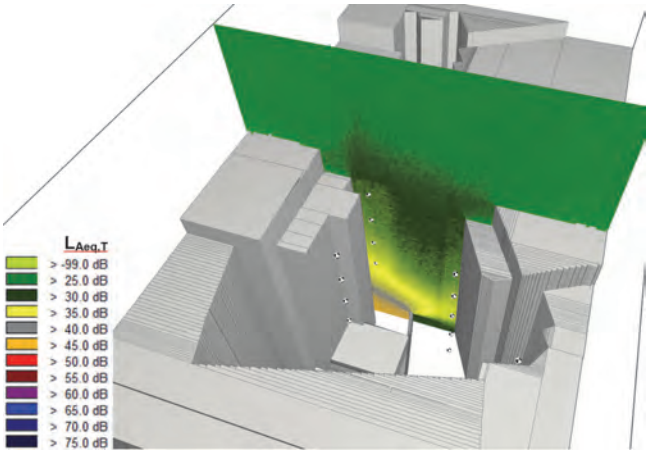

Figure 15 Noise field in the vertical plane after acoustic modifications, reduced HP operation (at night)

CONCLUSION

The results of the calculation after the acoustic protection were verified by noise measurements for the building approval at the control point approx. 6 m beside the canopy, further north of MP no.2, see Fig. 6. Table 2 shows the results of the noise measurements for the building approval and the calculated values of the A-weighted equivalent sound pressure level from the operation of the selected heat pumps.

Table 2 The results of the noise measurements for the building approval and calculated values from the day and night operation of the heat pumps, at the control point see Fig. 6.

Operation of the heat pumps	Measured $L_{Aeq,T}$ (dB)	Calculated $L_{Aeq,T}$ (dB)
DAY OPERATION – $L_{Aeq,8h}$	35.7 ± 1.8 dB	41.3 ± 2 dB
NIGHT OPERATION – $L_{Aeq,1h}$	32.5 ± 1.8 dB	33.3 ± 2 dB

The measured noise values are demonstrably in compliance with hygienic noise limits, according to [4]. For the day regime, the measured noise value is significantly lower than the calculated value, as the set daily heat pump regime for which the system is actually approved does not represent the maximum power of all the heat pumps of the daily programme. On the contrary, the measured noise value for night regime, where significantly stricter hygienic noise limits apply, corresponds to the calculated value, which is the same as the night operating conditions for the final approval and actually corresponds to the simulated mode.

ACKNOWLEDGMENT

The article was created with the support of grant SGS16/212/OHK2/3T/12 – Modelling, Management and Design of Environmental Technology Facilities and a grant from the Ministry of Education, Youth and Sports under the National Sustainability Programme I (NPU I), Project No. LO1605 – University centre for energy-efficient buildings.

We thank AKUSTPROJEKT s.r.o. for their cooperation and providing the results of the calculation and the measurements guidance.

REFERENCES

[1] ČSN EN 14 511-3: Air conditioners, liquid chilling packages and heat pumps with electrically driven compressors for space heating and cooling - Part 3: Test methods. April 2004.

[2] ČSN EN 12102: Air conditioners, liquid chilling packages, heat pumps and dehumidifiers with electrically driven compressors for space heating and cooling - Measurement of airborne noise - Determination of the sound power level. April 2014.

[3] KRÁLÍČEK, J., KRÁLÍČEK, J. Jr. Database of orders for acoustic studies and reviews of AKUSTPROJEKT s.r.o., 2016.

[4] Government Regulation No. 272/2011 Coll. on health protection from adverse effects of noise and vibrations - amendment: 217/2016 Sb., available from 30. 7. 2016.

[5] KRÁLÍČEK, J., KUČERA, M. Aerodynamic noise of blade grill HVAC systems at low Mach numbers. In: The 24th International Congress on Sound and Vibration, London, 2017. ISSN 2329-3675. ISBN 978-1-906913-27-4

[6] KRÁLÍČEK, J., KUČERA, M. Aerodynamic Noise of Blade Grill vs. Round Cylinder. Journal of Heating, Ventilating and Sanitary Installation. 2016. Vol. 25, Issue 5, pp. 268 – 273. ISSN 1210-1389.

[7] KRÁLÍČEK, J., KUČERA, M. Aerodynamic Noise of Blade Grill. Journal of Heating, Ventilating and Sanitary Installation. 2015. Vol. 24, Issue 3, pp. 118 – 123. ISSN 1210-1389.

[8] KRÁLÍČEK, J., KUČERA, M. Simulation of aerodynamic noise of blade and cylinder, Conference col-lection IBPSA, ISBN 978-80-270-0772-1, Brno. 2016.

[9] KUČERA, M. Reducing of Noise from Sources of Heat and Propagation of Sound. Journal of Heating, Ventilating and Sanitary Installation. 2016. Vol. 25, Issue 4, pp. 198 – 201. ISSN 1210-1389.

[10] VAVŘIČKA, R. Thermal Stress and Noise Aspects of the Pipeline Networks Operation. Journal of Heating, Ventilating and Sanitary Installation. 2016. Vol. 25, Issue 4, pp. 212 – 216. ISSN 1210-1389.

NOMENCLATURE

$L_{Aeq,T}$ A-weighted equivalent sound pressure level [dB]

Ing. Michal BROUM[1)]
doc. Ing. Tomáš MATUŠKA, Ph.D.[2)]
Ing. Jan SEDLÁŘ[2)]
Ing. Bořivoj ŠOUREK Ph.D.[2)]

[1)] Regulus s.r.o.
[2)] CTU in Prague, University Centre for Energy Efficient Buildings

PV and heat pump system with a seasonal storage for nearly zero energy building

FV systém s tepelným čerpadlem a sezónní akumulací pro téměř nulovou budovu

The energy system consisting of a combined ground-air source heat pump, PV system and seasonal ground storage unit for an energy passive family house has been developed and analysed by computer simulation. The heat pump, during summer operation, transforms the ambient heat to charge the seasonal ground storage with the use of PV electricity only. Winter operation relies on the heat stored under the house and results in low grid electricity consumption. The simulation analysis has shown the significant decrease in the use of the grid electricity needed for the house (the system's SPF increased from 3.1 for the reference borehole system to about 6.0) and an increase in usability of the local PV electricity production for energy supply (space heating, hot water) in the house. In total, more than 80 % of the energy supply for the house is renewable energy and the specific non-renewable primary energy needs of the house is under 17 kWh·m^{-2}·a^{-1} (for space heating, hot water and auxiliary energy).

Keywords: heat pump, seasonal storage, PV coupled operation

Pro energeticky pasivní rodinný dům byl vyvinut a počítačovou simulací analyzován energetický systém sestávající z kombinovaného tepelného čerpadla odebírajícího teplo ze země a vzduchu, FV systému a sezónního zásobníku tepla. Tepelné čerpadlo v letním období přeměňuje energie okolního prostředí pro nabíjení zemního sezónního zásobníku s využitím elektřiny pouze z FV systému. Zimní provoz spoléhá na teplo akumulované pod domem a výsledkem je nízká spotřeba elektrické energie ze sítě. Simulační analýza ukázala významný pokles potřeby elektrické energie ze sítě (sezónní topný faktor vzrostl z hodnoty 3.1 pro referenční případ se zemním vrtem a FV systémem na hodnotu okolo 6.0) a zvýšil využití produkce FV systému pro zásobování teplem v domě. Celkem více než 80 % energetické potřeby (vytápění, příprava teplé vody, pomocná energie) je dodáváno z obnovitelné energie a měrná potřeba neobnovitelné primární energie domu je menší než 17 kWh·m^{-2}·rok^{-1}.

Klíčová slova: tepelné čerpadlo, sezónní akumulace, provoz svázaný s fotovoltaikou

INTRODUCTION

The European Directive on the Energy Performance of Buildings [1] has brought a clear vision and an opportunity to transform the building stock to nearly zero-energy buildings (NZEB). There are a number of measures to improve the energy performance of modern buildings today. The space heating demand could be minimised to the limits of the technical and economical possibilities in the case of passive houses (envelope insulation, triple glazing, ventilation heat recovery, etc.). Domestic hot water systems could use energy saving showers, insulation of hot water piping, time and temperature control of hot water circulation runs, etc. Further savings can be expected with the use of heat recovery from waste water. Electricity demand has been continuously reduced with the introduction of appliances with energy class A and better and the implementation of modern daylighting principles together with proper control of LED artificial lighting.

The logical step ahead, in order to decrease the energy use in buildings, is the application of renewable energy sources. Heat pumps use renewable energy from the ambient environment, however they also need grid electricity to valorise the renewable heat to a useful temperature level for space heating and hot water preparation. However, the grid electricity in Europe, in general, has high primary energy conversion factors [2] dependent on the share of renewables in the grid in each country. The grid electricity in the Czech Republic originates from non-renewable fuels (brown coal and nuclear power plants) which disqualifies the use of such electricity in heating applications within the framework of building certification (primary energy factor *PEF* = 3.0). The non-renewable primary energy demand, as an integral quantity, has been adopted as the basis for comparison of a building's performance. Member states approach the definition with different strategies and different promptness. To define the target of a nearly zero-energy building, 30 kWh·m^{-2}·a^{-1} has been set for the purpose of the presented study as a half value of the criterion for a passive house. Despite the fact that the calculation of the non-renewable criterion is generally based on the simple annual balance between the imported and exported energy, it is ambitious target comparable e.g., with Danish legislation [3]. However, the export of local renewable electricity production to a public grid has already become complicated in several countries (huge administration, negligible feed-in tariffs) and new installations are focused on the local use of renewable electricity from PV systems integrated into buildings. An interesting way to NZEB could lie in the reduction of grid electricity (and other energy carriers) use. Production of electricity by PV systems and use of electricity by heat pumps, therefore, seems to be an ideal combination to significantly reduce the external supply of electricity from the public grid for space heating and hot water systems [4]. Such an approach also results in the need of the realistic evaluation of the locally produced electricity used in the system.

The paper shows an analysis of a proposed energy system under development which has been motivated by the situation mentioned above. The system combines the PV system and a heat pump for a family house to achieve a high share of renewable energy for space heating and hot water, to increase the self-sufficiency and even the strict goals defined for NZEB. On the other hand, the system has to use common technology, optimised or low-cost components because economic issues cannot be put aside.

SYSTEM CONCEPT

The concept of the system being developed is based on a combination of PV technology and an advanced heat pump system to increase the use of local renewable energy for space heating and hot water preparation in the family house by use of simple and low-cost seasonal storage realised within the building's foundations. The heat pump, with a variable speed compressor, is coupled with the PV system in order to adapt the heat pump power input to the actual PV system power output in operation. The target of the system concept is to reduce the annual external grid electricity demand for the house.

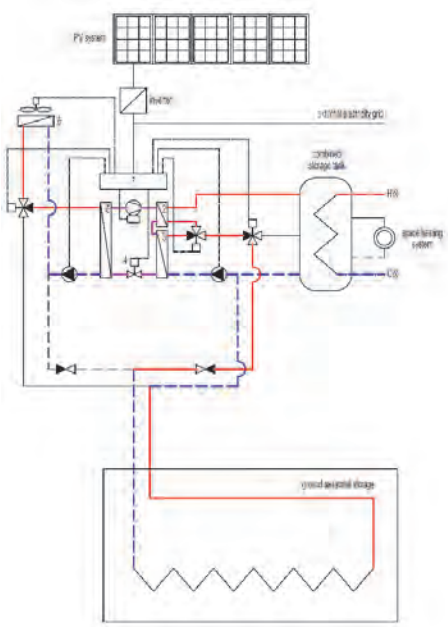

Figure 1 Diagram of the PV heat pump system concept: summer operation

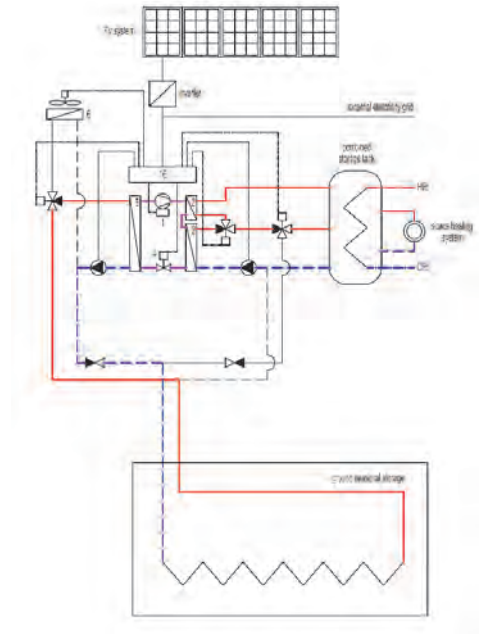

Figure 2 Diagram of the PV heat pump system concept: winter operation

The system concept and function are shown in Fig. 1 and Fig. 2 with the main components used but without respecting the heat transfer liquid here. The heat pump consists of an evaporator (5), a variable speed compressor (1), a condenser (3) with a separate desuperheater (2) to increase the usability of the rejected heat and to increase the total effectivity, an electronic expansion valve (4) and an integrated controller (7). The power input of the heat pump compressor could be controlled by an advanced algorithm using external information about the actual electric power of the local PV system. The integrated controller uses a mathematical description of the heat pump operation parameters and, according to actual conditions, predicts the power input of the heat pump and causes a change in compressor rotations.

A ground seasonal storage realised within the foundations under the house is an important component of the whole system. The heat pump, in the case of sufficient PV power production in summer season, adapts its power input to the PV system power and extracts heat from the ambient air by a heat exchanger / air cooler (6) and rejects it to the building for hot water production with a higher set-point in the combined storage tank (overcharges the volume of the storage tank) or to a ground seasonal heat storage, or the heat from the condenser can be stored in the ground at low condensation temperature 25 to 40 °C while heat from the desuperheater is used for hot water preparation at a temperature level of 50 to 60 °C in the top part of water storage tank (hot water zone). Such a function of the PV heat pump system could be achieved without any grid electricity input (see Fig. 1).

If the building demands the heat, but the PV system power has decreased under threshold electric power, i.e., during winter time or at night, the electric demand for the heat pump system operation is automatically covered from the grid. Then, the heat pump extracts the heat stored in the ground seasonal storage at a higher temperature (10 to 35 °C) than the ambient air temperature or conventional ground borehole and, thus, the system operates with a higher efficiency (see Fig. 2). This could reduce the grid electricity use and simultaneously increase the usability of the available PV system production over the whole year.

Compared to the conventional solution based on the heat pump system with a ground borehole and parallel PV system, the proposed system utilises several innovative components and provides a number of advantages:

- use of a desuperheater for hot water preparation at high temperatures without an increase of compressor electricity use – an increase in heat pump operation effectiveness;
- a combined water storage tank for hot water preparation and space heating with an optimised internal heat exchanger surface area distribution for hot water production – a larger part of the surface area located in the hot water zone reduces the required temperature difference between the water tank volume and the hot water output which causes the high effectivity of the heat pump operation, even for hot water preparation;
- use of excess renewable electricity from the PV system for the heat pump to charge the combined storage tank to a higher temperature than the required set-point and, thus, increasing its storage capacity to overcome the hot water load peaks – a significant increase of hot water demand coverage by renewable energy during the summer;
- use of excess renewable electricity for charging the ground seasonal storage – reduction of grid electricity use by the heat pump in winter season by the use of stored heat;
- the possibility to control the heat pump electric power according to the actual power output of the PV system (power adaptation) –

operation of the heat pump system without external grid electricity use during a significant part of the year.

FAMILY HOUSE

The energy efficient family house under construction (2016-2017) has been chosen for the analysis of the proposed PV heat pump system in the climate of the Czech Republic (see Fig. 3). The family house has two floors with a space volume of 935 m^3 and a total living floor area 190 m^2. The family house was designed in a passive house concept, the *U*-values of the individual envelope constructions meet the recommended values for such high-performance buildings. The foundations have been realised by a sacrificial formwork insulated by extruded polystyrene with a thickness of 160 mm. The base floor has been assembled from concrete slabs, the upper insulation has been realised from extruded polystyrene with a thickness of 240 mm and a floor heating system layer. The envelope brick system is based on cellular clay blocks filled with insulation and an external mineral insulation system with a thickness of 180 mm. The saddle roof has a slope of 40° with south-north orientation and the roof thermal insulation layer thickness is 240 mm.

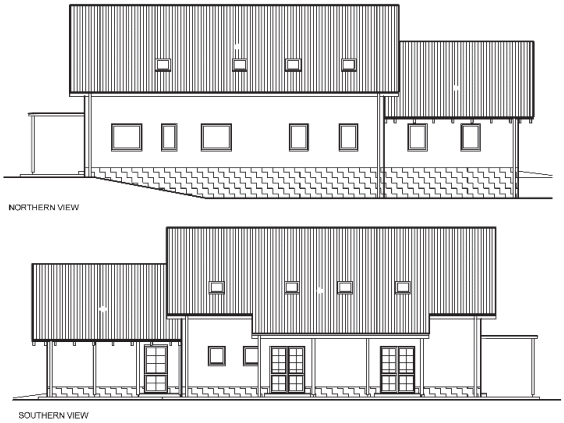

Figure 3 Family house used for the PV heat pump system analysis

The designed heat loss of the family house is 4.5 kW for ambient air temperature -15 °C. The low temperature floor space heating system has been used with design flow/return water temperatures 40/35 °C, respectively. Ventilation is provided by an air handling unit with a maximum flowrate of 275 $m^3 \cdot h^{-1}$ using heat recovery. The proposed system consists of an advanced heat pump with a heat output of 5.5 kW at B0/W35 (50 Hz) and a combined storage tank of volume 900 l with an internal heat exchanger with a surface area 9 m^2. The investor considered the large PV system installation with a peak power of 6 kW_p to increase the energy independency of the house operation.

During the construction stage, the ground seasonal storage has been realised with the use of a pipe heat exchanger (see Fig. 4) with a size of 14.4 m x 8.0 m within the foundations of the house, which are 1.5 m deep and thermally insulated on the external surface. The internal perimeter of the ground storage volume is also thermally insulated, but only to a depth of 0.5 m in order to eliminate thermal bridges from the charged storage to the interior through the envelope and foundations (see Fig. 4). The heat exchanger is made from plastic piping DN32 buried in the 300 mm deep trenches filled with cement and silicate sand mixture to provide a good thermal contact between the pipe and the ground. The distance between the pipes in the heat exchanger is 0.6 m. The heat exchanger has been realised in two loops, each 100 m in length. Two loops have been designed to reduce the auxiliary demand of the circulation pumps. Redundant thermal insulation with a thickness of 100 mm has been applied between the seasonal storage volume and the concrete floor slabs.

Figure 4 Realisation of a simple and a low-cost ground seasonal storage unit

SIMULATION ANALYSIS

The computer simulation analysis of the proposed PV and heat pump system has been undertaken in the TRNSYS environment [5]. The objective of the analysis was to prove the functionality of the system concept and to compare the performance with the conventional PV and heat pump system. To model the components of the system, both the available TRNSYS models and our own specifically developed TRNSYS models have been used [6-8]. The computer simulations have been completed with a time step of 2 minutes and two years of operation has always been simulated because of the ground massif use in both the proposed and conventional heat pump system. The results have been evaluated from the second year of the simulation. The properties of the ground massif have been defined: thermal conductivity of 2 $W \cdot m^{-1} \cdot K^{-1}$, density of 2100 $kg \cdot m^{-3}$ and specific capacity of 840 $J \cdot kg^{-1} \cdot K^{-1}$.

The building model has been built in TRNSYS based on the construction plans and used for separate simulations of space heating load to reduce the calculation time. The results for the space heating and hot water load have been used as inputs for the system simulations. The space heating demand is 3400 $kWh \cdot a^{-1}$ and the hot water demand is 3060 $kWh \cdot a^{-1}$.

RESULTS

A conventional ground source heat pump system with a borehole heat exchanger (75 m), a standard combined water storage tank (900 l) and a PV system (6 kW_p) has been modelled for the given house as a reference case. The total grid electricity use of the conventional system is 2061 $kWh \cdot a^{-1}$ and the system operates with a seasonal performance factor *SPF* = 3.1. The monthly values of the *SPF* range are around this value (see Fig. 7). The main reason of the low operation effectiveness for the conventional reference case is the large share of hot water heat demand in general combined with the necessity of charging the hot water zone in the storage tank to a temperature of 55 °C to eliminate the operation of the electric back-up heater. Despite the high installed power of the PV system, there is high electricity use and low utilisation of the produced PV electricity with the heat pump system. The reason is the mismatch between the hot water peak loads (morning, evening), space heating peak loads (winter season, night time) and PV electricity

production (summer season, daytime), see Fig. 5. The PV system annually covers 420 kWh from a total 2620 kWh system electricity demand only, despite the installed 6 kW_p power produces about 6020 $kWh \cdot a^{-1}$ of electricity.

The proposed system has been modelled with an advanced heat pump with a desuperheater and a variable speed compressor for adaptation of the power input to the PV system power production combined with a seasonal ground storage of ambient heat extracted by an air cooler in the summer and used as a source for the heat pump in the winter. The total grid electricity use (heat pump, circulation pumps, back-up heater, ambient air cooler minus the PV electricity used) is 1078 $kWh \cdot a^{-1}$ and the system operates with a seasonal performance factor of *SPF* = 6.0. Fig. 6 shows the energy balance of the whole system. It has been shown that very low grid electricity use resulted in the period of year outside the heating season. The monthly system seasonal performance factors reached the values far above 10 from spring to autumn. However, the monthly values of *SPF* ranges between 3.5 and 4.7 (see Fig. 7) even within the most severe months in the heating season due to favourable temperature conditions in the ground storage (see Fig. 8). Fig. 9 shows the process of charging and discharging of the ground storage under the house in the course of year (second year of simulation).

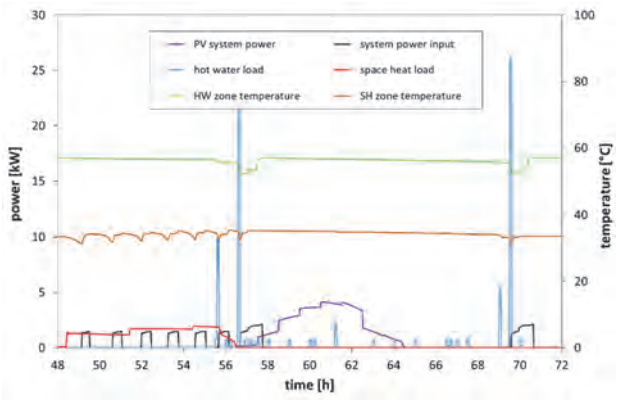

Figure 5 Detailed comparison of the production and load profile of the PV heat pump system in winter for the conventional system

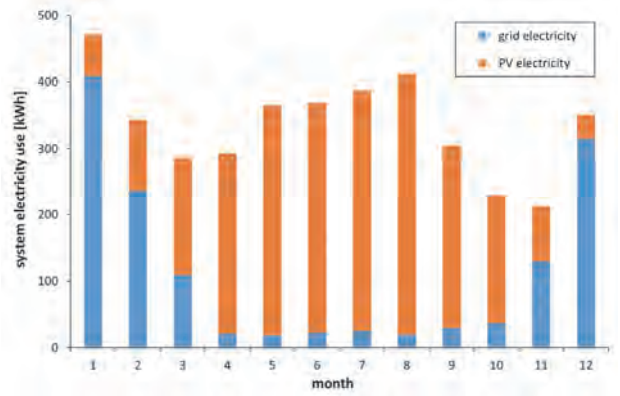

Figure 6 Electricity balance of the proposed PV heat pump system

The results have shown that the proposed system uses 83 % of renewable energy for space heating, hot water preparation and auxiliary consumption (parasitic system energy). If a strict non-renewable primary energy factor value of 3.0 for electricity is applied, the specific primary energy demand for space heating, hot water and auxiliary energy will be around 17 $kWh \cdot m^{-2} \cdot a^{-1}$. This is, finally, almost half of the original focused target. Moreover, this value results from the real balance of energy utilisation, not from a fictive annual balance of the PV electricity export to the external electric grid.

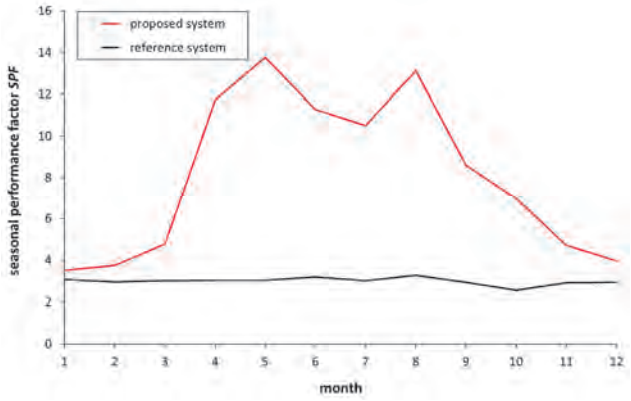

Figure 7 Comparison of the monthly seasonal performance factors for the reference and proposed system

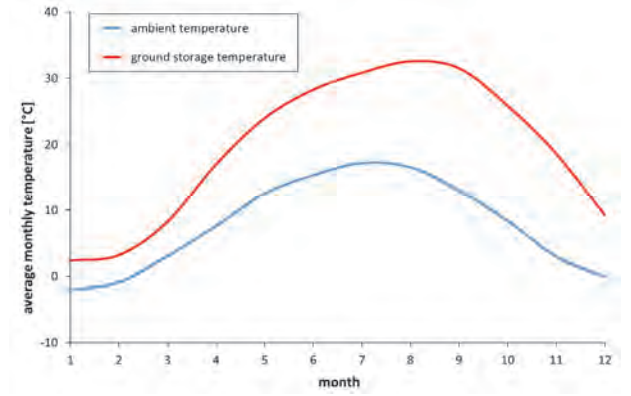

Figure 8 Development of the temperature in the seasonal ground storage

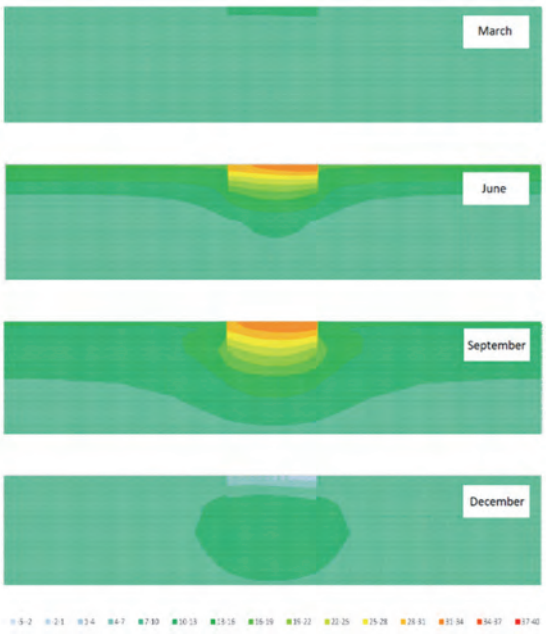

Figure 9 Charging and discharging of the ground storage during the year

CONCLUSION

The energy system consisting of a combined ground-air source heat pump, a PV system and a seasonal ground storage unit for an energy passive family house has been presented and analysed by computer simulation in TRNSYS. The simulation analysis has shown a significant decrease of the grid electricity needs for the house (the system's *SPF* increased from 2.9 for the reference borehole system to 6.0) and an increase in usability of the local PV electricity production for energy supply (space heating, hot water) in the house. In total, 83 % of the energy supply for the house is renewable energy and the specific non-renewable primary energy need of the house is lower than 20 $kWh \cdot m^{-2} \cdot a^{-1}$ (for space heating, hot water and auxiliary energy). This is in line with the strict criteria for nearly zero-energy buildings.

ACKNOWLEDGMENT

The analysis has been supported by the Technology Agency of the Czech Republic in the framework of the research project TA04021243 Sustainable energy source for nearly zero-energy buildings.

REFERENCES

[1] Directive 2010/31/EC (EPBD), of European Parliament and of the Council of 19 May 2010 on the energy performance of buildings (recast).

[2] MOLENBROEK, E., STRICKER, E., BOERMANS, T. 2011. Primary energy factors for electricity in buildings. Toward a flexible electricity supply. Ecofys.

[3] Nearly zero energy buildings definitions across the Europe. 2015. Buildings Performance Institute Europe (BPIE).

[4] International Energy Agency. 2014. Task 44/Annex 38 - Solar and Heat Pump Systems SHC Position Paper.

[5] Transient System Simulation Tool - TRNSYS 17.1. 2014. The University of Wisconsin, Madison, http://sel.me.wisc.edu/trnsys.

[6] SEDLAR, J. 2016. Type 260 – Variable speed ground source heat pump with desuperheater and subcooler. UCEEB, Czech Technical University.

[7] DRUCK, H. 2006. Multiport Store Model Type 340 - Stratified fluid storage tank with four internal heat exchangers, ten connections for direct charge and discharge and an internal electrical heater, version 1.99F. ITW Universität Stuttgart.

[8] WETTER, M., HUBER, A. 1997. Type 451 – Vertical Borehole Heat Exchanger, version 2.4, ZTL Lucerne

Ing. Jan SEDLÁŘ
CTU in Prague,
University Centre for Energy Efficient Buildings

Heat Pump for Water Preparation in a Block of Flats

Příprava teplé vody v bytovém domě tepelným čerpadlem

Recent trends in building construction in central Europe show a growing number of well insulated residential buildings. The heat demand for domestic hot water preparation is, in those applications, similar or higher than for space heating. Regular vapour-compression heat pumps reach a relatively low SPF 2.5 in such applications. The way to increase SPF is to use a heat pump with multiple heat exchangers on the high-pressure side (desuperheater, condenser, and subcooler) and a special hot water storage tank with three internal heat exchangers for good temperature stratification. A prototype of a heat pump with a desuperheater and subcooler was developed and a mathematical model of a refrigerant cycle was tested on it. The model of the heat pump describes the heating capacity and power input with an average relative deviation lower than 5 %. The validated model was used in simulations of a system for hot water preparation in a block of flats. The water draw in the simulation was set under the European standard and measured data from real applications. The results of simulations show SPF improvement by 26 % for a heat pump with a desuperheater and subcooler in comparison with a standard heat pump.

Keywords: subcooler; desuperheater; domestic hot water

Poslední trendy při výstavbě budov ve střední Evropě ukazují zvyšující se počet dobře zateplených budov. Potřeba tepla na přípravu teplé vody je podobná nebo může být i vyšší než pro vytápění. Klasická tepelná čerpadla se základním jednostupňovým parním cyklem dosahují při přípravě teplé vody relativně nízkého SPF 2.5. Jednou z možností zvýšení SPF je použití více výměníků tepla na vysokotlaké straně (kondenzátor + chladič par + dochlazovač) a upraveného zásobníku teplé vody pro dobrou teplotní stratifikaci. Pro určení potenciálního přínosu zmíněného uspořádání byl vyvinut prototyp a matematický model tepelného čerpadla s chladičem par a dochlazovačem. Model dokázal popsat chování tepelného čerpadla s průměrnou odchylkou 5 %. Validovaný model byl pak použit v simulacích systému pro přípravu teplé vody v bytovém domě. Výsledky simulací ukazují zlepšení SPF až o 26 % pro tepelné čerpadlo s chladičem par a dochlazovačem v porovnání se standardním zapojením.

Klíčová slova: chladič par, dochlazovač, teplá voda

INTRODUCTION

Heat pumps offer the possibility to substitute traditional heat sources like gas heaters, oil boilers, etc. and to reduce the primary energy consumption. The heat pump market shows growth in a number of installed units over the last three years [1]. With an increasing number of well-insulated buildings in central Europe brings a growing share of heat for hot water preparation in the total energy consumption of a building. The average energy consumption of space heating per m^2 is less than 70 % of its value from 1990 [2]. The energy demand for space heating is almost identical to water heating. A bigger portion of domestic hot water (DHW) in the total energy consumption of a household creates a demand for an increase in the energy efficiency of heat pumps in such applications. Heat pumps designed for DHW applications are measured under the standard EN 15147 [3]. The measured coefficient of performance (*COP*) [-] of a heat pump with a tapping profile can be recalculated into the energy efficiency of the hot water preparation and can be compared with other types of water heaters.

The portion of energy for water heating in the total energy consumption in a block of flats might be greater than for space heating due to the building envelope which is usually well insulated. The energy needed for water heating is higher than that in family house applications for the same water draw due to heat losses in the distribution system. In some applications, heat losses in distribution are comparable with the heat demand.

A typical block of flats in the Czech Republic is connected to a district heating system from a central gas boiler room or a heating plant. Energy savings over the last 15 years lowered energy consumption and made district heating systems less efficient. The maintenance and operational costs of the system did not change and the downswing in traded heat forced district heating providers to raise the price of heat [4]. This action is forcing the transformation from district to local heating systems and sometimes to systems with heat pumps in the long term.

This paper discusses the possibility of increasing the efficiency of the system with a heat pump (HP) in a block of flats application for water heating. The paper is based on an efficiency measurement of an air source HP in five blocks of flats construction over a one-year period. The paper includes a basic HP with a desuperheater and a subcooler model and its validation. The verified model of the HP was used in the TRNSYS [5] simulation software with a model of the DHW preparation.

THE MATHEMATICAL MODEL OF THE HEAT PUMP

To estimate the heat capacity and a power input of a brine/water source heat pump, a mathematical model of the heat pump (HPM) was developed. The HPM is comprised of compressor, condenser, evaporator, desuperheater and subcooler models. The model of the expansion valve is not included because the process in the expansion valve is considered adiabatic, which is valid for direct expansion evaporators [6]. Other devices and pipes in the refrigeration cycle are just considered as negligible pressure losses and are not taken into account in the model. The thermodynamic properties of a refrigerant are enumerated by Peng-Robinson equation of state [7]. The model is

simplified in general so that its parameters can be derived from the manufacturer's data sheets for each component.

Model assumptions

The model should approximate the performance of the HP prior to its construction. The only available data comes from the data sheets of the components, therefore, the model has to neglect any minor technical characteristics of the components. The list of assumptions and simplifications is here:

- a heat transfer area A [m^3] and an overall heat transfer coefficient U [W·m^{-2}·K^{-1}] value of each heat exchanger (HX) are stable and constant
- a stable superheat in the evaporator
- a stable subcooling in the condenser
- pressure losses are negligible
- there are no heat losses from the refrigerant cycle
- expansion in the expansion valve is adiabatic
- oil does not influence the refrigerant cycle and heat transfer

The assumption of a stable UA value in each HX is problematic. The UA value varies with flow rates, temperatures and other properties on both the refrigerant and water/brine side of the HX. However, a small change does not significantly influence the overall results. More complex model would make the simulation slower.

The stable superheat of the refrigerant in steady state conditions can be achieved by an electronic expansion valve in case of the superheat in the evaporator is higher than the minimal stable superheat [9]. The subcooling in the condenser is given by the refrigerant charge and in the case that refrigerant collector is situated between the condenser and expansion valve. Pressure losses influence the precision of the modelling [6]. However, it is difficult to estimate them without knowledge of the piping in the refrigerant cycle and the internal geometry of the HX. Heat losses can be neglected with insulated devices, especially when the compressor is insulated.

Model of the compressor

A simplified model of the real compressor is derived from the theory of piston compressors. It describes the mass flow of the refrigerant and the power input of the compressor in every working condition and can be derived from the manufacturer's data sheet. The refrigerant mass flow rate m_{ref} [kg·s^{-1}] is described as follows:

$$m_{ref} = V_{sw} \lambda_v \rho_{ref,s} n \quad [\text{kg·s}^{-1}] \tag{1}$$

In the above equation, V_{sw} is the swept volume of compressor [m^3], $\rho_{ref,s}$ is the refrigerant density [kg·m^{-3}] at the compressor suction, λ_v is the volumetric efficiency [-] and n is the compressor rotational speed [s^{-1}]. The swept volume V_{sw} is provided by the manufacturer of the compressor. The rotational speed n is given by the local electric network frequency. λ_v is changing with the different pressure and temperature state of the refrigerant in the suction and discharge of the compressor. It depends on the pressure ratio. In foregone applications of vastly used piston compressors, the volumetric efficiency was a function of the clearance volume when the piston was at top dead centre. Today's mostly used compressors in heat pumps applications are without the mentioned issue, λ_v is close to 1 and can be described as follows:

$$\lambda_v = 1 - C(\sigma - 1) \quad [-] \tag{2}$$

In the above equation, σ is the pressure ratio [-] and C is a constant [-]. The isentropic efficiency η_{ie} [-] describes the compressor's efficiency energy. The real compression process can be defined as polytropic with a varying exponent of compression. A simplified description of the real compression is undertaken through the difference between real and isentropic compression. η_{ie} in the model is described as follows [9]:

$$\eta_{ie} = D_1 + D_2\varphi + D_3\varphi^2 + D_4\varphi^3 + D_5 p_{con} \quad [-] \tag{3}$$

$$\varphi = \sigma^{1/n_{pol}} \quad [-] \tag{4}$$

In the above equation, p_{con} is the condensing pressure [Pa], D_1 [-] to D_4 [-] and D_5 [Pa^{-1}] are constants [-] for the parametrisation, and is defined in Equation (4), where n_{pol} is the average exponent of the isentropic compression [-]. The model of the compressor calculates the pressure ratio, the isentropic and volumetric efficiency according to the pressure at the suction and discharge.

Model of the heat exchangers

The model of the HX calculates the heat exchange rates from the calorimetric equations and the heat transfer equation. For steady state conditions, the heat flows of liquid on both sides are equal to the heat flow transferred through the working surface. It can be described as follows:

$$Q_{hx,1} = m_{ref}\, abs\left(h_{ref,in} - h_{ref,out}\right) \quad [\text{W}] \tag{5}$$

$$Q_{hx,2} = m_{liq} c_{p,liq}\, abs\left(t_{liq,out} - t_{liq,in}\right) \quad [\text{W}] \tag{6}$$

$$Q_{hx,3} = UA\delta_{\ln} \quad [\text{W}] \tag{7}$$

In the above equations, $Q_{hx,1}$, $Q_{hx,2}$ and $Q_{hx,3}$ are the heat exchange rates [W] on the refrigerant side, the secondary side and the heat transfer through the heat exchanger surface area rate, respectively. $h_{ref,in}$ and $h_{ref,out}$ are specific enthalpies [J·kg^{-1}] of the refrigerant at the inlet and outlet of the section, $c_{p,liq}$ is the specific capacity [J·kg^{-1}·K^{-1}] of the secondary liquid, m_{liq} is the mass flow rate [kg·s^{-1}] of the secondary liquid, $t_{lig,in}$ and $t_{liq,out}$ are the temperatures [°C] of the secondary side liquid at the inlet and outlet of the section, δ_{ln} is the logarithmic mean temperature difference [K]. The value of UA [W·K^{-1}] can be found in the data sheets of the HX. The heat pump model consists of four HX – condenser, evaporator, desuperheater, and subcooler. The heat exchangers are modelled in sections in accordance with the expected phase condition on each side:

- an evaporator - two sections,
- a condenser - two or three sections,
- a desuperheater - one or two sections,
- a subcooler - one section.

The operating parameters of the heat pump

Every heat pump works with some refrigerant. The thermodynamic properties are calculated with a mathematical model of the refrigerant in every time step. The type of refrigerant is given at the beginning of the simulation and does not change, therefore, it is the first parameter. Other parameters are set at the beginning of the simulation are:

- the superheating temperature difference in the evaporator,
- the subcooling temperature difference in the condenser,
- superheating in the compressor suction piping,
- the pressure loss in the compressor suction,
- the operating envelope of the compressor.

The operating envelope is necessary for system simulations. It limits the compressor working conditions. The model checks the maximum

and minimum operational pressure, the pressure ratio and the outlet temperature of the refrigerant. If the limited boundary is crossed, the model responds accordingly (e.g., when the temperature at the compressor discharge is over the maximum temperature model, the compressor turns off).

Cycle convergence algorithm

A special algorithm was developed in order to solve the HP model with three successive HXs on the high-pressure side of the refrigerant cycle. The algorithm can be divided into two parts. The first part searches for the optimal condensing temperature t_{con}, the evaporating temperature t_{ev}, the specific enthalpy at the outlet of the desuperheater $h_{des,out}$ and the temperature of the refrigerant at the outlet of the subcooler $t_{s,out}$ in sequential order to find a balance of energy between Eq. 5, 6 and 7 for every used HX. The second part calculates the model of the refrigerant system and the HX.

MODEL VALIDATION

The model of the heat pump was tested on a heat pump prototype. The schematic of the refrigerant cycle and test bench is shown in Fig. 1. The prototype contains a scroll compressor, a brazed plate HX and an electronic expansion valve. The list of the main components and properties for the model validation is shown in Table 1. The prototype also contains the superheater which was implemented solely for testing and it is not included in the validation. The prototype works with refrigerant R410A.

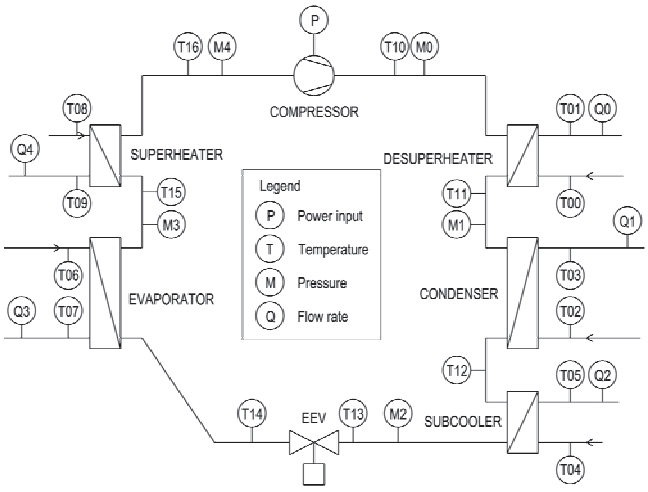

Figure 1 Diagram of the tested heat pump and measured values

Table 1 List of components used in the tested prototype

Component		Value	Unit
Scroll compressor	V_{sw}	21.7	cm^3
	C	$2.22 \cdot 10^{-2}$	-
	D_1	$-2.31 \cdot 10^{-2}$	-
	D_2	$8.31 \cdot 10^{-1}$	-
	D_3	$-2.48 \cdot 10^{-1}$	-
	D_4	$2.22 \cdot 10^{-2}$	-
	D_5	$1.36 \cdot 10^{-8}$	Pa^{-1}
Evaporator	UA_{con}	1494	$W \cdot K^{-1}$
Condenser	UA_{ev}	1306	$W \cdot K^{-1}$
Desuperheater	UA_{des}	100	$W \cdot K^{-1}$
Subcooler	UA_{sub}	300	$W \cdot K^{-1}$

The prototype was measured in various working conditions. The superheating controlled by the expansion valve was set at 4 K. The average subcooling in the condenser was 2 K. The results of the model validation are shown in Table 2 and in Fig. 2, 3, 4 and 5. $Q_{heat,total}$ is the total heat transfer on the high-pressure side of the HP. The average error of the *COP* is less than 5 % of its value. The model fits the measured data with good accuracy.

Table 2 List of errors of the model from the measured data

Working arrangement (on the high-pressure side)	*P* (%)		$Q_{heat,total}$ (%)		*COP* (%)	
	Avg.	Max.	Avg.	Max.	Avg.	Max.
Condenser	3.1	8.2	3.0	8.2	4.1	8.2
Condenser, desuperheater	4.0	10.2	3.7	10.0	4.2	9.6
Condenser, subcooler	5.6	10.0	5.3	8.9	1.2	4.0
Condenser, desuperheater, subcooler	4.3	10.4	5.3	10.0	1.8	3.8

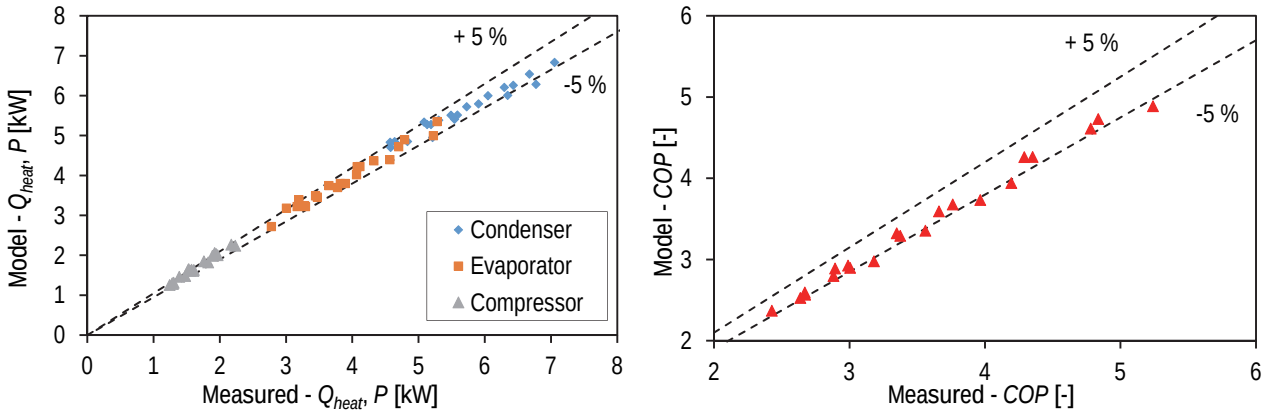

Figure 2 The deviation between the model and the measured data for the heating capacity, the power input (on the left) and the COP (on the right) in a condenser arrangement

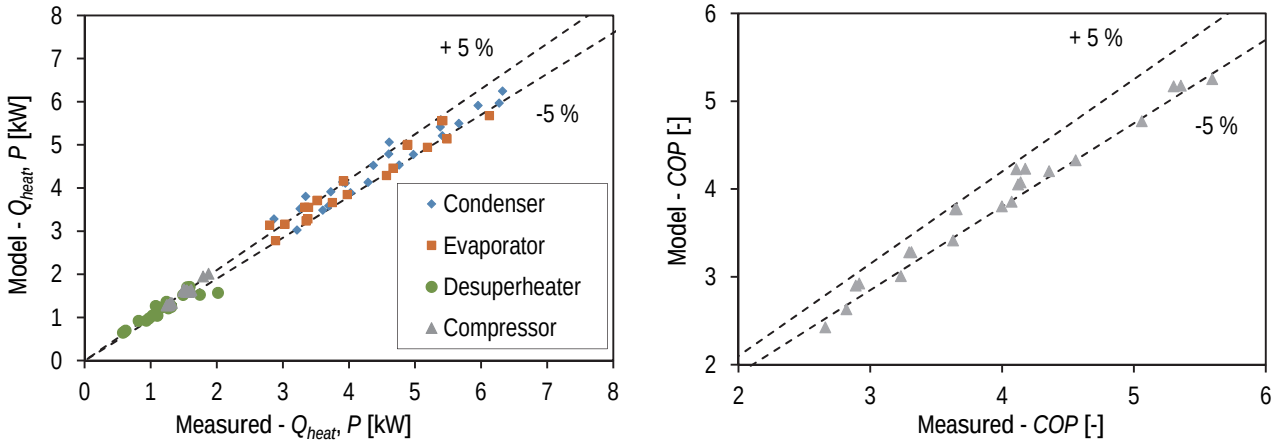

Figure 3 The deviation between the model and the measured data for the heating capacity, the power input (on the left) and the COP (on the right) in a condenser + desuperheater arrangement

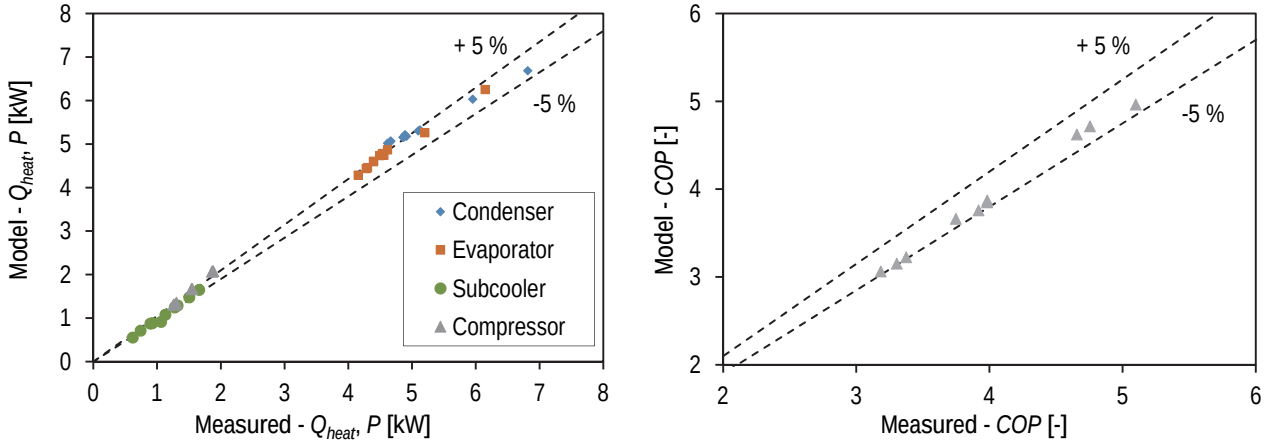

Figure 4 The deviation between the model and the measured data for the heating capacity, the power input (on the left) and the COP (on the right) in a condenser + subcooler arrangement

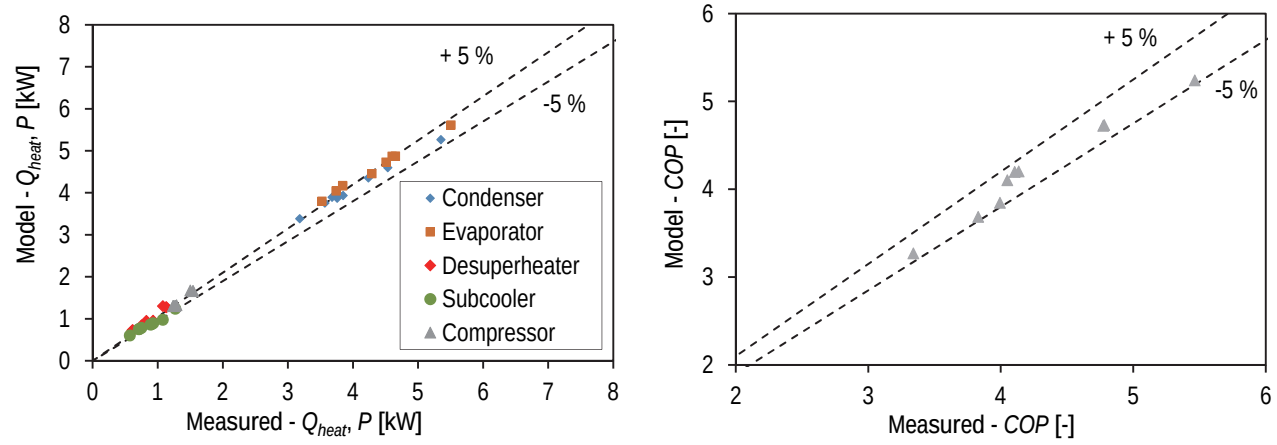

Figure 5 The deviation between the model and the measured data for the heating capacity, the power input (on the left) and the COP (on the right) in a condenser + desuperheater + subcooler arrangement

HOT WATER PREPARATION SYSTEM IN APARTMENT BUILDING

The validated model of the heat pump was used in the simulation of domestic hot water (DHW) preparation system in a block of flats application. The DHW consumption is modeled in TRNSYS simulation software and was dimensioned in accordance with the measured data from the real HP application. Fig. 6 shows the main characteristics of the measured system - supplied heat, electric energy consumption and measured SPF. The total electricity consumption is 36.5 MWh·a^{-1}, the total heat provided by the HP and the electric boiler is 91.3 MWh·a^{-1} and the SPF of the whole DHW system is 2.5.

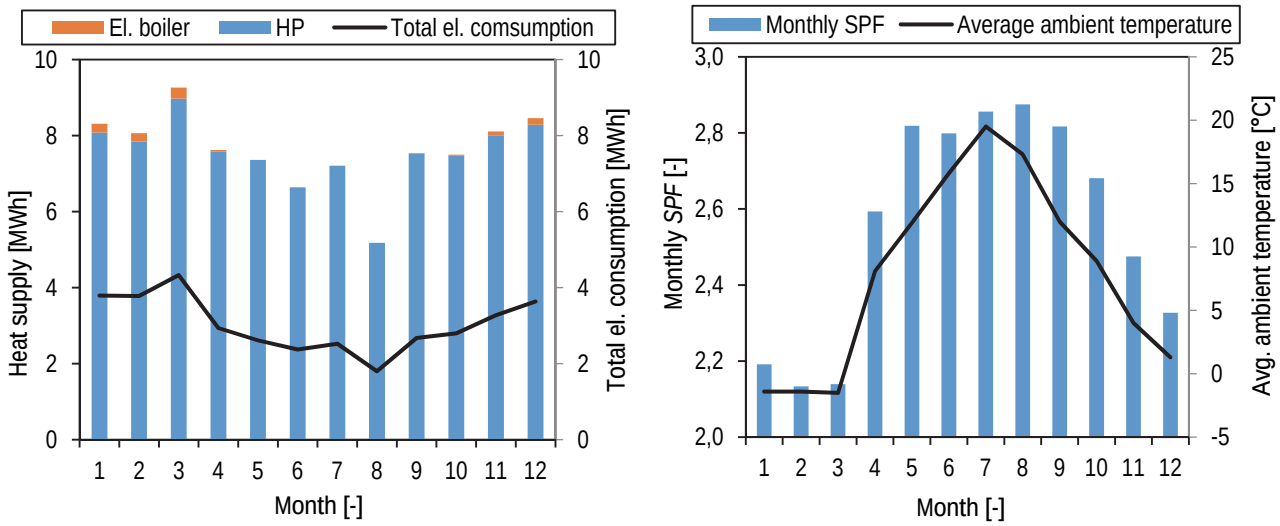

Figure 6 The measured data of the heat supply from the heat pump and the electric consumption (on the left), the calculated SPF of the system and the average ambient temperature (on the right)

The measured system is in the western part of the Czech Republic and is assembled with an air source HP. The nominal heating capacity of the HP (A7/W35) is 20.2 kW. The backup heater is an electric boiler. The heat pump regulation turns off the unit when the ambient temperature is lower than -10 °C and the whole energy consumption is then covered by an electric boiler. The block of flats has 48 housing units. The demanded temperature of the DHW to the circulation system is 55 °C. The DHW circulation system is needed to ensure comfort for residents and works nonstop, however it is estimated that 40 % of the energy is lost there. The accumulation of hot water is provided by a 6 m^3 water tank. The hot water tapping profile was modelled with respect to the standard EN 16147 [3] and the number of the housing unit. The tapping profile is shown in Fig. 7. Hot water consumption is not same during the year (see Fig. 6), therefore, a function describing the monthly profile was implemented in the simulation.

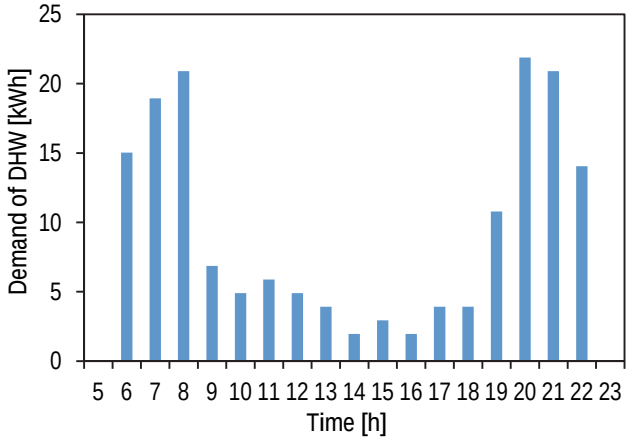

Figure 7 Daily hot water tapping profile

The model of the heat pump described in the chapter Model validation predicts the working behaviour of ground source HP. To describe the air source HP, correction of the heating capacity was undertaken. The correction is based on the ideal working behaviour of the ground source HP. The relative deviation between the ground source heat pump modelled data and the data sheet values is a function of the ambient temperature. The correction is well described by the hyperbole function of a higher order:

$$\xi = \frac{E_1}{t_{amb}^4 + E_2 \cdot t_{amb}^3 + E_3 \cdot t_{amb}^2 + E_4 \cdot t_{amb} + E_5} \quad [-] \tag{8}$$

The function which describes heating capacity is:

$$Q_{heating} = Q_{heating,GS}\left(1 - \xi\right) \quad [W] \tag{9}$$

In the above equations, ξ is the correction factor [-], t_{amb} [°C] is the air inlet temperature (equal to the ambient temperature in the model), $Q_{heating,GS}$ is the heating capacity [W] calculated by the ground source heat pump model, Q_{heat} is the heating capacity of the HP after the correction and E_1 to E_5 are unknown constants for parametrisation.

The model of the heat pump was parameterised to describe the manufacturer's data. The data fit is shown in Fig. 8. The heating capacity is the same for the 35 °C and 45 °C outlet temperature from the condenser. The model contains some unknown constants and, therefore, the parametrisation is precise enough. The average error of the fitted values is 0.53 % for the heating capacity, 3.86 % for the power input and 3.55 % for the *COP*.

SIMULATION MODEL OF THE DHW SYSTEM

The previously described DHW system was modelled in TRNSYS simulation software. The weather was modelled with meteorological data for Prague. The list of constants used in the HP simulation is shown in Table 3 and 4.

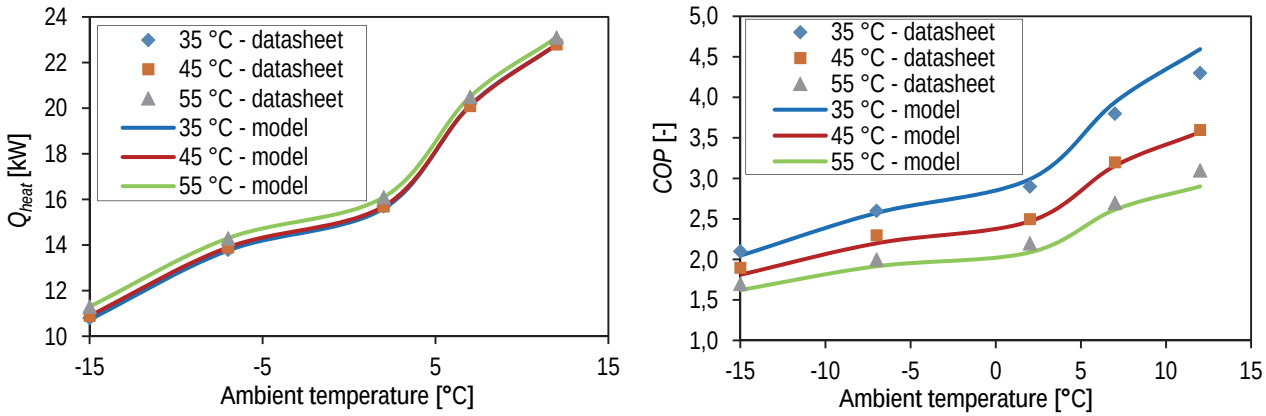

Figure 8 The heating capacity (on the left) and COP (on the right) as a function of the ambient temperature

Table 3 List of the constants used in the simulations

V_{sw}	C	D	E_1	E_2	E_2	E_4	E_5
(cm^3)	(-)	(-)	(-)	(°C^{-3})	(°C^{-2})	(°C^{-1})	(-)
97.2	$2.22 \cdot 10^{-2}$	See Table 1	-2.14	1.86	-2.83	-56.2	117.5

Table 4 List of the UA values used in the simulations

System	UA_{con} (W·K^{-1})	UA_{ev} (W·K^{-1})	UA_{des} (W·K^{-1})	UA_{sub} (W·K^{-1})
reference	6000	6000	0	0
+ desuperheater	5000	6000	1000	0
+ subcooler	5000	6000	0	1000
+ desuperheater and subcooler	4000	6000	1000	1000

Reference system

The working diagram of the reference system in shown in Fig. 9a. A type340 [10] with a volume of 6 m^3 was used for the hot water tank (HWT) simulation. The *UA* value of the internal HX is 3.4 kW·K^{-1} and has height of 2.5 m. The temperature of the incoming cold water is 10 °C. The HP is connected to the hot water tank by an inlet and outlet connection to 10 % and 90 % of its height, respectively. The position of the temperature sensor T1 is at 60 % of the height. The system of the measurement and regulation (MaR) controls operation of the HP and the circulation pump (P1) by measuring temperatures T1 and T2. In the case of hot water, overheating is measured on the temperature sensor T3 at the outlet of the HWT, the hot water is mixed with cold water. If the hot water does not reach the demanded temperature of the DHW, the electric boiler (EB) heats the water to the demanded 55 °C. The circulation pump (CP) works nonstop and its power input is excluded from the *SPF* calculation. Heat losses of the circulation system are included in the heating demand because they are indifferent to the heat source. Heat losses are simulated by a tube model. The length of the tube is 335 m. The ambient temperature around the tube varies from 10 °C to 40 °C during a year. The circulation return pipe leads the water both to the DHW pipe and the HWT according to temperature T4 to improve the temperature stratification in the HWT.

System with a desuperheater

The working diagram of the system is shown in Fig. 9b. The HP is connected to the HWT via two internal HXs. The condenser heats the two lower thirds of the HWT until the demanded temperature (40 °C) at T1 is reached. The desuperheater heats the upper part of the HWT until the HP is ON or the temperature at T5 is higher than 57 °C. The three-way valve V1 controls the water flow rate to the desuperheater so that temperature of water at the outlet from desuperheater is 60 °C. The piping connection between the condenser and the desuperheater ensures the minimal condensation of the refrigerant in the desuperheater. It is assumed that the water enters the desuperheater with a temperature approximately equal to the condensing temperature. The positions of T1 and T5 are at 40 % and 75 % of the HWT height, respectively. The *UA* values of the internal heat exchangers are divided in the same ratio as the *UA* values in Table 4 from the *UA* value of the reference system. The same rule is valid for the systems with the subcooler and both the subcooler and the desuperheater.

System with a subcooler

The working diagram of the system with a subcooler is shown in Fig. 9c. The subcooler preheats the lower third of the HWT. The condenser heats the upper two-thirds of the HWT. The subcooler and the circulation pump P2 always work when the HP is ON. The sensor T1 is positioned at 80 % of the HWT height.

System with a desuperheater and subcooler

A hydraulic connection combines previous cases. The subcooler heats the upper quarter of the HWT, the condenser the middle half and the subcooler the lower quarter of the HWT. The working diagram is shown in Fig. 9.d. The logic of the control is similar to the previous cases.

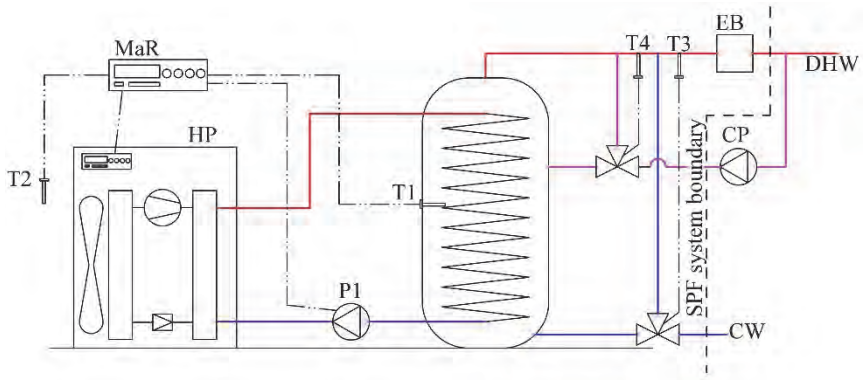

Figure 9a Reference system working diagram

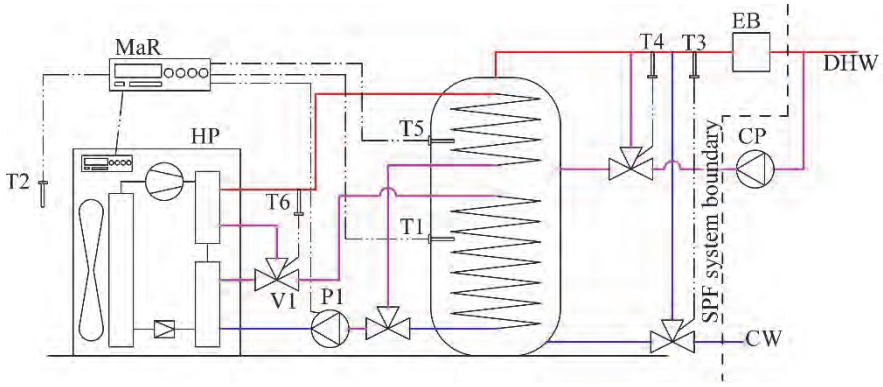

Figure 9b Working diagram of the HP with a desuperheater

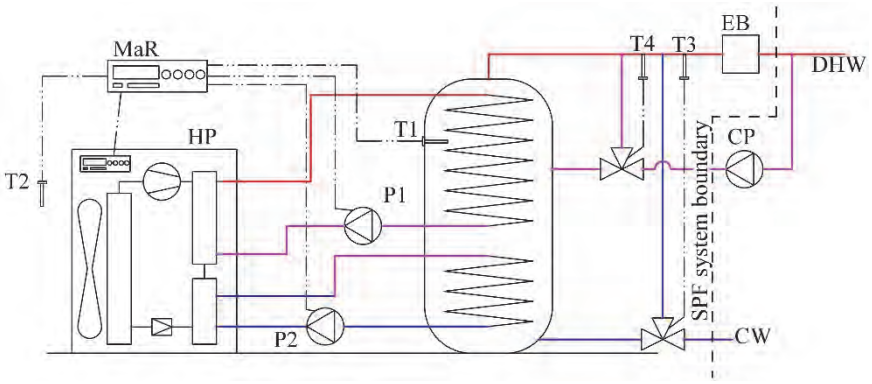

Figure 9c Working diagram of the HP with a subcooler

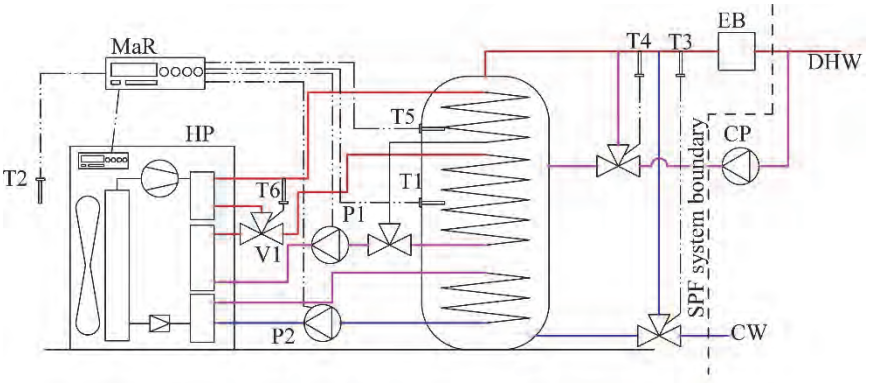

Figure 9d Working diagram of the HP with a desuperheater and a subcooler

RESULTS AND DISCUSSION

The summary of the results from the simulations for each described system is shown in Table 5. The heat consumption DHW system is 56.5 MWh and approximately 92 MWh together with circulation losses for all systems. The *SPF* of reference system is 2.55. The results of references are close to the measured data. The reference simulation, therefore, sufficiently describes the real behaviour of the system.

The *SPF* of the system with the desuperheater is 2.7, which is 6 % higher than the reference. The DHW circulation system, which is connected to the HWT, negatively influences the temperature stratification, therefore, the advantage of the desuperheater, which is in charge of the upper part of the HWT, is diminished.

The *SPF* of the system with the subcooler is 3.01, which is 20 % higher than the reference. The subcooler helps to preheat water for the condenser and the efficiency of subcooler grows with higher condensing temperatures.

The most complicated system with the desuperheater and the subcooler gives the best results. The *SPF* of the system is 3.17 which is 26 % higher than the reference. This option is comprised of the advantages of both previous systems.

The monthly results of the simulation of the system with the desuperheater and the subcooler are shown in Figure 10. The monthly *SPF* is a function of the ambient temperature and hot water consumption. In August, with a significant downswing of the DHW consumption, the *SPF* of the system decreases. The behaviour results from more significant losses in circulation. The heat supplied by the subcooler is stable during the year, contrary, the heat from the desuperheater varies more significantly with the ambient temperature.

Similar results as seen in Table 5 can be obtained with different heat exchangers. The main benefit of multiple HX heat pumps is in the better temperature distribution to the HWT. The size of the HX in the heat pump slightly influence the heat transfer which can result in a different *COP* of the HP. The *SPF* system is more dependent on the temperature distribution and the temperature stratification of the water inside the HWT.

CONCLUSION

The study mainly presented a possible increase in energy efficiency with a HP for the DHW application in a block of flats. The study is focused on the desuperheater and subcooler usage in such applications. The results proved the possibility to improve the *SPF* of the DHW system by 26 %.

The model of the air source HP for simulation is based on the ground source HP model (presented in the chapter Model validation) and the parametrisation of the data sheet values. The limitations of the air source HP model are unknown in frosting and defrosting behaviour of the HP on site. The correction function characterises ideal laboratory conditions and proved the described manufacturers data well.

The model of the ground source HP with the desuperheater and subcooler presented in the chapter The mathematical model of the heat pump describes the behaviour of the measured HP. However, the model limitation is in the assumptions (Section 4). The assumption of the constant *UA* of the HX, which is valid just in limited range of operating conditions, is also problematic.

The other limitation of the model of the DHW system as a whole is in the model of the HWT. The quality of the model and parameterisation was not tested on site. The deviation can negatively influence the error between the simulated and real *SPF* of the system. However, the same model of the HWT was used for all simulations (the only deviation was in the position of the sensors and internal HX), therefore, the ratios between the *SPF* of the systems should not vary.

Future research will focus on the connection between the HWT and HP on the impact of changing the relative positions of the sensors and the inlet and outlet port positions. The model of the HP can be improved by modelling a change of the *UA* value and implementing a compressor with capacity modulation. The system simulation should be tested on real applications via long-term measurements.

Table 5 Main results of the simulation

	Heat losses		HP					Circulation pumps	Electric boiler	*SPF*
	Circulation	HWT	Q_{con}	Q_{des}	Q_{sub}	P	COP			
	(MWh)	(MWh)	(MWh)	(MWh)	(MWh)	(MWh)	(-)	(MWh)	(MWh)	(-)
Reference system	35.6	0.24	90.5	-	-	35.3	2.57	0.23	0.56	2.55
HP with the desuperheater	36.0	0.25	58.5	32.9	-	32.4	2.82	0.24	1.39	2.70
HP with the subcooler	35.6	0.20	70.0	-	19.89	29.8	3.17	0.22	0.32	3.01
HP with the desuperheater and subcooler	35.9	0.25	44.15	27.15	21.48	28.75	3.23	0.22	0.19	3.18

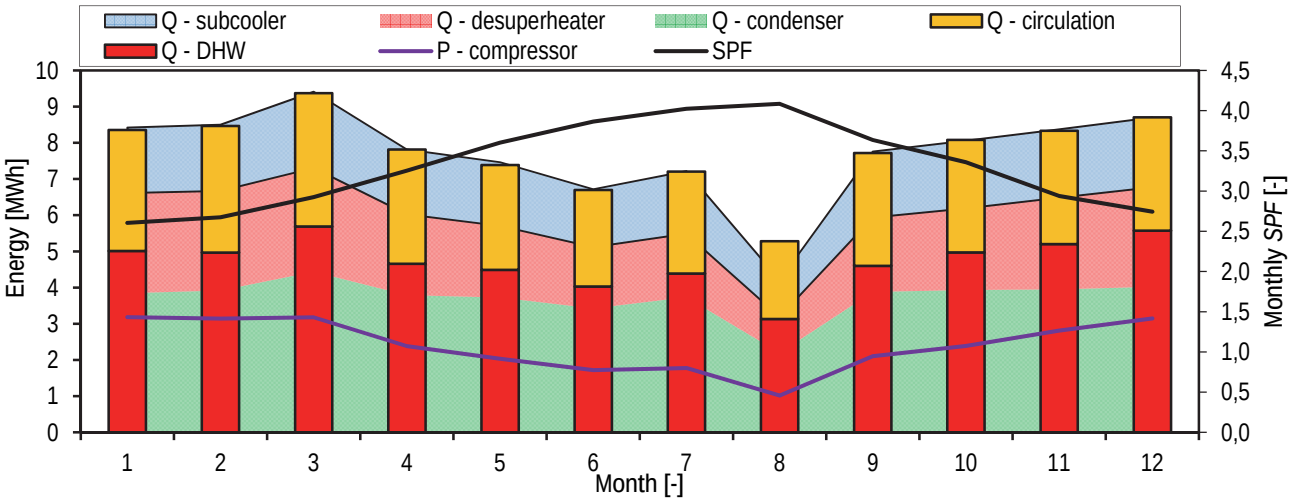

Figure 10 Monthly results of the simulation of the system with the desuperheater and the subcooler

ACKNOWLEDGMENT

This work has been supported by a project of the University Centre for Energy Efficient Buildings.

REFERENCES

[1] NOWAK, T. European Heat Pump Market and Statistics Report 2016. European Heat Pump Association (EHPA) 2016; Available at: http://www.ehpa.org/homepage/?eID¼dam_frontend_push&docID¼1930.

[2] Progress on energy efficiency in Europe. European Environment Agency (EEA) 2015; Available at http://www.eea.europa.eu/data-and-maps/indicators/progress-on-energy-efficiency-in-europe-2.

[3] EN 16147 Heat pumps with electrically driven compressors - Testing and requirements for marking of domestic hot water units. Brussel: CEN, 2011.

[4] Vyhodnocení cen tepelné energie k 1.1.2015. Energy Regulatory Office 2015; Available at: https://www.eru.cz/cs/teplo/statistika/vyhodnoceni-cen-tepelne-energie.

[5] Transient System Simulation Tool - TRNSYS 17.1 (2014), The University of Wisconsin, Madison, http://sel.me.wisc.edu/trnsys.

[6] ZAKULA, T., GAYESKI, N.T., ARMSTRONG, P.R., KEITH, L. Variable-speed heat pump model for wide range of cooling conditions and loads. HVAC&R Research 2011; 17:5, p. 670–691.

[7] PENG, D.Y., ROBINSON, D.B. New Two Constant Equation of State. Ind. Eng. Chem. 1976; 15:1, p. 59–63.

[8] SHANG, Y., WU, A., FANG, X. A study on modeling of minimal stable superheat for variable speed refrigeration system. International Journal of Refrigeration 2015; 59, p. 182–189.

[9] ERICSON, L. Rating Equations for Positive Displacement Compressors with Auxiliary Suction Ports. International Compressor Engineering Conference 1998, http://docs.lib.purdue.edu/icec/1282.

[10] DRUECK, H. Multiport Store Model for TRNSYS - Type 340. Transsolar GmbH 2006; Germany.

NOMENCLATURE

A	heat transfer area [m^2]
C	constant [-]
COP	performance factor [-]
$c_{p,liq}$	specific capacity of secondary fluid [J·kg^{-1}·K^{-1}]
D_1 - D_4	constants [-]
D_5	constant [Pa]
E_1, E_5	constants [-]
E_2	constant [°C^{-3}]
E_3	constant [°C^{-2}]
E_4	constant [°C^{-1}]
$h_{des,out}$	specific enthalpy at the outlet of desuperheater [J·kg^{-1}]
$h_{ref,in}$	specific enthalpy of refrigerant at inlet [J·kg^{-1}]
$h_{ref,out}$	specific enthalpy of refrigerant at outlet [J·kg^{-1}]
m_{liq}	mass flow rate of secondary fluid [kg·s^{-1}]
m_{ref}	refrigerant mass flow rate [kg·s^{-1}]
n	compressor rotational speed [s^{-1}]
n_{pol}	average exponent of isentropic compression [-]
p_{con}	condensing pressure [Pa]
P	electric power input [W]
Q_{con}	heat capacity of condenser [W]
Q_{des}	het capacity of desuperheater [W]
Q_{heat}	heating capacity [W]
$Q_{heat,total}$	heat capacity of high pressure side [W]
$Q_{heating,GS}$	heat capacity of ground source heat pump [W]
$Q_{hx,1}$	heat exchange rate of refrigerant [W]
$Q_{hx,2}$	heat exchange rate of secondary fluid [W]
$Q_{hx,3}$	heat transfer through HX area [W]
Q_{sub}	heat capacity of subcooler [W]
SPF	seasonal performance factor [-]
t_{con}	ambient temperature [°C]
t_{con}	condensing temperature [°C]
t_{ev}	evaporating temperature [°C]
$t_{liq,in}$	temperature of secondary fluid at inlet [°C]
$t_{liq,out}$	temperature of secondary fluid at outlet [°C]
$t_{s,out}$	temperature at the outlet of subcooler [°C]
U	overall heat transfer coefficient [W·m^{-2}·K^{-1}]
V_{sw}	swept volume [m^3]
δ_{ln}	logarithmic mean temperature difference [K]
η_{ie}	isentropic efficiency [-]
λ_v	volumetric efficiency [-]
ξ	correction value [-]
$\rho_{ref,s}$	refrigerant density in the compressors suction [kg·m^{-3}]
σ	pressure ratio [-]
Φ	polytropic correction [-]

Ing. Petr ZELENSKÝ[1),2)]
Ing. Martin BARTÁK, Ph.D.[1),2)]
prof. Dr. Ir. Jan L.M. HENSEN[1),3)]

[1)]CTU in Prague, Faculty of Mechanical Engineering
[2)]CTU in Prague, University Centre for Energy Efficient Buildings
[3)]Eindhoven University of Technology, Building Physics and Services

Simulation of Indoor Environment in the Concert Hall Housed in a Former Church

Simulace vnitřního prostředí v koncertní hale umístěné v objektu bývalého kostela

A previously developed approach to simplify the numerical modelling of heat sources based on the replacement of a heat source by a simple boundary condition (see VVI 5/2012) is applied in the real scenario of a recently refurbished former church built in the 14th century. The building is now used as a concert and conference hall with up to 350 visitors staying for different time periods during each day. The investor of the restoration was concerned about temperature fluctuations caused by the variable occupancy and the possible negative impact on the historical stucco decorations and on the original wooden trusses of the former church. Moreover, only natural ventilation through window openings on the street level and the windows in the roof is possible in order to preserve the original look of the building. The study elaborated upon in the paper is based on the results of the CFD simulations with simplified models of visitors acting as heat sources under two different occupancy scenarios.

Keywords: CFD (Computational Fluid Dynamics), indoor environment, heat sources, simplified model, convectional flow, thermal plumes interaction

Dříve vyvinutá metoda zjednodušení numerických modelů zdrojů tepla založená na náhradě zdroje tepla jednoduchou okrajovou podmínkou (viz VVI 5/2012) je aplikována na reálnou případovou studii nedávno zrekonstruovaného bývalého kostela ze 14. století. Budova je nyní vyžíván jako koncertní a konferenční prostor s obsazeností až 350 návštěvníků, kteří se zdržují proměnnou dobu během každého dne. Investor restauračních prací projevil obavu z teplotního kolísání způsobeného proměnnou obsazeností kostela, které by mohlo mít negativní vliv na historické štukové dekorace a na originální dřevěný krov bývalého kostela. Navíc je z důvodu zachování původního vzhledu budovy možné využít pouze přirozenou ventilaci okenními otvory na úrovni ulice a střešními okny. Studie vypracovaná v tomto příspěvku vychází z výsledků CFD simulací se zjednodušenými modely návštěvníků, kteří působí jako tepelné zdroje v rámci dvou různých scénářů návštěvnosti.

Klíčová slova: CFD (Computational Fluid Dynamics), vnitřní prostředí, zdroje tepla, zjednodušený model, konvekční proudění, interakce konvekčních proudů

INTRODUCTION

The former church of St. Anna is a 14th century gothic building located in the Old Town of Prague (hereinafter referred to as the church). It was desecrated at the end of the 18th century, recently completely reconstructed and it now serves as a community centre and universal space suitable for events such as concerts, conferences, etc., with the total capacity up to 350 visitors. The front part of the church interior after reconstruction is displayed in Figure 1.

Figure 1 Interior of the church, after reconstruction

Adaptation of historical buildings to a new function always brings a question about the influence of the indoor environment change on the building structures. This question arose also during the restoration works in 2001. The biggest concerns were indoor airflow velocities and air temperature distribution in the vicinity of the internal wall surfaces [1]. The design team had to take measures to protect original stucco decorations on the walls and the original wooden roof trusses, but at the same time only natural ventilation through window openings on the street level and through openings in the roof was possible, so that the original look of the building was preserved. Building energy simulation (BES) and computational fluid dynamics (CFD) were used to tackle this uneasy task [2].

CFD simulations can predict the influence of heat sources on natural ventilation and test different scenarios. However, for their effective use, it is especially vital to reduce the time to be spent on the model set-up as well as on the simulations. One of the possible ways to achieve this is to simplify computational models providing that the results accuracy will not be significantly lowered.

The high number of visitors acting as heat sources may have a crucial effect on the environment inside the former church. The main impact on the airflow is caused by convective currents generated by human bodies. Warm air is driven upwards by buoyancy forces and forms a rising thermal plume above each visitor.

Detailed CFD modelling and simulations of natural convective flows generated in ventilated and air-conditioned spaces are quite demanding for computing power and time. The original CFD simulation used by the design team in 2001 did not contain explicitly modelled indoor heat sources. The natural ventilation of the indoor space was emulated by the prescribed pressure difference between the internal

space of the church and the surrounding environment, which was pre-calculated using BES [1]. The floor of the model was heated in order to compensate the thermal gain from the occupants. Yet, the explicit modelling of heat sources is important, as they can be vital for the appropriate air change [3], [4] and they can significantly influence air flow distribution indoors as well as the indoor environment quality [5]–[7].

The current work elaborates on the CFD simulations of the indoor air flow inside the church with two different occupancy scenarios: 65 and 304 visitors. The models of heat sources were simplified according to the previously developed method based on the replacement of each heat source by a simple boundary condition of convective flow, which is determined in advance from a detailed simulation of a thermal plume above a comprehensive model of the heat source [8]. The influence of each heat source on the overall air-flow pattern is preserved, while the computational demands of the simulations are lowered, enabling, e.g., variant studies.

The target of this research was to investigate the influence of the visitors acting as heat sources on the stucco decorations and the wooden roof trusses of the church. The results of the simulations with 65 and 304 visitors are mutually compared and also with the simulation without the explicitly modelled visitors. The effect of the heat sources on the indoor air flow, temperature stratification and ventilation rates are studied. The paper also demonstrates the usability of the previously developed method to simplify indoor heat sources for real scenarios.

NUMERICAL MODEL OF THE CHURCH

The modelled building is a former single-nave church with the main enclosure of approx. 9,630 m^3 total volume and the basic external dimensions (width x length x height) of approx. 11.4 x 43.5 x 29.2 m. The rear half of the nave is divided by a gallery 6 m above the floor, see Figure 2.

The church has 3 large window openings on the street level and 11 small window openings in the roof (6 of them on the south-facing side and 5 of them on the north-facing side). As it is possible to use natural ventilation through these openings only, all of them were opened.

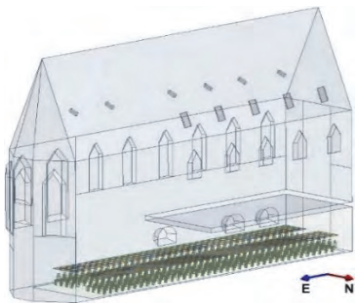

Figure 2 Model of the church, 304 seated visitors

Two numerical models of the church with a different number of seated visitors were created in the ANSYS Design Modeller. Both models included a 1.5 m wide region of external space surrounding the church, in order to correctly simulate the process of natural ventilation. The first model represents the almost fully occupied space, with 304 seated visitors, as displayed in Figure 2. The second model represents the low occupied space, with 65 seated visitors, distributed in two rows.

It was expected that the high number of visitors in the space of the church may have a significant effect on the indoor environment, for they act as heat sources driving natural ventilation. It was important to consider them in the CFD simulation. However, their models had to be simplified, in order to lower the computational demands.

METHOD TO SIMPLIFY MODELS OF HEAT SOURCES

The models of the visitors in the CFD simulations were simplified according to previously developed methodology [8], based on the replacement of each heat source by a simplified geometrical object and simple boundary conditions generating convective flow. All the visitors were considered as identical (with the same heat output). The preparation of the simplified model of the heat source was undertaken in two steps.

The model of a sitting thermal manikin with detailed geometry and boundary conditions of constant heat flux of 57.3 W/m^2 from its body was created as the first step. The total sensible heat output of the manikin was 90 W. Heat and momentum transfer near the manikin's surface were modelled using a dense boundary layer mesh (i.e., without wall functions), which is accurate but significantly increases the demands on the computer memory and prolongs the computational time. The CFD simulation was performed with the detailed model to obtain the velocity and temperature fields around the manikin, with the focus on the generated thermal plume.

The results of the detailed simulation were used to determine the temperature, velocity and turbulence profiles of the thermal plume at the height 0.7 m above the manikin, where the convective flow is considered as fully developed. The obtained profiles were parameterised using Curve Expert software and programmed in ANSYS Fluent by the User Defined Function (UDF). The velocity and turbulent quantities were prescribed as absolute, the temperature of the convective flow was prescribed as relative to the reference ambient temperature. The work flow of the programmed UDF was as follows:

1. set the local coordinate system with the origin in the geometrical centre of the subsidiary zone;
2. get the reference temperature in the vicinity of the subsidiary zone;
3. calculate the temperature profile of the convective flow, on the basis of the reference temperature;
4. prescribe the boundary condition for the temperature;
5. prescribe the boundary condition for the vertical velocity;
6. prescribe the boundary cond. for the turbulent quantities k and ε.

The heat sources were substituted by a geometrically simplified object with adiabatic surface, acting only as an obstacle to the airflow. The thermal plume rising above each heat source is induced artificially, by the velocity and temperature profiles calculated and prescribed in the UDF as boundary conditions at subsidiary zones created 2 m above the ground, see Figure 3.

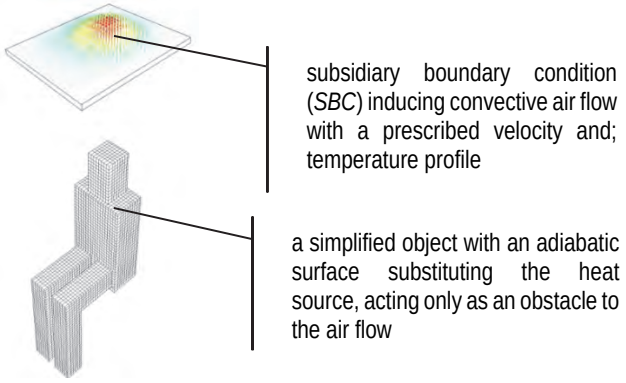

Figure 3 Simplified model of the sitting occupant

The previous development and testing of the method to simplify models of heat sources is described in the paper published in VVI 5/2012 [8]. Two additional studies were concluded prior to the simulation of the church. These studies targeted the optimal positioning of the subsidiary zone above the thermal manikin and the influence of the simplification on the merging of thermal plumes above multiple heat sources placed close to each other.

The CFD simulations were performed in the same manner as the simulations in the previously published studies [8]. The surface temperature of the room's walls was 19 °C, their emissivity was 0.94 and the emissivity of the thermal manikin surface was 0.98. The two equation k-ε turbulence model by Launder and Spalding [9] was used, with modification to account for the full buoyancy effects. This model has been found as the most suitable for CFD simulations of indoor spaces with the prevailing effect of natural convection [10]. Heat radiation was simulated using the surface-to-surface (*S2S*) model [11].

The *Body Force Weighted* scheme was chosen for the discretisation of the pressure equation as it is recommended for solving buoyancy driven flows [11]. The convective terms of the equation were solved using a second order upwind scheme. Pressure and velocity fields were coupled by the *SIMPLE* algorithm and the flow was considered as unsteady. 10 iterations for each time step of 0.1 s were computed in all the simulations. The residuals were in the order of magnitude of 10^{-5} or lower.

All the computational cases were simulated for a start-up period of at least 480 s after which the flow was considered fully formed and the results were then recorded for a further 120 s of the simulated time with a time step of 1 s. 120 data files were the outcome of each simulation. The values of temperature and velocity were recorded at appropriate points and averaged over the 120 s.

Optimal position of the subsidiary zone

The influence of the subsidiary zone position on the rising thermal plume was studied in the case of thermal manikin situated in the middle of a room. Four computational cases with different vertical positions of the subsidiary zone above the heat source were solved and compared to the reference case with a detailed model of the thermal manikin, see Figure 4.

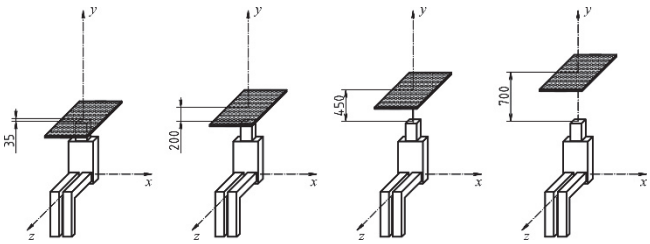

Figure 4 Vertical position of the subsidiary zone above the manikin's head (from left to right: 35 mm, 200 mm, 450 mm and 700 mm)

The velocity and temperature profiles determined for all the simulations with simplified models are close to the reference detailed case, especially in the higher regions of the room, i.e., above the subsidiary zones, see Figure 5 for example. The exception is the case with the subsidiary zone positioned 200 mm above the manikin's head. In this case, the comparison shows a slower velocity and lower temperature of the convection flow induced above the manikin. The most similar case corresponding to the reference case are the simulations with *SBCs* in the heights 450 and 700 mm above the manikin's head. The case with the *SBC* positioned 35 mm above the manikin reasonably corresponds to the reference case as well.

It can be advised to position the *SBC* rather higher above the heat source, where the thermal plume is fully developed, if the problem on hand allows it (i.e., in the simulation of a room with sufficient space above the heat sources, such as the church). If it is, for some reason, necessary to position the *SBC* in a closer vicinity to the heat sources (for example, rooms with a low ceiling), a CFD study should be performed, in order to test the correctness of the boundary condition defined from the reference detailed simulation.

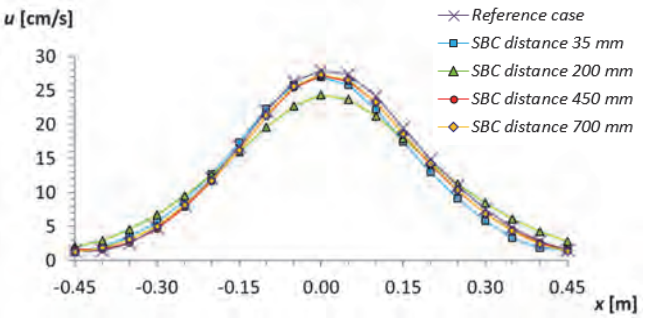

Figure 5 Velocity profiles at the height y = 1.975 m above the floor

Influence of the simplification on merging of thermal plumes

In the simulations with multiple heat sources, the merging of individual thermal plumes in higher regions must be considered. There was a concern how the developed method influences this physical process, especially as it is targeting simulations of spaces with a large number of heat sources possibly positioned close to each other, such as in the case of the church.

The numerical study was elaborated upon with the focus on the thermal plumes merging above multiple heat sources [12]. It compares a set of simulations with numerical models of four sitting thermal manikins in an enclosed room, which were modelled either in detail or simplified using the developed methodology, with the subsidiary zone placed 0.7 m above the thermal manikin. The group of manikins was placed in the middle of an enclosed room, with dimensions (width x length x height) 5 x 5 x 5.6 m, see Figure 6.

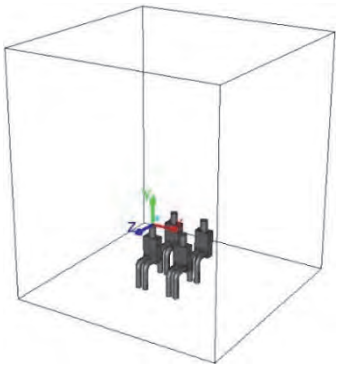

Figure 6 Thermal plumes merging simulation setup

The room dimensions and no obstacles around and above the manikins provided enough space for thermal plumes to develop sufficiently and merge. The height of the room was chosen according to the height of the space under the gallery, which divides the rear half of the church's nave, see Figure 2.

The results of the simulation with the detailed models were compared to the results with the simplified models of thermal manikins. The evaluation was focused on the phenomenon of the thermal plumes merging above the heat sources and the influence of the simplification of the heat source models on this physical process.

In both the simplified and detailed simulations, the thermal plumes are developing in a similar way, see Figure 7. Merging of the four thermal plumes is obvious in both cases, although it is more noticeable above the reference detailed models. Especially in the side view, it is possible to see that the thermal plume above the front seated manikin is, in this case, deflected more from the vertical direction and rises more towards the rear manikin than in the case with the simplified models. In the higher regions, the thermal plumes merge completely in both simulations, and adhere to the ceiling of the room and spread further to the vertical walls in a very similar way.

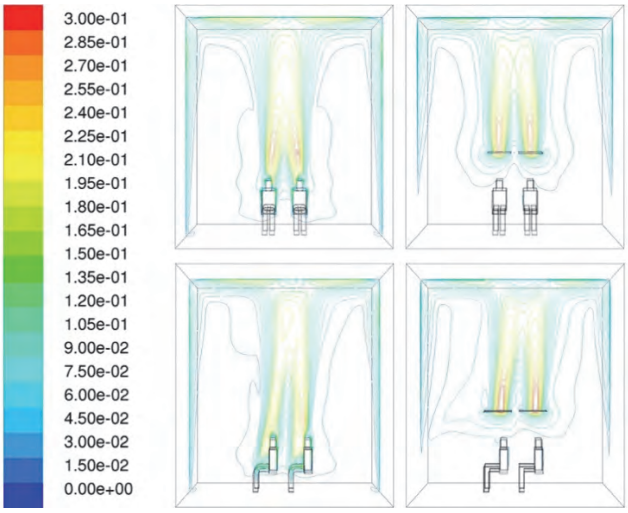

Figure 7 Velocity isolines [m/s], detailed model (left) and simplified model (right); top – front views; bottom – side views

It has been shown that the simplification affects the development of the thermal plumes considering their merging above the heat sources. However, the difference of the simplified simulation from the reference simulation decreases with the increasing height above the heat sources. The higher it is above the manikins, the more the thermal plumes resemble each other in the two simulated cases, see Figure 8 for example, presenting velocity profiles nearby the room's ceiling. Although the plumes in the simulation with the simplified models are not fully merged yet, they are very close to the plumes from the simulation with the reference models. The velocities, in both cases, are comparable and it can be expected that full merging in the simplified case is achieved if the space is higher. This deficiency could be solved by placing the prescribed boundary condition lower above the thermal manikins' heads, so the merging would be achieved sooner in the case with the simplified models also. However, in the case of the church, this was not necessary, as the primary interest was to simulate airflow high above the floor.

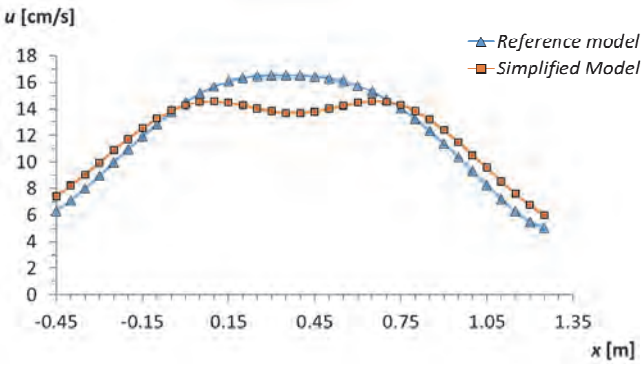

Figure 8 Velocity profiles 3.6 m above the floor (front view)

CFD SIMULATION OF THE CHURCH

The building interior (approx. 9,630 m^3), including the external space surrounding the building, was divided by an unstructured tetrahedral grid into more than 17.9 × 10^6 control volumes in the model with 65 visitors and more than 28.6 × 10^6 control volumes in the model with 304 visitors. The minimum size of a cell was in both cases 25 mm, the maximum was 250 mm.

The boundary conditions of the surfaces facing the surrounding environment (see Figure 9) were specified as a free boundary with zero pressure gradient. The external air temperature was –7 °C, as a winter scenario was considered. The church is partially, from two sides, surrounded by other occupied buildings with the indoor temperature being considered as 20 °C. The temperature of the ground under the floor was 5 °C. The composition of the building constructions was prescribed in the model and the solver calculated the temperature of the internal surfaces. Thus, the thermal conduction through the walls was taken into account. All the walls of the church are made from marlstone, the concrete floor is covered by tiles, the windows are single glazed.

Figure 9 Boundary surfaces facing the surrounding environment (red line)

The CFD simulations were solved in the software ANSYS Fluent 16.0 as a non-isothermal flow of incompressible ideal gas (air). The flow in the proximity of the walls was solved using wall functions and the dimensionless wall distance *y+* for the first cell near the walls of the church was in the range from 80 to 110. The two equation *k-ε* turbulence model by Launder and Spalding [9] – the so called *standard* – was used considering the influence of the temperature and buoyancy on the turbulence. This model has been previously found to be the most suitable for CFD simulations of indoor spaces with the prevailing effect of natural convection [10].

The *Body Force Weighted* scheme was chosen for the discretisation of the pressure term as it is recommended for buoyancy driven flows [11]. The convective terms were solved using a second order upwind scheme. A coupled and steady-state solver was used to obtain the pressure and velocity fields. Radiation was not simulated, as the visitors are sitting very close to each other and the balance of heat transfer among them should be close to 0. Radiation heat transfer should be more significant for the visitors sitting at the end of the rows only, which was neglected.

The evaluation of the results targeted at the influence of heat source on the indoor environment inside the church, especially on the airflow patterns, temperature stratification and air change rates. The results of simulations with 65 and 304 visitors were mutually compared and also against the simulation of the space without the modelled visitors [2].

RESULT ANALYSIS AND DISCUSSION

A CFD simulation of the indoor air flow with a prevailing effect of natural convection caused by low temperature differences is always challenging and the calculation tends to be slow and unstable. In our case, the convergence of the calculation was achieved after more than 4,000 iterations in the case of the simulation with 65 visitors and more than 5,000 iterations in the case of 304 visitors. All the residuals reached the order of 10^{-4} or less, excluding the residuals of continuity, which reached the order of 10^{-3}. This could have been caused by the instability of the convective flow. The convergence has been proven on the basis of the total mass flux balance in the whole computational domain, which approx. reached $4 \cdot 10^{-2}$ kg/s in both simulated cases. This is reasonable, considering that it is approximately 1 % of the absolute value of the mass flux in the computational case. The imbalance occurred on the boundary facing the surrounding environment. The balance of the total mass flux through the building's interior was 0 kg/s for both simulated cases, i.e., perfectly balanced.

Images of the simulated velocity and temperature fields in the church were evaluated after the convergence of each simulation. The velocity vectors, the isolines of velocity magnitude and the contours of temperature were studied in 1 vertical plane *y-z* (side view) intersecting the geometrical centre of the building and 5 vertical planes *x-y* (front view) intersecting the church with a spacing of 7 m.

Velocity fields

The velocity vectors and isolines of the velocity magnitude in the vertical plane *y-z* intersecting the centre of the church (side view) are displayed. See Figure 10, for the simulation with no explicitly modelled heat sources performed during the restoration works in 2001 [2] and Figure 11 and Figure 12 for the new simulations with 65 visitors and with 304 visitors, respectively.

Comparison of the velocity fields in the three presented simulations shows that the explicit modelling of the visitors acting as heat sources significantly affects the results of the simulation. In the case without the explicit models of visitors (Figure 10), there are two large circulation flows above the raised gallery in the rear part of the church and one large circulation flow in the front of the building. However, in both cases with the models of visitors (Figure 11 and Figure 12), the vortexes above the gallery merge in one large circulation flow. This may have been caused by a strong thermal plume, which is formed above the models of the visitors and rises from the space under the gallery. Also, it is possible to see that, in the case with 304 visitors, there is stronger air circulation in the space of the church than in the case with 65 visitors, although the airflow trajectories resemble each other.

The visitors have a strong influence also on the environment in their close vicinity. There is very low air circulation under the gallery in the simulation without the explicitly modelled visitors. The presence of the visitors in the space causes the airflow with strong mixing in the other two cases.

The large windows in the front of the building (on the left side of the displayed intersections) have another strong influence on the airflow in the church. The air is cooled down in their vicinity and falls down towards the floor. The falling flow does not fully reach the auditorium in the two simulations with the visitors, as it is turned upward by the convective flow rising from the space under the gallery, unlike in the case without the explicitly modelled heat sources. The air flow velocities did not exceed 0.65 m/s in any of the three simulated cases. The maximum velocities in both simulations with the explicit models of the visitors are in the space under the gallery, where the ventilation air enters the building through the three window openings on the street level. This may be the main concern, as the fast, cold flow directly enters the space with the sitting visitors, which could cause their discomfort. The visitors acting as heat sources consequently influence the distribution of this supplied air in the rest of the space. Nearby the walls, the airflow velocity does not exceed 0.45 m/s.

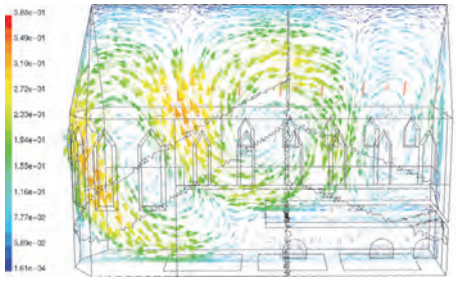

Figure 10 Velocity field in the case without heat sources, velocity vectors [m/s] [2]

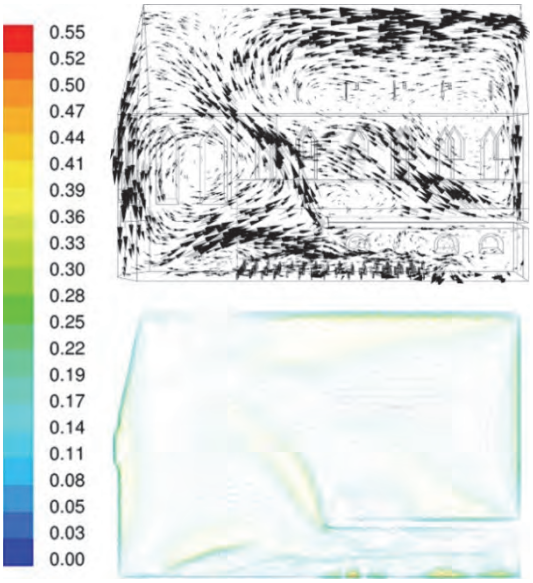

Figure 11 Velocity field in the case with 65 visitors, upper: velocity vectors, lower: velocity magnitude isolines [m/s]

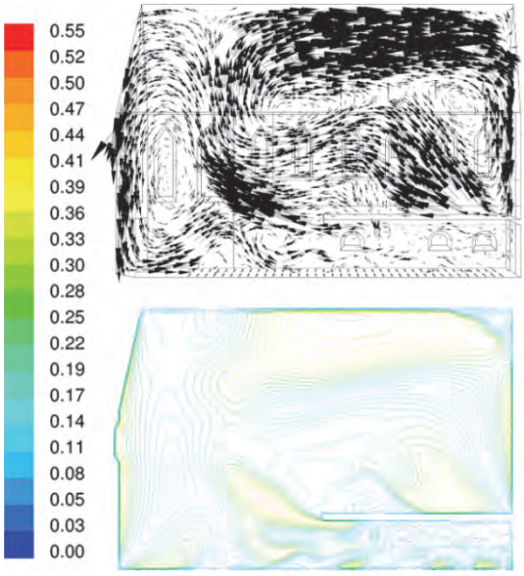

Figure 12 Velocity field in the case with 304 visitors, upper: velocity vectors, lower: velocity magnitude isolines [m/s]

The velocity vectors and isolines of the velocity magnitude were evaluated in 5 vertical planes x-y (front view) also in order to get more complete information about the velocity fields under the roof where the original wooden trusses are exposed to the air flow. See Figure 13 for example, showing a velocity field 21 m from the rear wall of the church. It has been confirmed that the maximum velocity near the sides of the roof does not exceed 0.45 m/s.

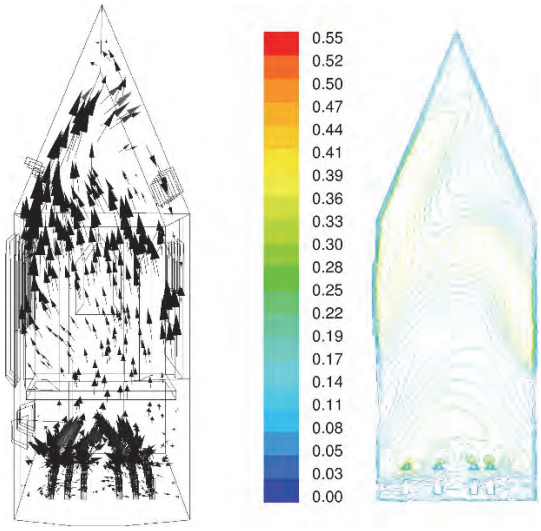

Figure 13 Velocity field in the case with 65 visitors - left: velocity vectors, right: velocity magnitude isolines [m/s]

Temperature fields

The temperature distribution in the church was evaluated on the basis of the temperature contours in 1 vertical plane *y-z* (side view) and 5 vertical planes *x-y* (front view). The selected cross-sections for the cases with 65 and 304 visitors are displayed in Figure 14.

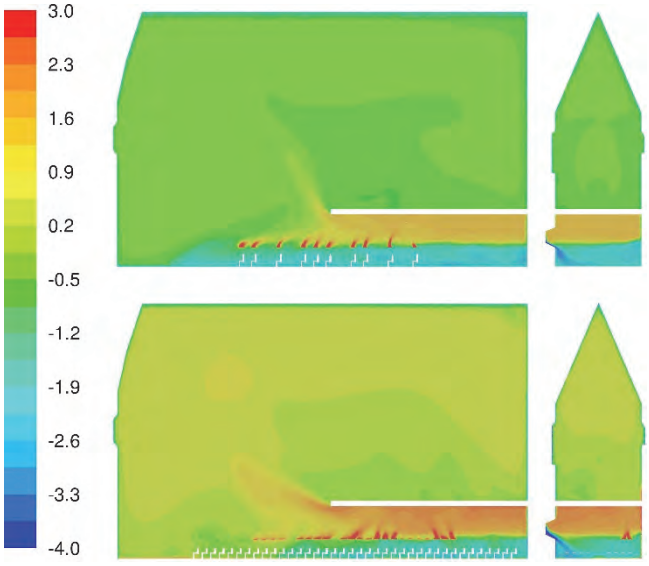

Figure 14 Temperature field, contours of the temperature [°C] 65 visitors (top), 304 visitors (bottom)

The influence of the visitors acting as heat sources is obvious. In the case with 65 visitors, the space below the gallery in the rear part of the church is colder, with more gradual stratification. In the case with more visitors, the supply air is heated up faster and the influence of the cold air flows from the low window openings is decreased.

While the lower regions of the church are strongly influenced by the visitors, the remaining space shows better thermal stability. The temperature fields in the higher regions are almost uniform in both simulations, without any significant stratification. The only disturbances are the warmer plumes rising from the space below the gallery, with the temperature higher by approx. 0.5 K than the surrounding air.

The average temperature in the church increased by 1.1 K due to the increase in the number of visitors from 65 to 304. This relatively small temperature change should not have a negative effect on the preserved internal constructions of the building. However, the average temperatures inside the church are, in both cases, just slightly above 0 °C, which is not acceptable considering the thermal comfort of visitors. A heating system should be used during winter.

It should be considered that the methodology used to simplify indoor heat sources does not perform well in the low regions above the ground. It can be expected that the temperature above the ground (up to a height of approx. 2 m) would be higher in reality, with a more gradual thermal stratification.

Ventilation flow rates

The ventilation flow rates have been evaluated for both simulated cases with the explicitly modelled visitors by summing the volume flow rates through the low window openings, see Table 1. The supplied flow rate per visitor was calculated.

Table 1 Ventilation rates

Simulated occupancy	Ventilation flow rate	Flow rate per visitor
65 visitors	1.07 m³/s	16.5 L/s
304 visitors	1.35 m³/s	4.4 L/s

The supplied volume of fresh air should be sufficient for this type of space. The minimum volume flow rate for the auditorium seating area is 2.7 L/s per person according to the ASHRAE standards [13]. The volume of fresh air per visitor in both simulated cases exceeds this minimal rate. However, according to the Czech standards, the minimal recommended volume flow rate for occupied spaces is 5 L/s [14]. Although this recommendation is indicated for forced ventilation systems only, it should be considered.

In situations with less visitors in the church, it can be advised to reduce the area of the window openings and reduce the airflow rates. In the simulated adjustment, the cold airflow supply enters the space of the seated visitors with the velocity reaching 0.65 m/s, which could cause discomfort. Partial closing of the window openings may reduce the risk of draught in the auditorium. In addition, the internal air temperature will increase.

CONCLUSION

Two CFD models of the former church with two different occupancy scenarios (65 and 304 visitors) were created in order to study the influence of the indoor heat sources (visitors) on the environment inside the building. The models of the heat sources were simplified following the previously developed methodology of substitution by simple boundary conditions generating thermal plumes. The CFD simulations were mutually compared and with the simulation without explicitly modelled heat sources also.

The presence of the visitors influences velocity patterns in the whole space and the temperature fields, especially in the regions close to the floor. The higher regions of the church show good thermal stability.

The simulation results show that it is possible to use the former church of St. Anna as a cultural space with large number of visitors, without negatively affecting the preserved building structures. The indoor air velocities in close vicinity to these structures do not exceed 0.45 m/s. The building's thermal environment shows good resistance to the occupancy fluctuation as well, especially in the higher regions, at the location of the preserved building structures and the original wooden roof trusses. The increase in the number of visitors from 65 to 304 caused a rise in the average temperature in the space of only 1.1 °C, with only a small change in the temperature fields in the higher regions.

It has been shown that natural ventilation of the building in the winter period is possible. However, it is recommended to use a heating system during winter, as the indoor air temperature is very low even in the case with 304 visitors, which would have a negative effect on the comfort of the visitors. Another concern may be the cold air supply from the low window openings that directly enters the space of auditorium, with the velocity reaching 0.65 m/s. This fast, cold air flow could be reduced by partial blocking of the window openings. However, in the situation with 304 visitors this should be accompanied by the installation of a heating system in the church, so the driving force of the natural ventilation will increase. Otherwise, the volume flow rate per visitor may not meet the values recommended by the Czech standards.

It has been shown that the previously developed methodology [8], [10] to simplify the models of the indoor heat sources is suitable for this type of study. The proposed method enabled the simplification of the heat sources' geometry and of the computational mesh around them also, but it preserved the rising thermal plumes patterns. Thus, the possibility of the variant CFD simulation study was enhanced.

REFERENCES

[1] BARTÁK, M., DRKAL, F., HENSEN, J.L.M., LAIN, M., MATUŠKA, T., SCHWARZER, J., ŠOUREK, B. Simulation to Support Sustainable HVAC Design, in *Proceeding of the 18th International Conference on Passive and Low Energy Architecture*, 2001, Floriánopolis, Brazil, pp. 7–9.

[2] BARTÁK, M., DRKAL, F., LAIN, M., SCHWARZER, J. *Obrazy proudění v kostele Sv. Anny v Praze 1* [in Czech]. Czech Technical University in Prague, Report no. 01002, 2001.

[3] XING, H., HATTON, A., AWBI, H.B. A study of the air quality in the breathing zone in a room with displacement ventilation. *Building and Environment*, 2001, 36(7), pp. 809–820.

[4] SKISTAD, H., MUNDT, E., NIELSEN, P.V., HAGSTROM, K., RAILIO, J. *Displacement ventilation in non-industrial premises*. REHVA Guidebook No. 1. Trondhaim: Tapir, 2002.

[5] AWBI, H. B. *Ventilation of Buildings*. 2nd ed. London: Spon Press, 2003.

[6] ZBOŘIL, V., MELIKOV, A., YORDANOVA, B., BOZHKOV, L., KOSONEN, R. Airflow Distribution in Rooms with Active Chilled Beams, in *Proceedings of the 10th International Conference on Air Distribution in Rooms – Roomvent 2007*, Helsinki, Finland, pp. 1-7.

[7] ZUKOWSKA, D. *Airflow interactions in rooms - Convective plumes generated by occupants* [PhD thesis]. Technical University of Denmark, 2011.

[8] ZELENSKÝ P., BARTÁK M., HENSEN J.L.M. Model sedící osoby jako zdroje tepla ve vnitřním prostředí [in Czech]. *Vytápění, větrání, instalace,* 2012, vol. 5, pp. 22–26.

[9] LAUNDER, B.E., SPALDING, D.B. The numerical computation of turbulent flows. *Computer Methods in Applied Mechanics and Energy*, 1974, (3), pp. 269–289.

[10] ZELENSKÝ P., BARTÁK M., HENSEN J.L.M. Faktory ovlivňující CFD simulaci konvekčního proudu nad zdrojem tepla ve vnitřním prostředí [in Czech]. *Vytápění, větrání, Instalace*, vol. 5, pp. 2–8, 2013.

[11] ANSYS Inc., *ANSYS Fluent User's Guide*. USA: ANSYS Inc., 2013.

[12] ZELENSKÝ, P., BARTÁK, M., HENSEN, J.L.M., VAVŘIČKA, R. Influence of turbulence model on thermal plume in indoor air flow simulation, in *Proceedings of the 11th REHVA World Congress "Energy Efficient, Smart and Healthy Buildings" – Clima 2013*, Prague, Czech Republic.

[13] ASHRAE. 2003. *Ventilation for Acceptable Indoor Air Quality*. ANSI/ASHRAE Standard 62-2001.

[14] EN 13 779 *Ventilation for non-residential buildings - Performance requirements for ventilation and room-conditioning systems.* 2010.

NOMENCLATURE

c	specific thermal capacity [J/kg·K]
d	thickness [m]
k	turbulence kinetic energy [m^2/s^2]
$y+$	dimensionless wall distance [-]
ε	turbulent dissipation rate [m^2/s^3]
λ	thermal conductivity [W/m·K]
ρ	density [kg/m^3]
SBC	subsidiary boundary condition

Ing. Marek BEGENI
doc. Ing. Vladimír ZMRHAL, Ph.D.

CTU in Prague,
Faculty of Mechanical Engineering

Energy Demand and Operating Costs Associated with Mechanical Ventilation of Classrooms

Potřeba energie a náklady spojené s provozem nuceného větrání učeben

The aim of the contribution is to determine the energy demand for ventilating classrooms with the inclusion of heat gains and to analyse the energy benefits of high heat recovery efficiency. On a simple model of the classroom, a calculation was performed in an ESP-r energy simulation programme and the operating costs of the mechanical ventilation were determined. Part of the contribution is also an analysis of the selected local ventilation units, which leads to the determination of specific financial costs for the operation of the mechanical ventilation. It was found that the total cost of continuous mechanical ventilation with a defined air flow rate is not a crucial element of a school budget.

Keywords: ventilation, school, energy demand, heat gains, heat recovery

Cílem příspěvku je stanovit potřebu energie na větrání učeben se započítáním tepelných zisků a analyzovat energetické přínosy vysokých teplotních faktorů zpětného získávání tepla. Na jednoduchém modelu učebny byl realizován výpočet v energetickém simulačním programu ESP-r a stanoveny náklady na provoz nuceného větrání. Součástí příspěvku je také analýza vybraných lokálních větracích jednotek, která vede ke stanovení konkrétních finančních nákladů na provoz nuceného větrání. Bylo zjištěno, že celkové náklady spojené s provozem trvalého nuceného větrání vybaveného zpětným získáváním tepla s definovanou dávkou vzduchu nejsou pro rozpočet školy nikterak zásadní položkou.

Klíčová slova: větrání, učebny škol, potřeba energie, tepelné zisky, zpětné získávání tepla

INTRODUCTION

The issue of school ventilation is often completely neglected, not only in the Czech Republic, where the vast majority of school buildings are equipped with openable windows with the possibility of natural ventilation [5], but air quality in classrooms is largely inadequate [4]. Natural ventilation is not automatic and depends on many factors (outdoor climatic conditions, outdoor air quality, classroom location, building location in the landscape, surroundings, building solution, human factor, etc.). Often the natural ventilation system does not ensure that the basic requirements for indoor air quality are met.

A number of studies have shown that the degraded quality of the indoor environment in schools has a negative impact on the attention and performance of pupils [1], [11]. Similarly, this is also the case for higher morbidity, which is associated with absence, including the impact on health problems that are manifested by allergies, asthma, etc. [7], [8], [9], [10]. It is certain that ventilation (whether natural or mechanical) entails operating costs (energy payments). Energy savings due to the reduction of the ventilation may seem to be justified in the context of lowering school running costs (little money for education), at a time when there is considerable pressure to reduce the energy consumption of buildings. However, the issue is much wider, has a societal character and interferes with other sectors (health, education, industry). These costs are hardly quantifiable and argumentation in favour of a healthy indoor environment in schools is extremely difficult.

Requirements for ventilating schools

According to Decree No. 410/2005 Coll. as amended, No. 343/2009 Coll. [13], the ventilation airflow rate of school buildings is 20 to 30 m^3/h per pupil, practically representing continuous ventilation. The German VDI [16] states that the permissible concentration of CO_2 is 1000 ppm in the classroom. Interestingly, however, the German VDI Directive lists relatively high CO_2 emissions from children (15.6 l/h.pupil for the 1st-4th classes, 18.9 l/h.pupil for the 5th-13th classes in the years of education), which results in relatively high airflow rates per pupil (Table 1). Higher concentrations of CO_2 than the German directive [16], but not more than 1500 ppm [14], can be accepted in the interior. The CO_2 concentration in the outdoor unpolluted environment is assumed to be 400 ppm.

Table 1 Requirements for ventilation of classrooms according to selected regulations

Regulation	Concentration limits CO_2 [ppm]	Airflow per pupil [m^3/h.pupil]			
		3 - 6 y.o.	6 - 10 y.o.	10 - 15 y.o.	15 - 18 y.o.
		Nursery school	Elementary school		High school
Decree No. 343/2009 Coll	-	20 – 30			
EN 15251	1 200	-	14 – 36		
ÖNORM H 6039:2008	1 200	-	15	19	24
VDI 6040-1	1 000	-	26	31	31

Where outdoor air is not significantly polluted, carbon dioxide CO_2 is used as an indicator of indoor air quality. On the basis of the CO_2 balance in the interior space, the minimum airflow per pupil can be determined, according to the pupil's age, resp. of school attendance. CO_2 production depends on the activity and physical proportions of a person (weight, height). The modified ASHRAE [1] relationship can be used for the calculation:

$$\dot{V}_{CO2} = 1.742 H^{0,725} W^{0,425} M \ \text{[l/h]} \quad (1)$$

For the determination of CO_2 production, the physical proportions of children can be advantageously used by standard growth charts used by paediatricians to control the correct growth of the child. The common (expected) proportion of the child is the 50% percentile, and it was used for the calculations.

The results of the airflow calculation based on CO_2 production for different limit concentrations are shown graphically in Figure 1. Table 2 shows the limit values of the air flow rate for the different levels of the educational process. As can be seen from Tab. 1, the Austrian Standard (ÖNORM H 6039:2008) permits similar considerations [17].

Table 2 Airflow rates determined on the basis of CO_2 in the room

Air quality	Concentration limits CO_2 [ppm]	Airflow per pupil [m³/h per person]			
		3 - 6 y.o.	6 - 10 y.o.	10 - 15 y.o.	15 – 18 y.o.
		Nursery school	Elementary school		Secondary school
I.	1 000	12	17	25	27
II.	1 200	9	12	18	20
III.	1 500	7	9	13	15

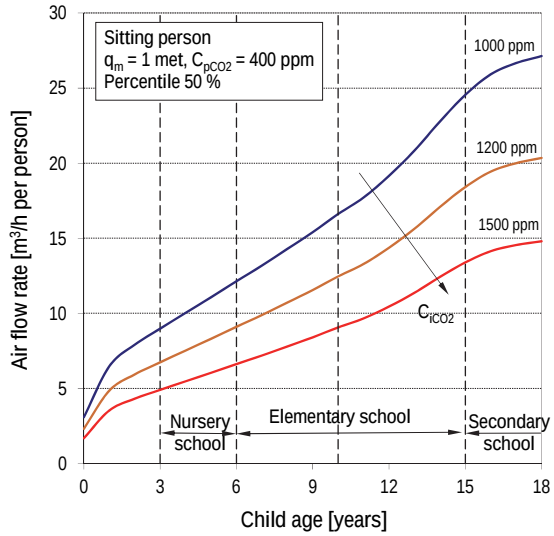

Figure 1 Airflow rate per pupil based on CO_2 balance

ENERGY REQUIREMENTS FOR VENTILATION

With today's construction requirements, heat gains significantly contribute to the overall heat balance. From the point of view of school buildings, it is mainly the internal heat gains caused by the presence of people (children) and their activities, as well as the thermal gains from the outdoor environment caused by the sun's radiation. The resulting heat flux consists of three basic items:

1) heat transmission through the wall and window,
2) heat loss by ventilation,
3) heat gains (internal and external).

Table 3 List of examined cases

A previously published analysis of the energy demand calculation for classroom ventilation [3] is based on a simplified calculation, and heat gains are practically not included (except fan gain). For a detailed analysis, it is more advantageous to use an energy simulation calculation that provides the prediction of heat loads, heat losses, indoor environment parameters, and energy demands for a given zone with the specified outdoor climate condition, usually with an hourly time step.

MODEL CASE

For the analysis, a simulation model of the classroom was constructed, the ground plan of which is shown in Fig. 2. The total floor area of the classroom is 70 m², the volume of the classroom is 245 m³.

For the purposes of this study, a classroom located in the inner building of a building with one outer wall with windows (adjacent rooms are classrooms with similar traffic and a corridor) was investigated. The orientation of the classroom was either southern or northern. The classrooms of an Elementary School, 1st level (1st to 5th years) and a Secondary School were examined. The air temperature in the classroom is considered as a constant 22 °C. The classroom is designed for 30 pupils and 1 teacher. Classroom availability for students is assumed to be 90% (27 pupils) at the time of operation, every day of the week from 8.00 to 13.00. The heat gain from the pupil was determined according to [12].

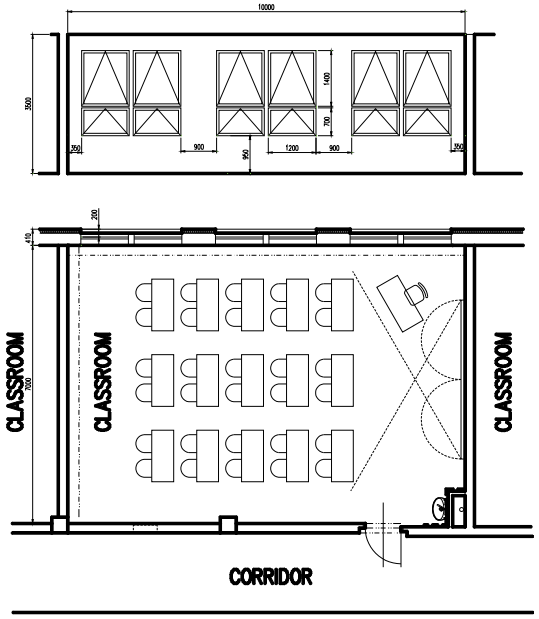

Figure 2 Floor plan of the classroom with external facade arrangement

Heat balance of the classroom

The resulting heat flux Q_t can be determined on the basis of a simplified heat equation including heat loss by walls $Q_{hl,t}$, ventilation $Q_{hl,vent}$, and internal heat gains $Q_{hg,i}$:

$$\dot{Q}_t = \dot{Q}_{hg,i} - \dot{Q}_{hl,vent} - \dot{Q}_{hl,t} \ \text{[W]} \quad (2)$$

The sign "-" in the heat equation means heat loss, the sign "+" means heat gain. For simplification, we will neglect heat gains from the sun (we are considering a north-facing room where the gains from the sun in winter are negligible - see below).

Case	Description	Outside airflow		Heat recovery efficiency Φ [%]	Supply air temperature
		Elementary school	Secondary school		
1	Infiltration ventilation / micro-ventilation	0.1 h^{-1}		0 %	t_o
2	Natural ventilation	12 m^3/h.pupil	20 m^3/h.pupil	0 %	t_o
3	Mechanical ventilation	12 m^3/h.pupil	20 m^3/h.pupil	80 %	$\Phi (t_i - t_o) + t_o$
4	Controlled ventilation as required	12 m^3/h.pupil	20 m^3/h.pupil	max. 80 % + controlled bypass	variable

The calculations were realised for the different boundary conditions outlined in Tab. 3. Case 1 represents a classroom with insufficient ventilation, Case 2 is then with sufficient natural ventilation. Cases 3 and 4 represent mechanical ventilation with heat recovery. In Case 4, the demand controlled ventilation was used with respect to the classroom heat load removing.

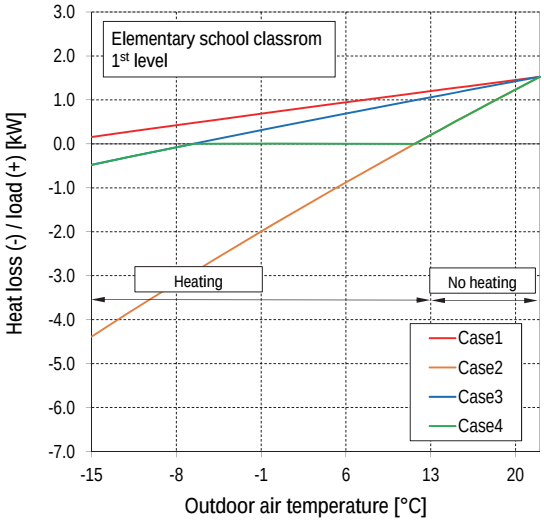

a) Elementary school, 1st level

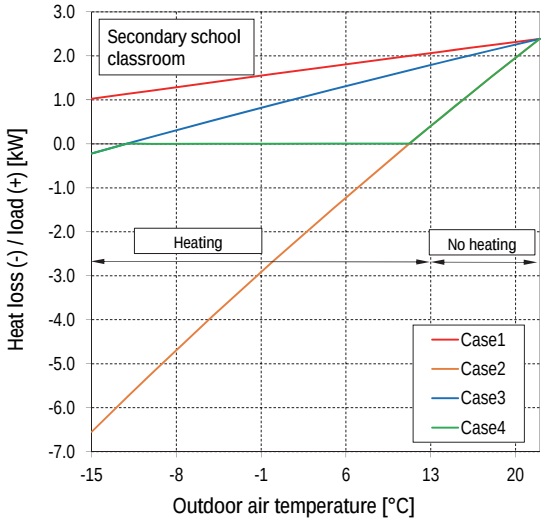

b) Secondary school

Figure 3 Heat balance of the Elementary school and Secondary school classrooms

The heat balance results are shown in Figures 3a (elementary school) and 3b (secondary school) for all the variants examined. It is clear that classroom in Case 1 is burdened by heat gains throughout the year (the resulting equation is positive - red dependence), despite the fact that we neglect the solar radiation, as a result of which the air temperature in the classroom will rise, the non-ventilated classrooms tend to overheat, which is also known from practical experience. If the permanent natural ventilation is admitted (Case 2) the effect will be the opposite - practically the whole heating period needs to be heated (orange line). In addition, commonly used heating systems cannot flexibly react to the continuous supply of outdoor air. Mechanical ventilation with high efficiency of heat recovery (Case 3) is also not an ideal solution, because the classrooms are overheated again for a significant part of the year. High requirements for the heat recovery efficiency [13] are justified, as they will only apply on the coldest days of the year (for t_o < -5).

These considerations lead to the need for **controlled ventilation** of the classrooms so that the resulting Equation (2) is zero as far as possible (Q_t = 0) – Case 4 (green dependence). This applies to the **air flow control** (based on the aiflow requirements and heat load) as well as to the **regulation of the air supply temperature**. In order to remove heat loads, it is possible to use the outside air (most of the school year t_o < 22 °C), without the use of mechanical cooling. It is advisable to regulate the air supply temperature by bypassing the heat recovery exchanger.

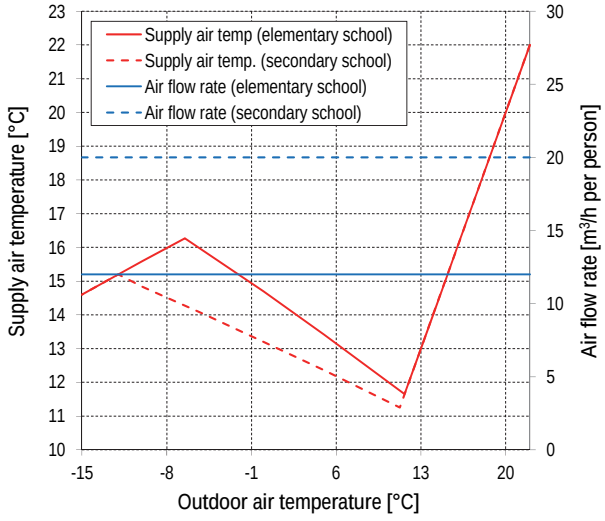

Figure 4 The supply air temperature for case no. 4

It can be seen in Fig. 4 that the air supply temperature for the thermal load discharge is relatively low (for the secondary school $t_{s,min}$ = 11.5

°C) and the difference in temperature of the inlet and supplied air is Δt_s = 10.5 °C. An integral part of the ventilation system must be, in addition to a controlled bypass, a suitable air distribution system (diffusers ensuring the diffusion of the supplied air into the space without any negative effects on the people). The heat load discharge can, of course, also be solved by increasing the air flow if the device allows it.

For temperatures t_o > 13 °C, natural ventilation with higher airflows can be applied to a maximum extent. From an energy point of view, this does not pose any problem as the heating system is no longer in operation.

SIMULATION

The energy demand for air heating is normally included in the need for heating. In most cases, it is difficult to separate these two values from each other, especially when heat gains enter the equation.

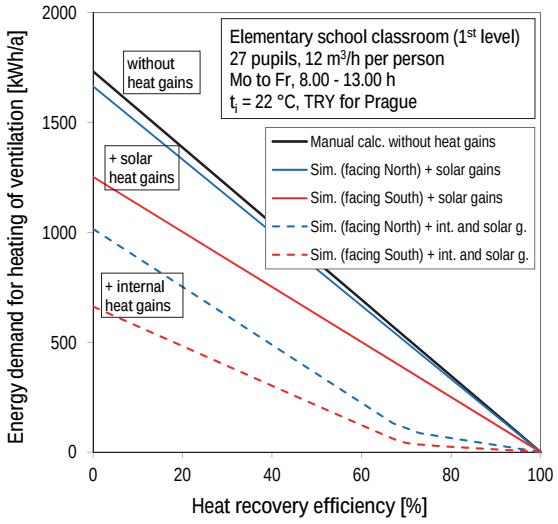

a) Elementary school, 1st level

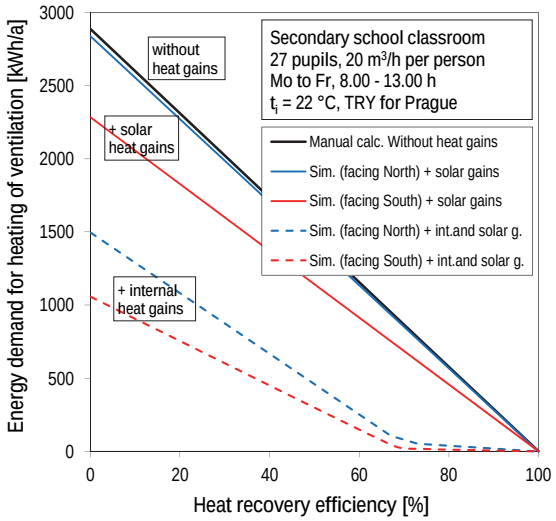

b) Secondary school

Figure 5 Energy demand for outdoor air heating - results

Figure 5 shows the heat demand for ventilation depending on the efficiency of the heat recovery exchanger. The heat recovery efficiency is equal to 0% when the ventilation system is not equipped with a heat recovery, e.g., natural ventilation or under pressure mechanical ventilation. The heat recovery efficiency represent the yearly average value at the time the device is operating. The black curve represents the results of the manual calculation published in the article [3] (without considering the heat gains). The remaining dependencies were obtained based on the simulation. The red curve applies to the south-facing room, blue to the north. Dashed curves represent the realistic simulation results with consideration of both internal and external heat gains.

The heat demand for the ventilation of a model elementary school equipped with mechanical ventilation with a temperature factor of 67% (minimum requirement in accordance with [13]) is 131 kWh/year (for a north-facing classroom). In the case of a south-facing classroom, it is 61 kWh/year. At the average heat price of 500 CZK/GJ (€ 19.2/GJ) (it can actually range from 300 to 700 CZK/GJ, i.e., € 11.5 to € 30/GJ), this represents a cost of max. 236 CZK/year (€ 9/year) for a north-facing classroom and 163 CZK/year (€ 6.3/year) for a south-facing classroom, **i.e., a max. 6 CZK/year per pupil (€ 0.34 or € 0.23 respectively per year per pupil)!** In fact, this amount is even lower, as the heat gain from the intake fan (see below) will be reflected in the final equation. Similar results were also obtained in the secondary school room calculations. The heat demand for mechanical ventilation with heat recovery (HR) should not be an obstacle to its operation.

Note: Exchange rate for calculation 1 € = 26 CZK

Heated air from the fan

All the power of the fan, which is placed in the air stream together with the electric motor is converted to heat and contributes to the heating of the air. We assume that the supply fan takes one half of the total power consumption of the unit. The total heat demand for outside air heating reduced by the input fan for one of the examined variants is shown in Fig. 6 (*SFP* is the specific fan power).

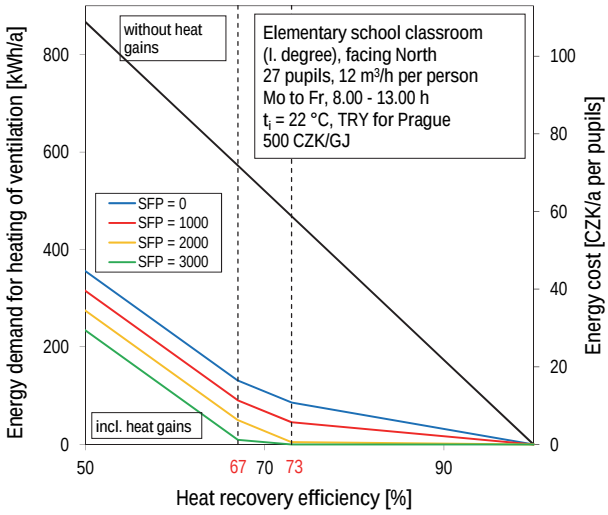

Figure 6 Energy demand for outdoor air heating when considering the heating of the air from the supply fan

The results are displayed for different *SFP* (coloured curves) values. The black line shows the heat demand without considering the heat gains. From the analyses of the ventilation units on the Czech market (see below) it was found that most units reach *SFP* values up to 3000 W.s/m³. For units with *SFP* > 3000 W.s/m³ and heat recovery Φ > 67%, it is not practically necessary to heat the air. This, of course, does not mean that the use of high-power units (high *SFP*) is energy efficient. The price for electricity is often higher than the price for thermal energy.

Figure 6 also sums up the indicative cost of heating the ventilating air for the examined classroom per pupil. The results take the heat load and heated air in the intake fan into account. As already mentioned, the cost of heating the ventilation air using mechanical ventilation is very low. The price for thermal energy may vary according to the heat source used or by region (district heating is used in about 1/3 of the schools) [5].

VENTILATION OPERATING COST

Figure 7 summarises the total ventilation cost per one pupil of the elementary school room considered, taking the need for electric power to drive the unit into account. The points in the graph represent the specific parameters of the ventilation units. For the purposes of this article, 19 local heat recovery ventilation units available on the Czech market (without specification) were analysed with a nominal flow of 350 resp. 540 m³/h, the transport pressure of the units was considered to be 50 Pa (the price for electric energy was considered to be 4.25 CZK/kWh).

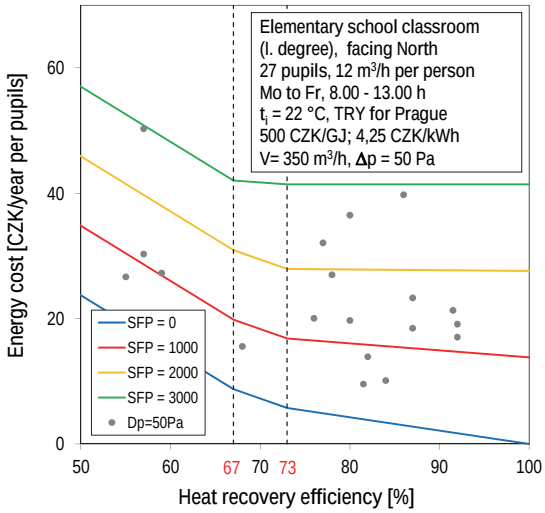

a) Elementary school, 1st level

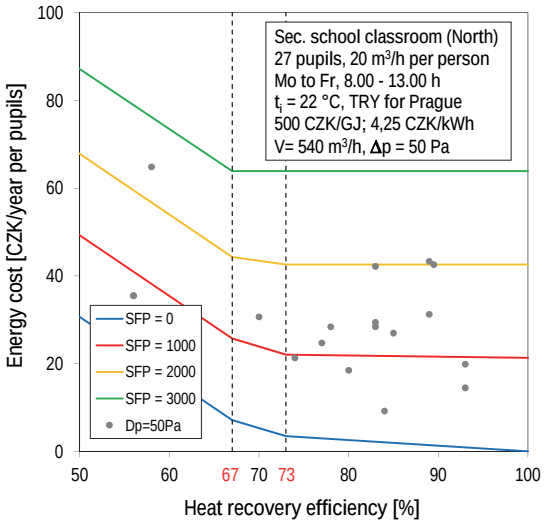

b) Secondary school

Figure 7 Operation cost of mechanical ventilation for different types of local ventilation units

The technical data, i.e., the power input and the efficiency of the HR, was taken from the technical documentation of the HVAC manufacturers. It is clear from Fig. 7 that most units achieve *SFP* values up to 3000 W.s/m³.

The cost of ventilation operation, depending on the type of local ventilation unit used, with heat recovery efficiency $\Phi \geq 67\%$, ranges from 10 to 52 CZK / year per pupil (€ 0.38 to € 2 per year per pupil), for the classroom located in the internal tract buildings facing north). As you can see, the cost of the ventilation operation depends on the unit type, its specific fan power *SFP* and the efficiency of the HR. It is evident from Fig. 7 that a higher efficiency of the HR does not mean lower operating costs. The power input of the unit and, of course, the energy prices are essential. The actual consumption differs from the presented energy demand results - for mechanical ventilation with HR, this difference is not very significant.

CONCLUSIONS

In addition to maintaining indoor air quality, ventilation helps to reduce heat load and prevents the room overheating, even during the winter months. Due to the possible discomfort, it is not possible to continuously supply outside air without heating. On the other hand, it appears that it is necessary to bring air into the classroom at a lower temperature than the air temperature in the room for most of the year, which leads to the consideration of the need to use exchangers with high heat recovery efficiency and their benefits. Devices with a lower heat recovery efficiency will probably have less pressure loss, resulting in lower fan power consumption.

From these analyses it is clear that the operation costs of mechanical ventilation with heat recovery are minimal. In fact, it will also be necessary to consider the cost of filter replacement (usually once every 3 months), maintenance and service. The calculation is subject to some inaccuracies because it works with the energy demand rather than the energy consumption. The real heat consumption will be affected by the efficiency of the individual building HVAC systems i.e., heat sources, heating systems, power distribution, etc. These analyses were beyond the scope of the presented study.

REFERENCES

[1] ASHRAE Handbook 2009 Fundamentals. 2009, Atlanta: ASHRAE. ISBN – 978-1-933742-55-7

[2] BAKÓ-BIRÓ, Z., et al. Ventilation rates in schools and pupils' performance. Building and Environment, 2012, 48: 215-223.

[3] BEGENI, M., ZMRHAL, V. Energy Demand for Classrooms Ventilation. In: Heating, ventilation, Sanitary Installation. 2015, Vol. 24, Issue 5, pp. 218-222. ISSN 1210-1389

[4] BEGENI, M., ZMRHAL, V. Ventilation of Elementary School Classroom. In: Heating, ventilation, Sanitary Installation. 2014, Vol. 23, Issue 4, pp. 180-183. ISSN 1210-1389

[5] BEGENI, M., ZMRHAL, V. A questionnaire survey of the state of school buildings. In: TZB info. ISSN 1801-4399. 2015.

[6] CLEMENTS-CROOME, D. J., et al. Ventilation rates in schools. Building and Environment, 2008, 43.3: 362-367

[7] DAISEY, J. M.; ANGELL, W. J.; APTE, M. G. Indoor air quality, ventilation and health symptoms in schools: an analysis of existing information. Indoor air, 2003, 13.1: 53-64

[8] MENDELL, M. J., et al. Association of classroom ventilation with reduced illness absence: a prospective study in California elementary schools. Indoor air, 2013, 23.6: 515 - 528.

[9] SIMONI, M., I. ANNESI-MAESANO, T. SIGSGAARD, et al. School air quality related to dry cough, rhinitis and nasal patency

in children. European Respiratory Journal [online]. 2010, 35(4), 742-749 [cit. 2016-09-21]. ISSN 0903-1936.

[10] SUN, Y., Y. ZHANG, L. BAO, Z. FAN a J. SUNDELL. Ventilation and dampness in dorms and their associations with allergy among college students in China: a case-control study. Indoor Air [online]. 2011, 21(4), 277-283 [cit. 2016-09-21]. ISSN 09056947.

[11] WARGOCKI, P, WYON D., P., a P. Ole FANGER. The performance and subjective responses of call-center operators with new and used supply air filters at two outdoor air supply rates. Indoor Air [online]. 2004, 14(s8), 7-16 ISSN 0905-6947

[12] ZMRHAL, V. Heat Gains from the People as a Basis of Energy Simulation. In: Heating, ventilation, Sanitary Installation. 2016, Vol. 25, Issue 4, pp. 234-239. ISSN 1210-1389

[13] Czech decree no. 410/2005 (343/2009), on hygiene requirements for premises and operation of facilities and facilities for education and education of children and adolescents.

[14] Czech decree no. 20/2012, about technical requirements on building construction.

[15] Comission Regulation (EU) No 1253/2014 of 7 July 2014 implementing Directive 2009/125/EC of the European Parliament and of the Council with regard to ecodesign requirements for ventilation units.

[16] EN 15251: 2011 Indoor environmental input parameters for design and assessment of energy performance of buildings-addressing indoor air quality, thermal environment, lighting and acoustics

[17] VDI 6040 Air-conditioning - Schools - Requirements (VDI Ventilation Code of Practice, VDI Code of Practice for School Buildings

[18] ÖNORM H 6039:2008 Ventilation and air conditioning plants – Controlled mechanical ventilation of classrooms, training rooms or common rooms as well as of rooms for similar purposes – Requirements, dimensioning, design, operation and maintenance

NOMENCLATURE

H	height of the body [m]
M	metabolic heat [met]
Q	heat flux [W]
SFP	specific fan power [W.s/m^3]
t_i	indoor air temperature [°C]
t_o	outdoor air temperature [°C]
V_o	ventilation air flow rate [m^3/h]
V_{CO2}	production of CO_2 [l/h]
W	weight of the body [kg]
Φ	heat recovery efficiency [%]

Abbreviations

CZK	Czech crowns
HR	heat recovery
HVAC	heating, ventilation and air-conditioning
SFP	specific fan power

Ing.arch. Vojtěch MAZANEC
Ing.arch. Martin KNY, Ph.D.
prof. Ing. Karel KABELE, CSc.

CTU in Prague,
University Centre of Energy Efficient Buildings

The impact of the Human Body's Convective Boundary Layers on the Design of a Personalized Ventilation Diffuser

Vliv mezních vrstev lidského těla na návrh vyústky pro osobní větrání

The paper deals with the specifications of a settable range of air volumes for a personalized ventilation system to provide an appropriate fresh air supply to the user. It mainly deals with the interaction of fresh air flow and human convective boundary layers and the difference in various volumes and velocities. Measurement of the flow interaction was taken by a Particle Image Velocimetry (PIV), using a thermal manikin to simulate the environment around the human body.

Keywords: diffuser, personalised ventilation, PIV, convective boundary layers

Článek se zabývá vhodným zvolením rozsahu možného nastavení objemu přiváděného vzduchu pro personalizované větrání, aby bylo dosaženo vhodné distribuce k uživateli. Primárně se tak potýká s interakcí přiváděného vzduchu s konvektivními mezními vrstvami okolo lidského těla s proudem přiváděného vzduchu při různých objemech a tedy i rychlostech. Měření vzájemné interakce proudění bylo prováděno metodou Particle Image Velocimetry, za použití termálního manekýna k simulaci prostředí okolo lidského těla.

Klíčová slova: vyústka, osobní větrání, PIV, konvekční hraniční vrstvy

INTRODUCTION

Personalized ventilation is one of the modern alternatives to solve efficient air distribution and to create a pleasant microenvironment in offices and any other fixed workspace [1] [6]. The efficiency lies in distribution of the fresh air direct to the user by personalized local diffusers, which are mostly mounted on the table. It sounds simple, but there are many influences in the local place, which can dramatically decrease the effect of the personalized ventilation. One of those things is the user himself, specifically the user's body. The human body produces metabolic heat and this heat is emitted to the surrounding air. The temperature gradient between this heated air and the surroundings creates a convective upward airflow around the body [2] [3] [4]. The velocity and impact of these convective boundary layers depend on the temperature difference between the body and the environment. The convective boundary layers are capable of carrying many pollutants created by the human body to the person's breathing zone, and those pollutants can negatively impact the perceived air quality [2].

Figure 1 Convective boundary layers around the sitting human body.

It has been proven that convective boundary layers interact with the ventilation system [2] [5] and especially with personalised diffusers [3]. The study of the interaction between personalised ventilation and human convective boundary layers [3] shows that the real impact of personalised ventilation can be quite different due to the boundary layers. In the mentioned study of personalised ventilation, only 30 % of the supplied fresh air reached the user's breathing zone, when the boundary layers were fully developed. On the contrary, when the boundary layers were broken by a movable table panel or air intake, the effectivity of the inhaled air increased to 90 %.

In our task, we designed personal ventilation diffusers for use in a workspace of air traffic dispatcher. The air flow rate is manually controlled by the user, but according to the previous mentioned studies, there are flow rates with absolutely inefficient velocities, which would not even reach the user and can be even less effective than mixed ventilation. On the contrary, high velocities are efficient, but may become really uncomfortable over longer use.

The main task of this measurement was the range of the controller that we should use to make our system both comfortable and efficient for the user.

PROTOTYPE MEASUREMENT

To measure the diffuser and boundary layers flow interaction, we used a Particle Image Velocimetry (PIV) system. This system uses fast capturing cameras to track small particles diffused in the air. To specify the measured particles, a laser layer is used to light up the particles. From the captured images, it is able to calculate the exact velocity vectors of the airflow.

To study the interaction, we divided the measurement into three parts. The first measurement was focused on the airflow of the selected diffuser. The second one measured the velocities of the convective boundary layers around the body of the thermal manikin and the third combined the two previous ones to measure the interaction between them. We measured three different flow rates, which means three different velocities at the diffuser.

PIV setting

For our measurement, we used oil bubbles with a size of 100 – 1000 nm as tracing particles. The particles were equally dispersed in the room's air without any supplementary flow and they were dispersed in the supply air in the measurements of the diffusor.

For the diffusor and manikin measurement, only one camera was used. But to capture the flow interaction, we used two cameras next to each other to increase the measured area.

The calculation of the average velocities was made from fifty continually captured images.

The room ventilation system was turned off to provide steady air conditions. The air temperature was set to 23 °C with a deviation up to 0.5 K. The measured ambient air velocity in steady conditions was in the range from 0.03 to 0.12 m/s. Measurements were made for isothermal flow, it means that the temperature of the supply air was the same as the temperature of the ambient air.

Thermal manikin setting

Because convective boundary layers depend on the temperature gradient, they are different with each different kind of clothing. From our research questionnaire, we approximated some standard clothing that the dispatcher's wear at work and we used that to simulate some standard situation in the office. We used a long-sleeved shirt and trousers to set the thermal insulation value to 0.54 clo.

The manikin was set to a standard surface temperature of 35 °C. The manikin was not breathing in order to measure the average speed around the breathing zone without the velocity of the breath.

The diffuser measurement

At first, we just measured the diffuser to get the main information about the flow. We measured both the vertical and horizontal plane. The diffuser was mounted to the table as it should be in the real situation. The supply air had the same temperature as the environment.

The size of the diffuser is 50 x 300 mm and is set in a vertical position, 140 mm above the table plane. It is divided by 5 partitions on the vertical plane and there are 9 lamellae to shape flow on the horizontal plane. The size is based on the conditions of the dispatcher's workspace, which are quite limited, and to provide 25 m^3/s with an average velocity of 0.2 m/s in the diffuser plane. We used 25 m^3/s of supply air for the measurement of the flow according to actual legislature.

We can easily notice the partitions on the vertical plane. However, it forms one united flow after a distance of 350 mm. The flow forms cylinder with higher velocities in its core. The core is about 270 mm above the table, which is planned to correspond with the height of the upper part of the chest bone of the sitting user. Dispersion in the vertical plane is higher than in the horizontal one, which is not the effect we hoped for, but it was given by the size of the diffuser.

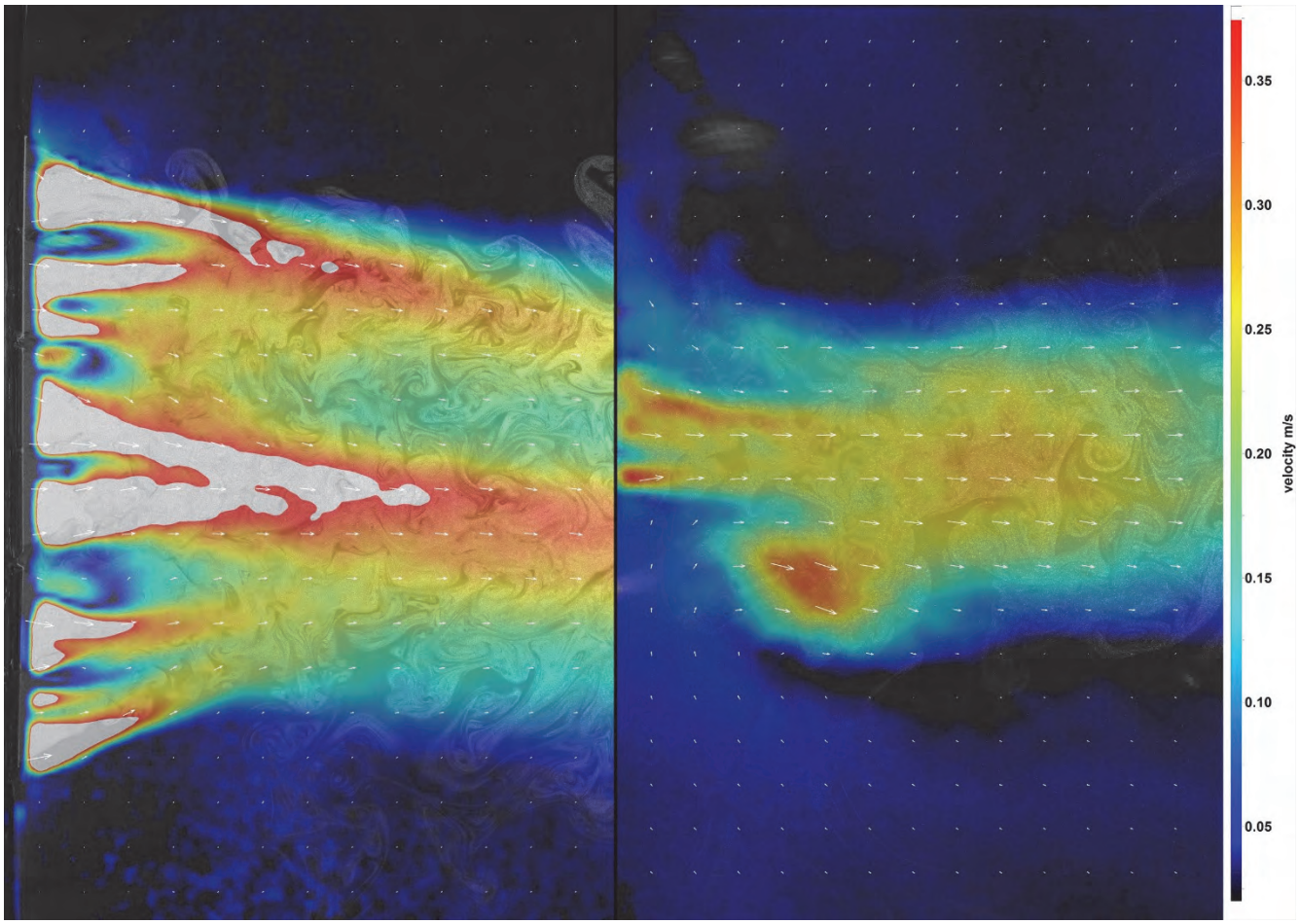

Figure 2 PIV vertical (left) and horizontal (right) vector field of the diffuser

Measurement of the convective boundary layers

The second measurement was focused on the boundary layers around the body. To simulate the human body, we used a thermal manikin to reach its steady state when the diffuser is turned off. The results of the measurement are shown in Figure 3.

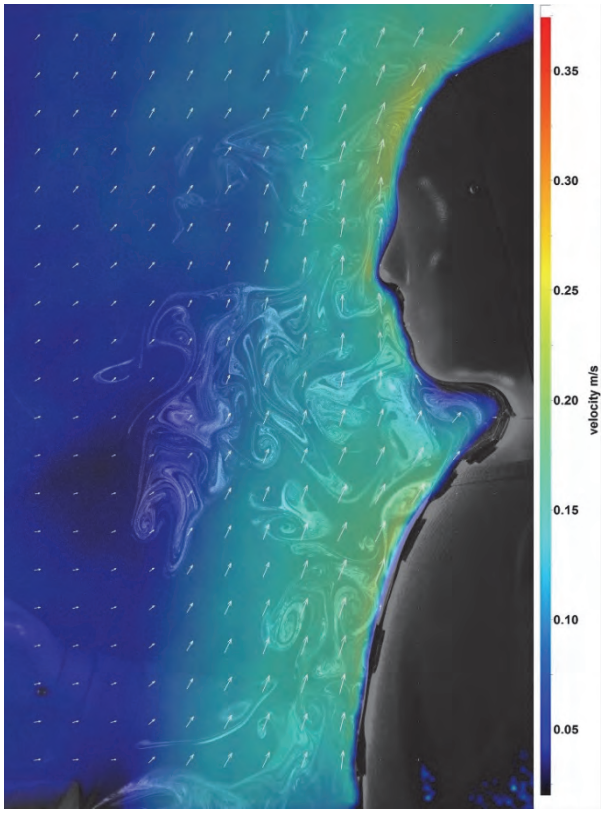

Figure 3 Vector field of the boundary layers

We can see the upward flow of the boundary layers around the manikin. The velocity range is from 0.1 m/s to 0.25 m/s and the width of the layer is about 100 mm at the height of the chest and about 70 mm at the height of the head. The fastest flow is around the large surfaces, like the chest, and around the head of the manikin. Also, the hands have their own influence, but it is only partially involved in the measured layer.

The figure shows the impact of the boundary layers to our comfort and environment. In steady air conditions, we mainly breathe the air that came from around our feet. When it reaches the breathing zone, it is already polluted by body odours and pollutants.

Measurement of the flow interaction

The third measurement combines two previous ones. We measured the thermal manikin and the diffuser together to measure the interaction of those two flows. The manikin and diffuser were set to the same settings as before.

The diffuser was in front of the manikin at a distance of 950 mm from the manikin's body. The laser layer was set from behind the diffuser in order to exactly measure the flow around the body. The settings of the measurement are shown in Figure 4. The measured plane captures the distance of 600 mm in front of the manikin.

We divided the measurement into parts with different speeds, to find out which speed is sufficient to penetrate the layers. Three different air flow volumes were used: 15 m³/h, 25 m³/h and 30 m³/h, parallel to the average velocities 0.12 m/s, 0.2 m/s, and 0.24 m/s in the plane of the diffuser. From the previous testing, we assumed that the first flow rate will not be sufficient to penetrate the boundary layers, the second should one be, but with limited efficiency, and the third should be the most efficient, but on the edge of comfortable use.

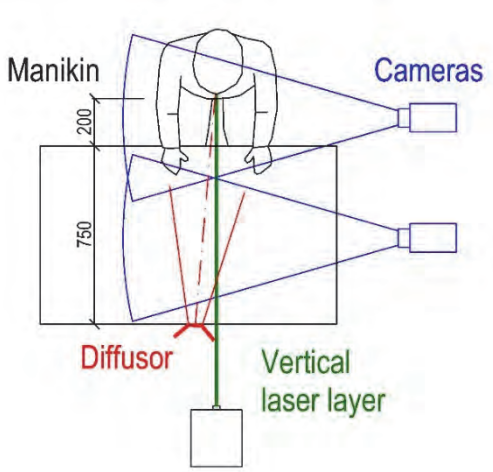

Figure 4 Settings of the flow interaction measurement

The lowest flow rate (of 15 m³/h) results are shown in Figure 5. We can see that the core is reaching a maximum velocity of 0.18 m/s at the maximum measured distance (600 mm from the manikin), but it decreases toward the manikin. At the distance of 220 mm (the gap between the pictures), the flow is almost scattered and has almost no influence on the boundary layers. Most of the fresh air just moved upward with the boundary flow and the effect of the ventilation with these velocities is marginal for the user.

We can see better results in Figure 6, where the results of the second flow rate of 25 m³/h are shown. The velocity in the core is higher, about 28 m/s, and it makes a real difference. The airflow from the diffuser is combined and mixed with the air transported by the boundary layers in the breathing zone. That means a user will partially breathe fresh air and partially breathe the polluted air transported by the upward flow. However, the boundary layers still have a great influence on the air in the breathing zone.

In the third situation, the flow rate of 30 m³/s, we can see a difference. The results of the measurement in Figure 7 show how the higher velocities affect the flow around the body.

The core velocity is up to 0.38 m/s and the flow reaches the manikin in the velocity of 0.25 m/s at the upper chest and neck. But there is a real difference in how it affects the boundary layers. In the previous measurements, the main source of heat was the chest and head, but in this situation, the airflow from the diffuser cools those surfaces and lowers the temperature difference. Then the body generates a weaker upward flow, which causes the supply air not to flow upwards, as in previous situation, but it goes around the neck behind the manikin (This effect was also measured with radiant cooling panels [2]). Both effects have a real impact on the effectivity of personalized ventilation, because most of the fresh air now reaches the breathing zone. We can say that increasing the air volume by 5 m³/h has a much greater positive effect.

On the other hand, it can have a negative impact on the personal temperature comfort, because it cools the sensitive parts of the body, like the neck and upper torso.

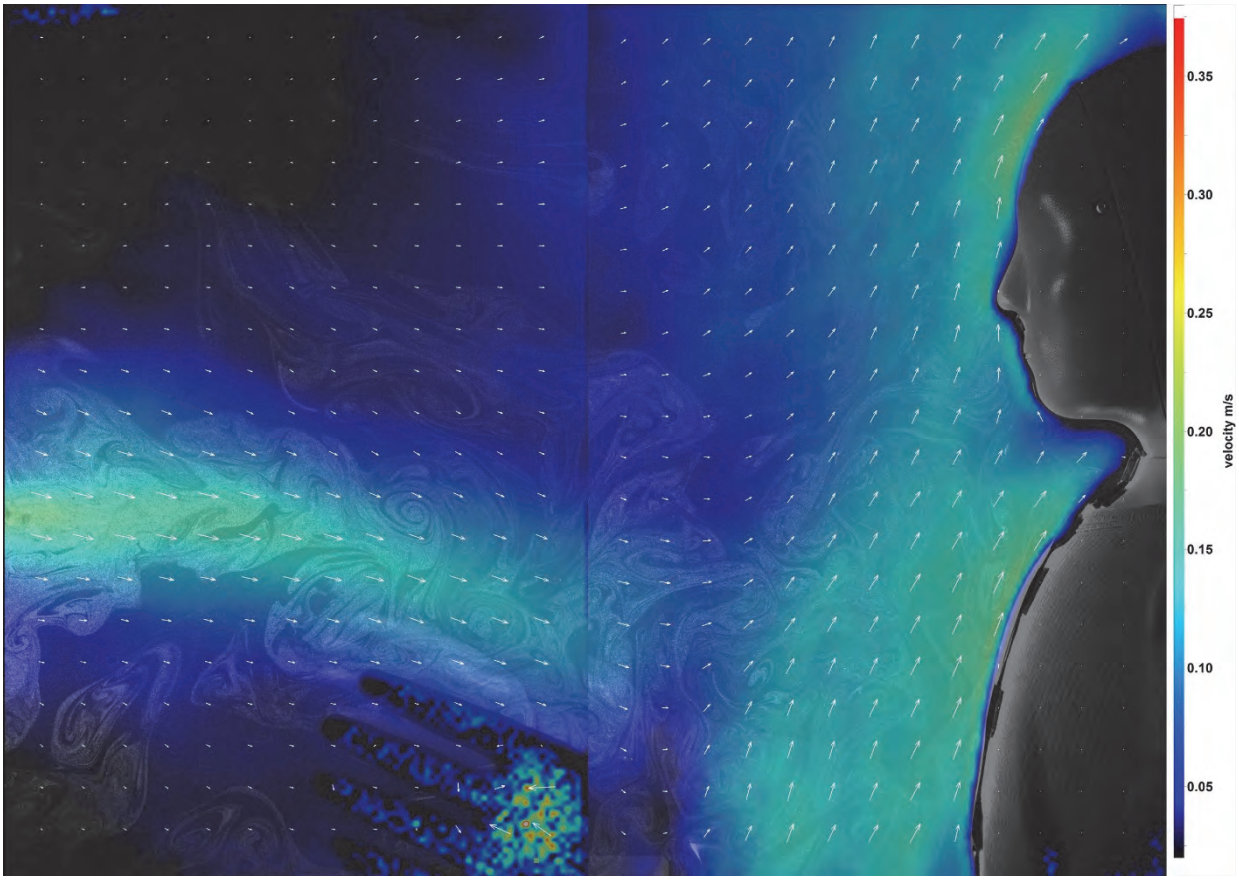

Figure 5 Interaction of the flows with a supply of 15 m³/h

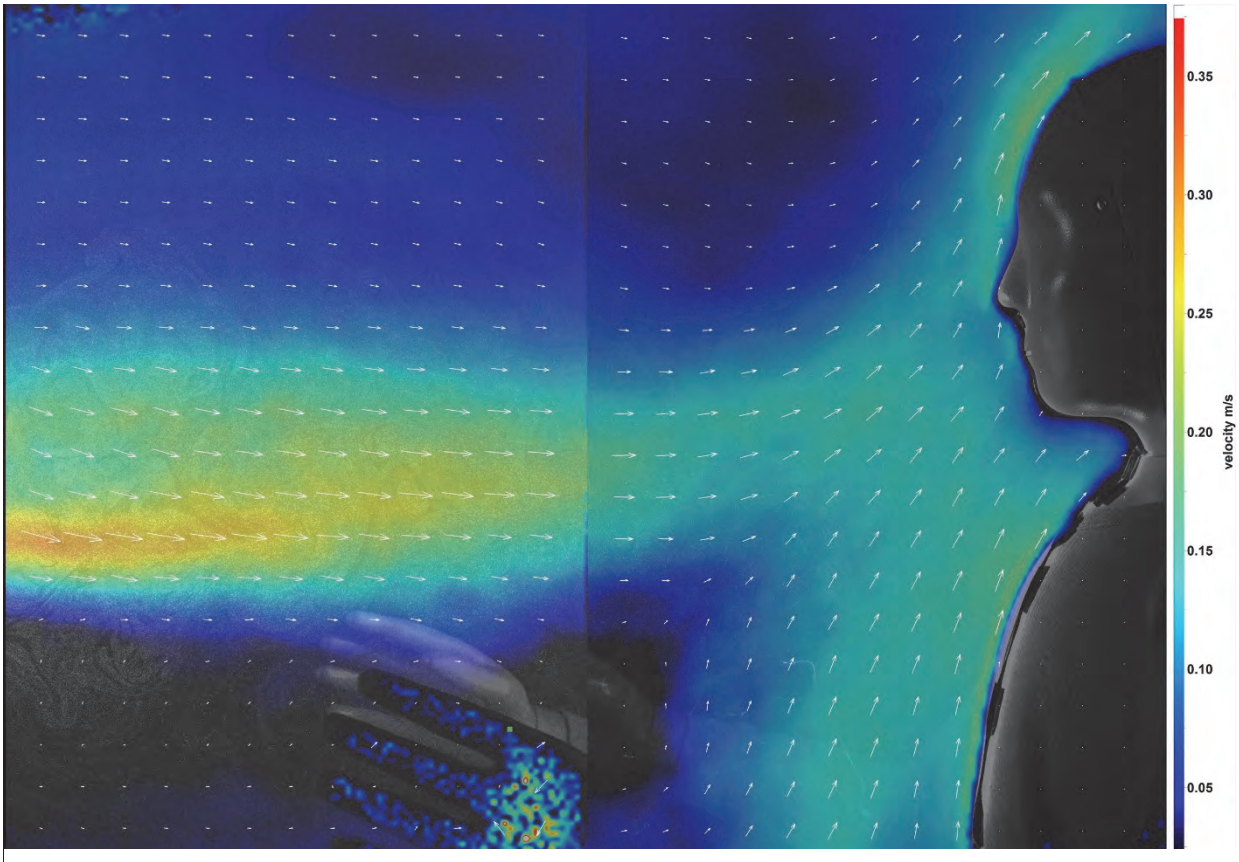

Figure 6 Interaction of the flows with a supply of 25 m³/h

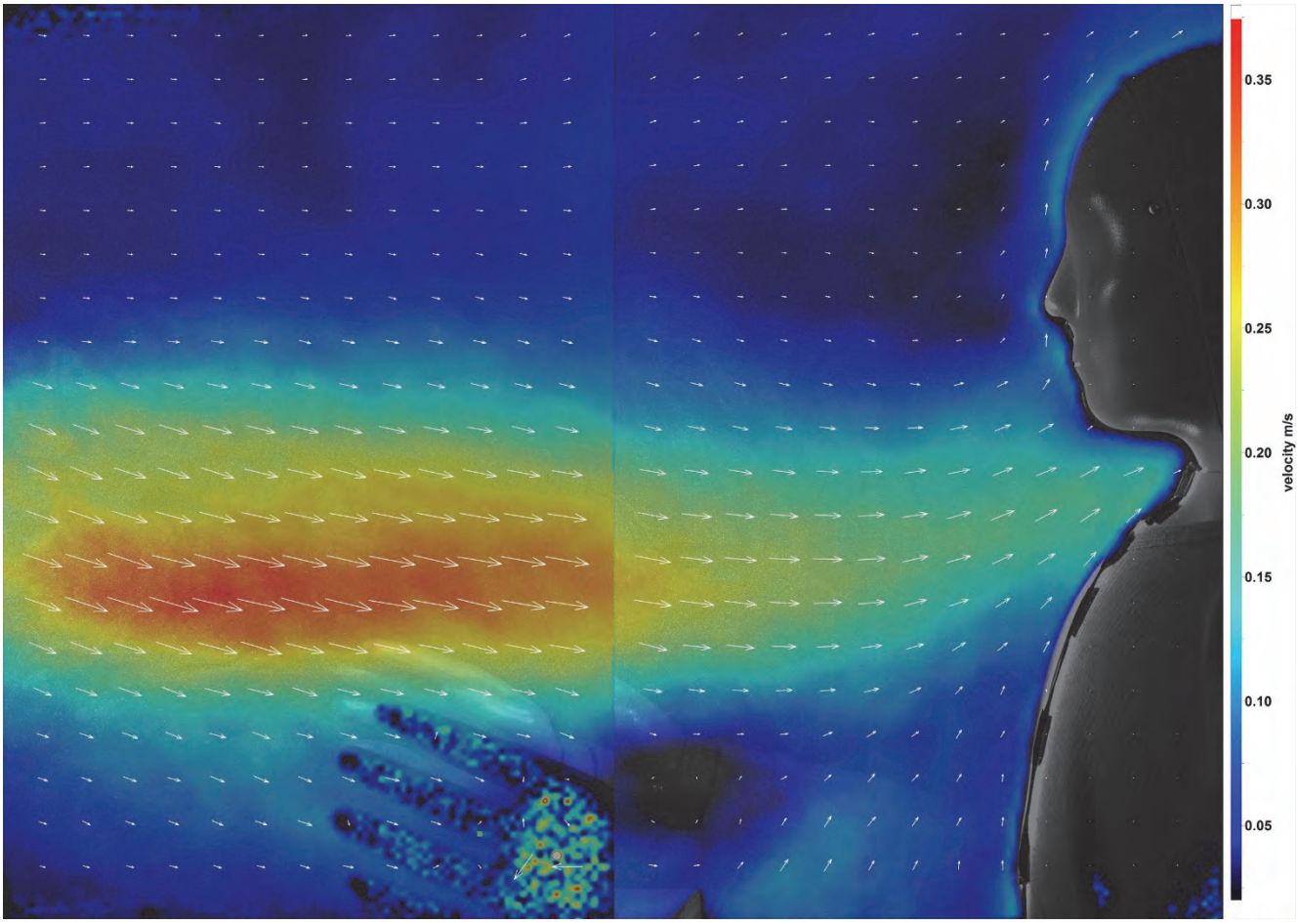

Figure 7 Interaction of the flows with a supply of 30 m³/h

CONCLUSION

We measured three different flow rates to get information about what range we should choose to personalise the flow rate. We can say from the results that the lower limit for the controller should be around 20-22 m3/h, where the ventilation starts to have a positive effect to the user. The upper limit should be set to around 30 m³/s, where it is already around the maximum efficiency. However, the upper limit is not only dependent on measured effectivity itself. The upper limit should be more exactly determined by the thermal comfort of the user. In the next study, we should use a thermal manikin to measure the influence of higher velocities on the body's temperature to set the point more exactly.

ACKNOWLEDGMENT

This work has been supported by the Ministry of Education, Youth and Sports in the project NPU I no. LO1605 - University Centre for Energy Efficient Buildings - Sustainability phase

REFERENCES

[1] MELIKOV, A. K. *Advanced air distribution: improving health and comfort while reducing energy use*. Indoor Air 2016, 26: 112–124. doi:10.1111/ina.12206

[2] LICINA, D., MELIKOV, A., SEKHAR, C. and THAM, K. W., *Human convective boundary layer and its interaction with room ventilation flow.* Indoor Air 2015, 25: 21–35. doi:10.1111/ina.12120

[3] MELIKOV A. K. *Human body micro-environment: The benefits of controlling airflow interaction.* Building and Environment. 2015; 91:70-77. Available from, DOI: 10.1016/j.buildenv.2015.04.010

[4] LICINA D, MELIKOV A. K, SEKHAR C, THAM K. W. *Air temperature investigation in microenvironment around a human body.* Building and Environment. 2015; 92:39-47. Available from, DOI: 10.1016/j.buildenv.2015.04.014

[5] HOMMA, H. AND YAKIYAMA, M. *Examination of free convection around occupant's body caused by its metabolic heat*, ASHRAE Trans., 94,104–124.

[6] ČERMÁK, R. MELIKOV A. K. *Personalized Ventilation*. Vytápění, větrání, instalace 5/2003, pp. 199-202. ISSN 1210-1389.

Ing. Aleš VLK
Ing. Jiří NOVÁK, Ph.D.

CTU in Prague,
Faculty of Civil Engineering

Impact of Airtightness on the Heat Demand of Passive Houses in the Central European Climate

Vliv vzduchotěsnosti na potřebu tepla na vytápění pasivních domů v klimatických podmínkách střední Evropy

This calculation study investigates the impact of the airtightness of a building envelope on the heat demand of a single-family house and a multi-family residential building in the Central European climate (Prague). Both model buildings are passive houses, equipped with a balanced mechanical ventilation system with heat recovery. For the purpose of this study, transient thermal and air infiltration models were developed using Matlab – Simulink. The single-family house was modelled as a single zone building. In the multi-family building, each flat and the staircase were considered as separate pressure zones. Iterative approaches were adopted for the reliable coupling of the thermal and air infiltration models (different in the single and multi-zone models). Their heat demand was calculated as a function of the envelope airtightness (n_{50} varying from 0 to 1 h^{-1}). Several combinations of leakage distribution over the building envelope, wind shielding and alternatives of the internal leakage paths between the zones were considered. The heat demand increases noticeably with the building envelope air permeability. The increase is more pronounced in the case of the residential building (e.g., 3 kWh/(m^2·a) per unit of n_{50} against 2 kWh/(m^2·a) for the single-family house under the same conditions). The wind shielding and the leakage distribution significantly influence the results. The internal air leakage does not significantly affect the heat demand of the residential building, which mostly depends on the air leakage of the envelope and its distribution. However, significant air flow rates were detected between the zones (up to 24 m^3/h between the flats). The internal leakage may, therefore, cause an issue for indoor air quality, ventilation system function and fire safety.

Keywords: Airtightness, air leakage, heat demand, thermal simulation, airflow simulation, passive houses

Tato výpočtová studie zkoumá vliv vzduchotěsnosti na potřebu tepla na vytápění rodinného a bytového domu v klimatických podmínkách střední Evropy (v Praze). Obě zkoumané budovy jsou pasivní domy, vybavené nuceným rovnotlakým větracím systémem se zpětným získáváním tepla. Pro obě budovy byl v prostředí Matlab – Simulink sestaven nestacionární tepelný model a model proudění vzduchu. Rodinný dům byl modelován jako jediná teplotní a tlaková zóna. V případě bytového domu bylo každé podlaží s byty a schodišťový prostor modelováno jako samostatná tlaková zóna. Vzájemné propojení tepelného modelu a modelu proudění využívá iterační postupy – odlišné v případě jednozónové a vícezónové budovy. Potřeba tepla na vytápění obou budov byla počítána opakovaně, v závislosti na vzduchotěsnosti obálky budovy (různé hodnoty n_{50} od 0 do 1 h^{-1}). Uvažovaly se různé kombinace rozložení netěsností po ploše obálky budovy, stínění budovy proti větru a vzduchotěsnosti vnitřních konstrukcí. Potřeba tepla na vytápění se znatelně zvyšuje s rostoucí průvzdušností obálky budovy. Nárůst je vyšší v případě bytového domu (o 3 kWh/(m^2a) při zvýšení n_{50} o 1 h^{-1} oproti 2 kWh/(m^2a) v případě rodinného domu za stejných podmínek). Stínění proti větru a rozložení netěsností po ploše obálky významně ovlivňuje výsledky. Netěsnosti ve vnitřních konstrukcích potřebu tepla na vytápění bytového domu příliš neovlivňují. Podstatná je velikost netěsností v obvodových konstrukcích a jejich rozdělení po ploše obálky budovy. Šíření vzduchu mezi jednotlivými zónami (průtok vzduchu mezi byty dosahoval až 24 m^3/h) by však mohlo negativně ovlivnit kvalitu vnitřního vzduchu, správnou funkci větracího systému a požární bezpečnost.

Klíčová slova: Vzduchotěsnost, proudění vzduchu, potřeba tepla na vytápění, simulace tepelného chování budovy, simulace proudění vzduchu budovou, pasivní domy

INTRODUCTION

Excessive air leakage through the building envelope may substantially increase the infiltration heat loss. Consequently, the heat demand increases, which results in a lower energy efficiency of the building. This impact is particularly significant in the case of well insulated buildings equipped with a mechanical ventilation system with heat recovery, where the transmission and ventilation heat losses are minimised. This is the reason why strict airtightness requirements were set for this category of buildings (e.g., n_{50} < 0.6 h^{-1} for passive houses).

Compliance with such a low limit value of n_{50} requires special design approaches during the planning phase, particular care, systematic control and use of special products during construction. Although the building industry has progressively adopted suitable strategies to achieve very good airtightness, building practitioners and investors still ask whether strict requirements are justified and which effect would produce a deviation for them (both upwards and downwards) in terms of energy consumption. Therefore, it is still important to study, how and how much the airtightness influences the energy efficiency of different types of buildings in different climates.

Numerous studies e.g. [7, 8] were published over the last several years which have investigated the impact of the airtightness on the energy efficiency of buildings in different European countries. A similar study has not been carried out in the Czech Republic until now. In pursuit of filling this gap, the authors present a numerical investigation of the impact of the airtightness of the building envelope on the heat demand of a single-family house and a multi-family residential building in a central European climate (Prague). Several combinations of leakage distribution over the building envelope and wind shielding conditions are considered. In the case of the multi-family residential building, the impact of the internal air leakage is studied as well. With regard to the increasingly tighter energy efficiency policies, this work is focused on buildings with low energy consumption (passive houses) and very low airtightness levels.

CALCULATION METHODS

In order to calculate the heat demand, a simplified transient model was developed in Matlab – Simulink. This model consists of two parts coupled to each other: the thermal model and infiltration model. The calculation time step is one hour and the model uses hourly weather data. The model was first developed as single-zone and then adapted in order to allow for multi-zone simulations.

Thermal model

Fig. 1 shows the thermal model network (single-zone case). The model only requires a limited amount of input data and its simplicity allows the coupling with the infiltration model to be handled easily. Based on the results of its validation, it is supposed to provide reasonable accuracy for the purpose of this study [4].

The thermal model calculates the internal air temperature, the corresponding heat loss and heat demand. The heat capacity is calculated considering an effective thickness of 100 mm for all building components in contact with the internal air. The effect of heat recovery from the exhaust air is obtained by reducing the supply air flow rate by a factor (1-η), where η is the heat recovery efficiency. The supply air flow rate (as well as the internal heat gains) follows an occupancy schedule. The infiltration air flow rate is taken from the infiltration model.

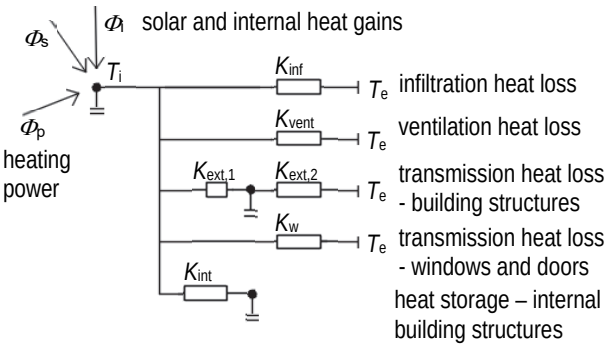

Figure 1 The thermal model network.

Infiltration model

The infiltration model calculates the infiltration air flow rate as a sum of air flow rates through the individual leakage paths. The air flow rate through the leakage paths is calculated using the power law equation as a function of the pressure difference, taking the air flow coefficient *C* and the air flow exponent *n* as leakage path characteristics. The pressure differences are calculated with regard to the wind pressure and stack effect. The pressure difference induced by the balanced ventilation system was supposed to be low in comparison with the wind and stack effect and, therefore, neglected in the calculation.

The pressure difference due to the stack effect is calculated from the leakage path position on the building envelope (height above the 1st floor) and the internal air temperature. Since the infiltration air flow rate and the internal temperature influence each other, the internal temperature is corrected by means of an iterative approach as explained in the section "Coupling of thermal and infiltration model".

The wind pressure is calculated as a function of the wind speed at the building's height and the wind direction. The wind speed taken from the weather data is corrected in order to account for the building height and the surrounding obstacles (wind shielding effect) according to [1]. Wind pressure coefficients C_p for the façades and the roof as a function of the wind incidence angle are taken from [6].

The infiltration model was validated with the computer programme CONTAM. A single-zone building model (the single-family house of this study) was modelled in CONTAM with the same settings. The difference between the results did not exceed 1.4 % for the air flow rate through the individual leakage paths and 0.3 % for the total air flow rate.

Coupling of the thermal and infiltration model

For each calculation time step, the infiltration model calculates the infiltration air flow rate based on an initial internal air temperature. The resulting infiltration air flow rate is transferred to the thermal model, which calculates the internal air temperature. Since the calculated internal air temperature may differ from the initial one, the calculated temperature is sent back to the infiltration model in order to adjust the stack effect pressure differences and recalculate the infiltration air flow rates. For each calculation time step, this iterative process is repeated until the difference between the internal air temperatures and infiltration air flow rates from two successive iterations is less than a pre-set limit.

CASE 1 – A SINGLE-FAMILY HOUSE

Building description

The size, the thermal performance and building services of the studied building (Fig. 2) are representative for a typical single-family passive house recently built in the Czech Republic. The building has two storeys and it is intended for a four member family. The floor area is 132 m^2 and internal air volume is 352 m^3. The mean thermal transmittance of the building envelope is U_{em} = 0.21 W/(m^2·K) and the heat demand calculated by means of a monthly method according to (EN ISO 13790) is 16.1 kWh/(m^2·a). The building is equipped with a balanced mechanical ventilation system with heat recovery. The heat recovery efficiency is η = 75 %.

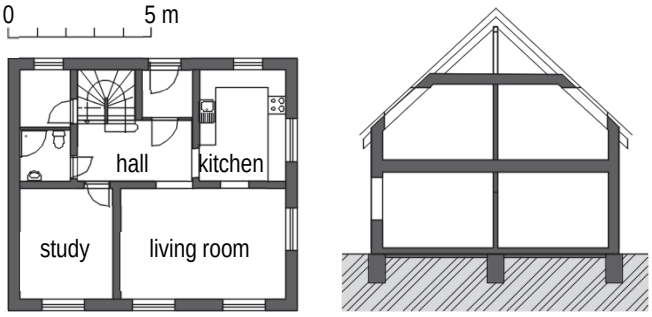

Figure 2 The studied single-family house. Left - first floor plan. Right - cross section.

Simulated alternatives

The objective of this work is the evaluation of the impact of the building airtightness on the heat demand. In this study, the building airtightness is expressed in terms of the air change rate at 50 Pa, n_{50} [h^{-1}]. The heat demand of the building was calculated several times with n_{50} varying stepwise from 0 to 1.0 h^{-1} with an increment of 0.1 h^{-1}. This range was supposed as typical for energy efficient buildings equipped with the ventilation system in question. For example, the Czech technical standard [2] recommends one to fulfil the limit value of n_{50} = 1.0 h^{-1} in the case when buildings are equipped with a mechanical ventilation system with heat recovery and n_{50} = 0.6 h^{-1} in the case when buildings with very low heat demand are equipped with the same ventilation system (typically passive houses).

Since the wind can significantly influence the infiltration, the study of the airtightness impact on the heat demand as described above was repeated three times, considering the following wind shielding conditions:

- no wind (hypothetical case, the infiltration is driven by the stack effect only),
- heavy shielding (buildings in city centres),
- moderate shielding (buildings in suburban or wooded areas),
- no shielding (buildings in an open terrain).

Single-family houses are usually built in suburban areas of larger towns or in smaller villages surrounded by buildings and trees of similar height. The villages are rarely situated in completely open country exposed to undisturbed wind. Therefore, moderate shielding can be considered as typical for this category of buildings.

For the case of moderate shielding, the impact of the leakage distribution over the building envelope was studied. On each of the building faces, the air leakage was concentrated into the leakage paths (spots) located at different heights (Fig. 3):

- the lower leakage path 0.5 m above the 1st floor – representing the leakage through the external wall/slab on the ground interface and other leakages in the lower part of the external wall (e.g., electrical boxes),
- the middle leakage path 4.05 m above the 1st floor – representing the leakage through the external wall/pitched roof interface and other leakages in the upper part of the external wall (e.g., electrical boxes on the 2nd floor, penetrations of structural elements – joists, etc.),
- the upper leakage path 5.82 m above the 1st floor – representing the leakage through the pitched roof/ceiling interface and other leakages in the upper part of the external wall (e.g., electrical boxes on the 2nd floor, penetrations of structural elements of the roof truss),
- the leakage paths in the middle-height of the building openings (windows, doors) - representing the leakage through the window or door/external wall interface and the leakage of the element itself.

Note that the horizontal position of the leakage paths has no significance for the infiltration calculations, since the average wind pressure coefficients C_p apply for the whole area of each building face. Tab. 1 shows the five studied alternatives of the overall building envelope leakage distribution.

In all the studied alternatives, the building was modelled as a single zone. The reasons are that the internal doors commonly remain open in a single-family house and the ventilation system considered in this study requires interconnections allowing for air flow between the rooms. The same time schedules (Tab. 2) and the same weather data (test reference year for Prague) were used in all simulations.

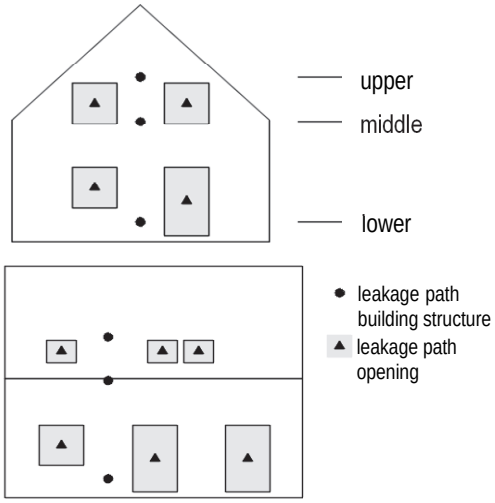

Figure 3 The position of the leakage paths.

Table 1 Overview of the studied alternatives of the leakage distribution over the building envelope

leakage path	share of the leakage path on the overall envelope air leakage				
	Alt. 1	Alt. 2	Alt. 3	Alt. 4	Alt. 5
lower leakage paths	30 %	70 %	10 %	40 %	50 %
middle leakage paths	30 %	10 %	10 %	10 %	0 %
upper leakage paths	30%	10 %	70 %	40 %	50 %
leakage paths of openings	10 %	10%	10 %	10%	10 %

Table 2 Time schedules for single-family house simulations

		0:00 ÷ 8:00	8:00 ÷ 16:00	16:00 ÷ 0:00
Number of people	[-]	4	0	4
Ventilation air flow rate	[m^3/h]	100	35*)	100
Internal heat gains	[W]	500	100	500

*) *corresponds to an air change rate n = 0.1 h^{-1}*

Results

In all the studied alternatives, the heat demand increases linearly with the air change rate at 50 Pa, n_{50} (Fig. 4 and Fig. 5). The increase in the heat demand may range from approx. 2 to 4 kWh/(m^2·a) per unit of n_{50}, depending on the wind shielding and the leakage distribution. For the likely, most common case, i.e., almost a uniform distribution of air leakage (Alt.1 in Tab. 1) and moderate wind shielding, the heat demand corresponding to the building with n_{50} = 0.6 h^{-1} is about 8 % higher than the heat demand of an ideally airtight building. In the case of a building with n_{50} = 1 h^{-1}, the increase in the heat demand reaches 14 %.

Unfavourable shielding conditions can significantly strengthen the impact of the airtightness on the heat demand. Considering the same level of airtightness, the increase in the heat demand of the studied house would be approx. 50 % higher in the case of “no shielding”

compared to the case of “moderate shielding”. On the other hand, the difference in the heat demand between the cases “moderate shielding” and “heavy shielding” is rather small. Under moderate and heavy shielding (usual conditions) the stack effect is the dominant driving force of air infiltration.

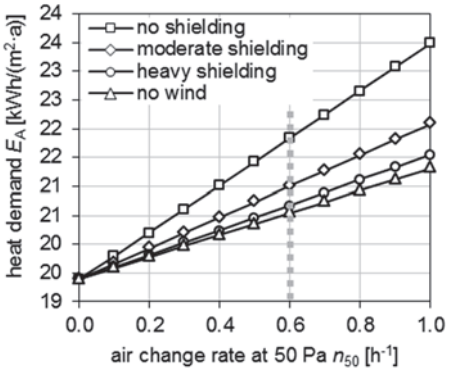

Figure 4 Simulation results for the single-family house. Influence of wind shielding, the leakage distribution corresponds to Alt. 1 in Table 1.

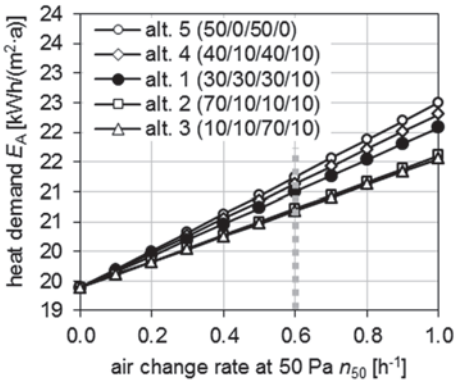

Figure 5 Simulation results for the single-family house. Influence of leakage distribution, moderate shielding

The influence of the leakage distribution is noticeable, but seems to be not really significant in comparison with the impact of the wind shielding. The lowest heat demand is obtained if the air leakage is concentrated either on the top or on the bottom of the building envelope (Alt. 2 and Alt. 3 in Tab. 1). Splitting the air leakage half on the top and half on the bottom of the building with no or a small leakage in the middle height of the building leads to the highest heat demand (Alt. 4 and Alt. 5). The uniform leakage distribution leads to the heat demand being rather closer to the unfavourable cases.

CASE 2 – A MULTI-FAMILY RESIDENTIAL BUILDING

Building description

The studied building (Fig. 6 and Fig. 7) represents an example of a real multi-family residential passive house. The building was built in a suburb of Prague in 2012. Its airtightness was tested and studied in detail [5]. Therefore, data concerning the envelope airtightness, the leakage distribution and data concerning the airtightness of the internal partitions are available.

The building has 4 residential floors above the ground level and a parking area underground. In the residential part, 14 flats are spread around the central staircase including an elevator shaft. The flats are of different sizes, the expected number of inhabitants is 40. The buildings height above the ground is 12.3 m. The floor area of the heated residential part is 1173 m^2 and its internal volume is 3933 m^3. The mean thermal transmittance of the building envelope (heated zone) is U_{em} = 0.3 W/(m^2·K) and the heat demand calculated by means of a monthly method according to [3] is 14.1 kWh/(m^2·a). The building is equipped with a decentralised balanced mechanical ventilation system with heat recovery (the efficiency is η = 75 %.). Each flat has its own air handling unit. The air change rate at 50 Pa, resulting from the overall airtightness test carried out at the time the building was commissioned is n_{50} = 0.48 h^{-1}.

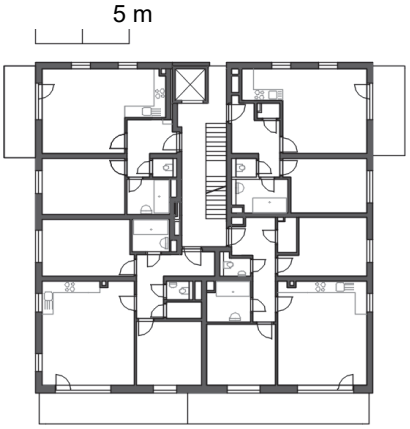

Figure 6 The studied multi-family residential building. 3rd floor plan.

Figure 7 The studied multi-family residential building. Completed building

Simulated alternatives

The heat demand of the multi-family residential building was calculated as a function of the n_{50} value ranging from 0 to 1 h^{-1} with an increment of 0.2 h^{-1}. In such a markedly compartmented building, the use of the single-zone model is not suitable. Therefore, the original thermal and infiltration models were adapted, including their coupling, in order to allow for multi-zone simulations.

In the thermal model, the heated space consists of two zones: one zone representing all the flats and a second zone representing the staircase. The infiltration model consists of five pressure zones. The flats of each floor are grouped into one zone (four zones, referred to as flats hereafter). The staircase is considered as a separate zone. The following alternatives of connection between the pressure zones were considered (Fig. 8):

- Alt. 1 no internal air leakage between the zones (airtight internal partitions),

- Alt. 2 each flat connected with the staircase (air leakage between the flats is not allowed),
- Alt. 3 each flat connected with the staircase and neighbouring flats (air leakage between the flats is allowed).

The characteristics of the internal leakage paths were estimated from the results of the airtightness tests [5]. These characteristics were kept constant in all simulations, regardless of the airtightness level of the building envelope.

In the case of the residential building, a more detailed distribution of the wind pressure coefficient C_p over the envelope was considered. Each face of the building was divided into several regions with characteristic C_p values for high-rise buildings [6].

Identical air leakage distribution was considered in all simulations (i.e., unlike in the single-family house study, the effect of leakage distribution over the building envelope was not studied here). The total air leakage through the building envelope was distributed between the envelope area enclosing the flats (61 % of the total air leakage) and the envelope area enclosing the staircase (39%). This proportion reflects the real leakage distribution deduced from the results of the airtightness testing. The proper air leakage of each of these two areas was equally divided among the four floors (25 % each). In the case of the flats, this "floor leakage" was equally divided between the two leakage paths: one at the top and one at the bottom of the zone height, as shown in Fig. 6. In the case of the staircase, the "floor leakage" was concentrated into one leakage path in the mid-height of the floor (Fig. 7).

Table 3 Time schedules for the multi-family residential building simulations

			0:00 ÷ 8:00	8:00 ÷ 16:00	16:00 ÷ 0:00
Flats (total figures)	Number of people	[-]	40	0	40
	Vent. air flow rate	[m³/h	1000	230*)	1000
	Internal heat gains	[W]	5400	1400	5400
Staircase	Number of people	[-]	0	0	0
	Vent. air flow rate	[m³/h	34	34	34
	Internal heat gains	[W]	0	0	0

**) corresponds to an air change rate n = 0.1 h^{-1}*

The same time schedules (Tab. 3) and the same weather data (test reference year for Prague) were used in all the simulations.

Results

The increase in the heat demand ranges from approx. 3 to 5 kWh/(m^2·a) per unit of n_{50}, depending on the wind shielding. Under moderate wind shielding, the heat demand corresponding to the building with n_{50} = 0.6 h^{-1} is about 13 % higher than the heat demand of an ideally airtight building. These figures are markedly higher than in the case of the single-family house showing a more significant impact of the airtightness on the heat demand in the case of residential buildings (compare Fig. 4, Fig. 5 and Fig. 9, Fig. 10, respectively). Since the residential buildings are higher, they suffer from stronger wind pressure than low-rise single-family houses (higher C_p values).

Different alternatives of the connections between the pressure zones led to very similar results in terms of heat demand (Fig. 9). However, the airtightness of the internal partitions strongly affects the distribution and magnitude of the internal air leakage. Significant air flow rates were identified from the staircase to adjacent flats and between neighbouring flats (Fig. 11).

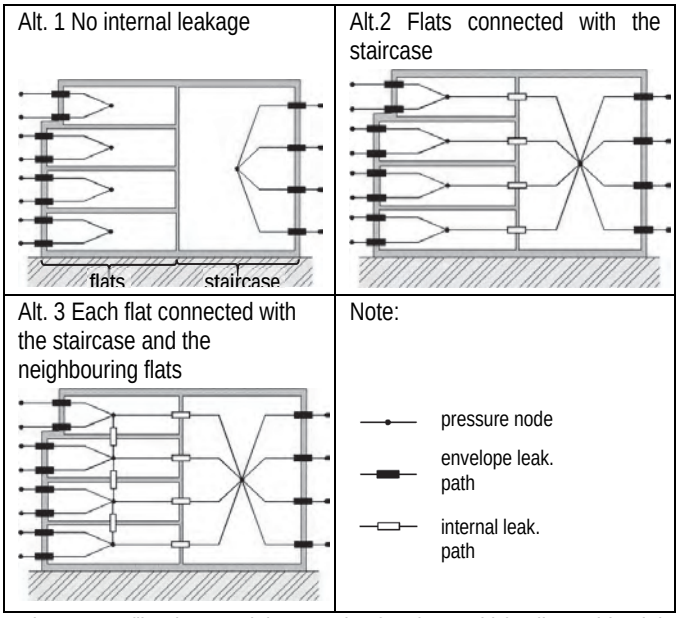

Figure 8 Infiltration model networks for the multi-family residential building - schematic cross sections

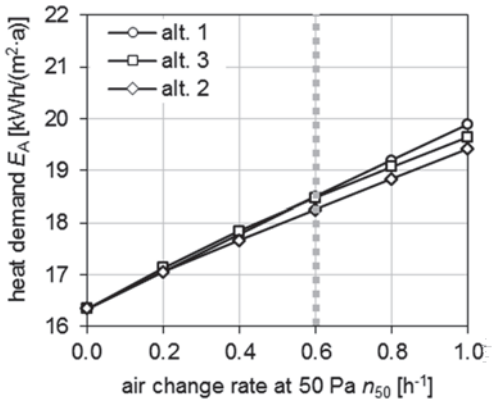

Figure 9 Simulation results for the multi-family residential building. Influence of internal leakage, moderate shielding.

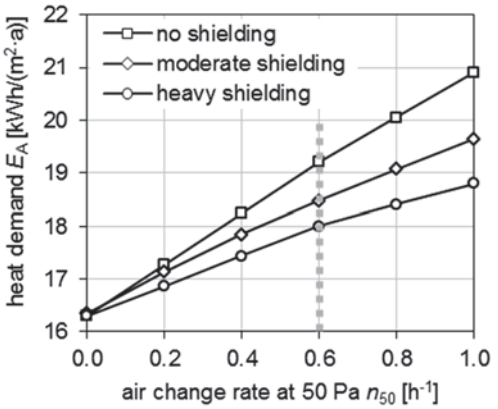

Figure 10 Simulation results for the multi-family residential building. Influence of wind shielding, no internal leakage (airtight internal partitions).

Alt. 2, flats connected with the staircase, air flow rates in [m³/h]

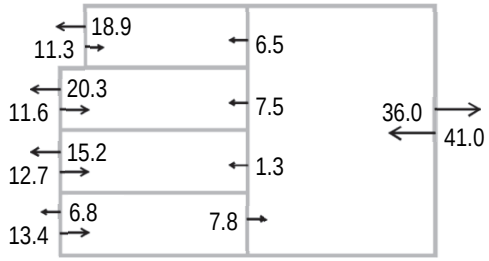

Alt. 3, each flat connected with the staircase and neighbouring flat, air flow rates in [m³/h]

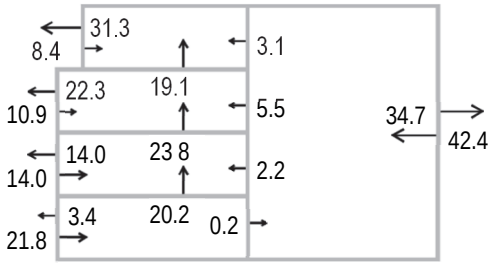

Figure 11 Average air flow rates between the pressure zones for January (schematic cross section).

DISCUSSION AND CONCLUSIONS

This study confirms the significant impact of air leakage through the building envelope on the heat demand of passive houses in the Central European climate. This impact is more pronounced in the case of taller residential buildings. Exposure to the wind considerably amplifies the impact of the air leakage. Even under typical wind exposure (moderate shielding), the air leakage corresponding to n_{50} = 1 h^{-1} can increase the heat demand of about 14 % (single-family house) or 20 % (residential building), with reference to an ideally airtight building. Hence, seeking an even better airtightness remains a meaningful challenge.

Despite the simplifications and limited extent of this study, one can try, based on the results, to estimate approximately an appropriate level of airtightness requirements for passive houses in the Central European climate. Generally, a factor causing an increase in the heat demand higher than 10 % can be perceived as a critical threat for energy efficiency targets. On the other hand, a factor causing an increase lower that 5 % would obviously be of minor significance (e.g., due to the uncertainties in the determination of the factor itself and in the calculation method). Therefore, let us set lower and upper limits of an acceptable increase in the heat demand due to the air leakage to 5 and 10 %, respectively, with reference to an ideally airtight building. Then, we can find a corresponding range of n_{50} being about 0.4 ÷ 0.7 h^{-1} for single-family houses and 0.2 ÷ 0.5 h^{-1} for residential buildings. From this point of view, the commonly accepted limit value of n_{50} = 0.6 h^{-1} seems to be appropriate for single-family houses, but could be further reduced for residential buildings. The achievement of n_{50} values ranging from 0.2 to 0.5 h^{-1} should not represent an issue in the case of residential buildings due to the usually favourable envelope area to the volume ratio (*A/V*). Moreover, field experience proves that such values can be achieved in practice, in particular, if a systematic control is required (mandatory airtightness testing).

An unfavourable distribution of the air leakage over the building envelope can strengthen the increase on the heat demand. The worst case occurs if the air leakage paths are concentrated at the bottom and at the top of the height of a pressure zone. Therefore, the design and construction of the connections between the building elements in these locations merit particular attention.

The influence of the internal air leakage on the heat demand was found negligible. However, leaky internal partitions result in a significant air exchange between adjacent pressure zones causing the potential interference with the ventilation system. Transport of contaminants (or fumes in the case of a fire) due to the internal air leakage represents a potential IAQ (indoor air quality) issue and fire safety risk. Further investigation is needed in order to decide whether, and to what degree, the airtightness of the internal partitions should be required.

Authors contact: ales.vlk@fsv.cvut.cz, jiri.novak.4@fsv.cvut.cz

ACKNOWLEDGEMENTS

This work has been supported by the Ministry of Education, Youth and Sports within the National Sustainability Programme I, project No. LO1605. This paper has been published in the Proceedings of the 38th AIVC Conference, Nottingham, September 2017.

REFERENCES

[1] ASHRAE (2001). 2001 ASHRAE Handbook - Fundamentals, American Society of Heating, Refrigeration and Air-Conditioning Engineers, Inc. Atlanta. ISBN 1-883413-88-5

[2] ČSN 730540-2: 2011. Thermal performance of buildings – Part 2: Requirements. Czech office for standards, metrology and testing.

[3] EN ISO 13790:2008. Energy performance of buildings – Calculation of energy use for space heating and cooling. European Committee for Standardisation

[4] KOPECKÝ, P. (2016). Comparative testing of simplified lumped parameter building thermal models. Proceedings of conference CESB 16 - Central Europe towards sustainable building 2016, 22nd – 24th June 2016, 789 – 796. Grada Publishing a.s. ISBN 978-80-271-0248-8

[5] NOVÁK, J. (2013). Airtightness of a multi-family passive residential building in the Czech Republic. Proceedings of the 8th International BUILDAIR-symposium 2013, Hannover

[6] ORME, M., LIDDAMENT, M., WILSON, A. (1998). Numerical Data for Air Infiltration and Ventilation Calculations. Coventry: AIVC. ISBN 1 946075 97 2.

[7] RICHIERI, F. et al. (2008). Numerical evaluation of the airtightness impact on energy needs in mechanically ventilated dwellings. Proceedings of the 8th International BUILDAIR-symposium 2013, Hannover.

[8] JOKISALO, J., KURNITSKI, J., VINHA, J. (2007) Building leakage, infiltration and energy performance analyses for Finnish detached houses. Building and Environment, Volume 44, Issue 2, February 2009, Pages 377-387.